Spin liquids: mean field and beyond

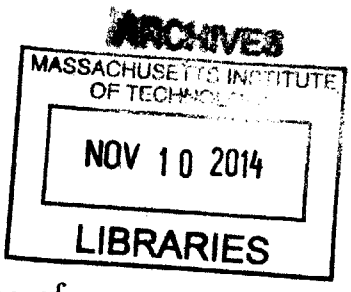

by

Maksym Serbyn

Submitted to the Department of Physics
in partial fulfillment of the requirements for the degree of

Doctor of Philosophy

at the

MASSACHUSETTS INSTITUTE OF TECHNOLOGY

September 2014

© Massachusetts Institute of Technology 2014. All rights reserved.

Signature redacted

Author .....
Department of Physics
August 28, 2014

Signature redacted

Certified by....
Patrick A. Lee
William & Emma Rogers Professor of Physics
Thesis Supervisor

Signature redacted

Accepted by .....
Krishna Rajagopal
Associate Department Head for Education

Spin liquids: mean field and beyond

by

Maksym Serbyn

Submitted to the Department of Physics
on August 28, 2014, in partial fulfillment of the
requirements for the degree of
Doctor of Philosophy

Abstract

Spin liquids are fluid-like ground states of spin systems, where spins do not order at zero temperature. These states have long-range entanglement and concomitant exotic properties, such as fractionalized excitations and emergent gauge field. In this thesis we use mean field approach and its extensions to address spin liquid states of spin-1 system which has no analogue for spin-1/2. Also, we consider impurity as a probe of spin-1 system, and spinon-phonon interactions in Dirac spin liquid.

In Chapter 2, using a fermionic representation for spin-1 system, we find a state where one flavor of spinons has a Fermi surface, while other flavors are gapped out by $d + id$ topological pairing [1]. Despite the existence of a Fermi surface, this ground state has fully gapped bulk spin excitations. Within Variational Monte Carlo techniques we study phase diagram of different spin-1 generalizations of Heisenberg model [2]. For an SU(3)-invariant model with sufficiently strong ring-exchange terms, we find a $d+id$ paired quantum spin liquid with a Fermi surface of deconfined spinons.

Chapter 3 addressed the behavior of Kondo $s = 1/2$ impurity embedded in a two-dimensional $S = 1$ U(1) spin liquid with a Fermi surface [3]. This problem contains an interplay between non-Fermi-liquid behavior induced by a gauge field, and a non-Fermi-liquid fixed point in the overscreened Kondo problem. We find that the gauge field leads to observable changes in the physical properties of the system at the overscreened Kondo fixed point. Thus, realization of overscreened Kondo physics in U(1) spin liquid can be used as a probe of fermionic spinons.

Finally, in Chapter 4 we study the interaction of Dirac spinons with $S = 1/2$ with lattice vibrations [4]. We establish the general procedure for deriving spinon-phonon interactions which is based on a symmetry considerations, and illustrate it for different algebraic spin liquids. Despite all considered algebraic spin liquids have identical low energy description, spinon-phonon interaction probes the microscopic details and is set by representation of projective symmetry group. We estimate the attenuation of ultrasound, and discuss its experimental prospectives as probe of spinons.

Thesis Supervisor: Patrick A. Lee
Title: William & Emma Rogers Professor of Physics

Acknowledgments

Over the five years spent at MIT physics department I had countless number of interaction with different people. Now I understand that it is these interactions that molded and shaped me as a physicist. Acknowledging everybody who had some influence on me seems a daunting task, and I shall attempt at least naming people whose imprint cannot go unnoticed by any means.

First I would like to thank to my advisor, Patrick Lee, who introduced me to the physics of strongly correlated systems – a *terra incognito* for me at the time of my arrival to MIT. My explorations into the physics of spin liquids, supervised by Patrick constitute the body of this thesis. It has been a great pleasure to work under the guidance of Patrick, and I am grateful for all our discussions and his generous advice. His deep physical intuition that sees the essence, or, physics, beyond complicated equations and models fascinated me from the beginning of our work together, and will remain a "gold standard" I will aim at. Another aspect, I am especially grateful for was the freedom to work on problems that interested me. I am thankful for Patrick's graciousness, patience and encouragement.

The work presented in this thesis was done in collaboration with T. Senthil, and was fueled by his enthusiasm and relentless flow of ideas. I have learned a lot from my interactions with Senthil, in particular about the field-theoretical language of Condensed Matter – Senthil's "native" language. I also enjoyed collaborating with Samuel Bieri on numerical approaches, and I am grateful for his introduction to method of Variational Monte Carlo.

During my PhD I also worked on problems not related to spin liquids. It was a great pleasure to work with Dmirty Abanin and Zlatko Papic on the problem of many-body localization. Working with Dima was rewarding in a number of different aspects. Dima possesses an ability to balance between thinking in a practical way, while still finding fundamental and conceptually interesting problems. His driving energy and enthusiasm along with high intellectual standards have left an indelible mark on me. In addition, I am grateful to Dima for being a mentor and a friend, and

I have benefitted a lot from our philosophizing and his counsel.

During my time at MIT, I was also lucky to interact with several experimental groups. Working hand-in-hand with experimentalists and casting some light on real experimental data was truly rewarding for me as a theorist. I learned a lot from the fast-paced work on topological crystalline insulators done together with Liang Fu in collaboration with experimental group of Vidya Madhavan, and, in particular, with Yoshinori Okada. I also acknowledge interactions with Pablo Jarillo-Herrero and Leonardo Campos on the physics of trilayer grapehene.

I would like to express my gratitude to other that surrounded me throughout my years at MIT. I am grateful to Leonid Levitov for his help and advices. I am very grateful to Tim Chen and Justin Song with whom I spent many an hour talking about physics, and truly became friends. I am especially grateful to Justin for his advice on writing and proofreading of my papers – every other article in this thesis belongs to him. I am also indebted for many discussions to Evelyn Tang, Matthew Pinson, Brian Swingle, Maissam Barkeshli, Abolhassan Vaezi, Andrew Potter, David Mross, Rahul Nandkishore, Fa Wang, Karen Michaeli, Rebecca Flint and many others.

I would like to thank people I met before I came to MIT. First and foremost I am grateful to my master's thesis advisor, Mikhail Skvortsov, who gently introduced me into the field of Condensed Matter Physics. Along with Mikhail, I would like to acknowledge Andrei Varlamov and Alexei Morozov for working with me and teaching me physics, and mentoring me throughout my years in Moscow.

The time I spent in Boston would not be so exciting and easy without the support from my friends. I am very grateful to Alexey Vikhlinin for his support and generous hospitality from my very first days in Boston, for his mentorship, ruminations on life, and sincere arm in friendship. From the start Mark Mezei and Anna Posfai have been a blessing. Mark and Anna were always offering a helping hand, and when we most needed it – never failed including everything from cake disposal to babysitting our daughter. I am also very indebted to Maxim Imakaev, Veronica Stelmakh and Jason Hill, Vasily and Dasha Dzyabura for their help and support.

The Holy Epiphany parish in Boston made us feel at home; it was a single big

family. I am honored to be part of this family and I am grateful to the countless number of exceptional people I have met there over past few years. I cannot list all their names, but I am especially grateful to the Boldewskul, Bolberov, Medzhidov, Parkhitko, and Soykin families.

I cannot express my gratitude to my wife Dasha for her endless love, patience, and courage to follow me to the United States. All my endeavors over last five years, would not be possible without Dasha; truly, all of them have been *our* endeavors. Our lives would be much less colorful without our children, Marfa and Tikhon, who have filled it with joy and adventure. Despite the physical distance that has separated me from my parents and sister, I have felt their constant love, support, and confidence in me. They have been a source of inspiration. I also thank my grandparents and my in-laws for their love, support, and understanding.

Contents

List of Figures

List of Tables

Chapter 1

Introduction

This introductory chapter aims to provide background and motivation for the results presented in Chapters 2, 3, and 4. We start with introducing the concept of emergence and definition of quantum spin liquid in Sections 1.1-1.2. Section 1.3 introduces the mean field description and its extensions. Afterwards, in Section 1.4, we briefly summarize our results in the context of open questions in the field of spin liquids. We conclude with a discussion of perspective and challenges of the mean field approach to spin liquids.

1.1 Defining spin liquid

The physics of strongly correlated systems is a collective notion for a variety of phenomena where interactions play a leading role. Despite recent progress made over the last few decades with the development of such fields as high-temperature superconductivity and heavy fermion materials, there still remain a plethora of open questions concerning strongly correlated matter.

The major difficulty in the physics of strongly correlated systems comes from strong interactions. As a consequence, conventional methods, e.g. *perturbing* with respect to some simple system like the free electron gas, breaks down. On the other hand, this difficulty brings a promise. The fact that relevant physics cannot be smoothly accessed from non-interacting limits, often indicates that it is *qualitatively*

different from known non-interacting examples. Perhaps the most celebrated example of such *emergence* are fractionalized excitations in the fractional quantum Hall effect. There, a system of interacting electrons in magnetic field has elementary excitations that are drastically different from electrons or holes; these emergent excitations have a charge that is a fraction of the electron charge.

Quantum magnets is another family of systems where such emergence is known to occur. Magnetism inherently lies in the realm of strongly-correlated physics, as it arises due to the quantum mechanical nature of electrons and atoms. Moreover it is quantum-mechanical interactions that are relevant for the majority of magnetic effects. Akin to a quantum harmonic oscillator that retains its zero point motion even in the ground state, one can imagine an interacting system of spins in which its "quantumness" prevents ordering down to zero temperature. Such a ground state bears the name of *quantum spin liquid*, reflecting the failure of spins to "freeze into a solid" due to quantum mechanics (hence, "quantum") and will be a main subject of this thesis.

The simplest example of quantum spin liquid is realized in one-dimensional systems. However, one dimension is well-known to be special – restricted phase space and strong quantum fluctuations lead to many exotic phenomena such as integrability, spin-charge separation, and so on. Beyond the one-dimensional wonderland, a very simple picture of quantum spin liquid state was proposed by Anderson [8]: the resonant valence bonds state (RVB). In this proposal Anderson suggested that the most intuitive way to get rid of spins is to pair them into singlets. For just two spins of 1/2 such a singlet, $(\uparrow\downarrow - \downarrow\uparrow)/\sqrt{2}$, gives us a spin-0 object, see top row of Figure 1-1. This is to be compared with the Neel-type product state $\uparrow\downarrow$, where one has zero total spin only after average. Note, that such a singlet, or a single valence bond is a maximally quantum entangled state of two spins. For a lattice of spins one can construct the RVB state by taking superposition of all possible tilings of the lattice with such nearest-neighbor singlets.

The original Anderson construction features emergent fractionalized excitations. Excluding a single pair of spins from participating in singlets produces a single ex-

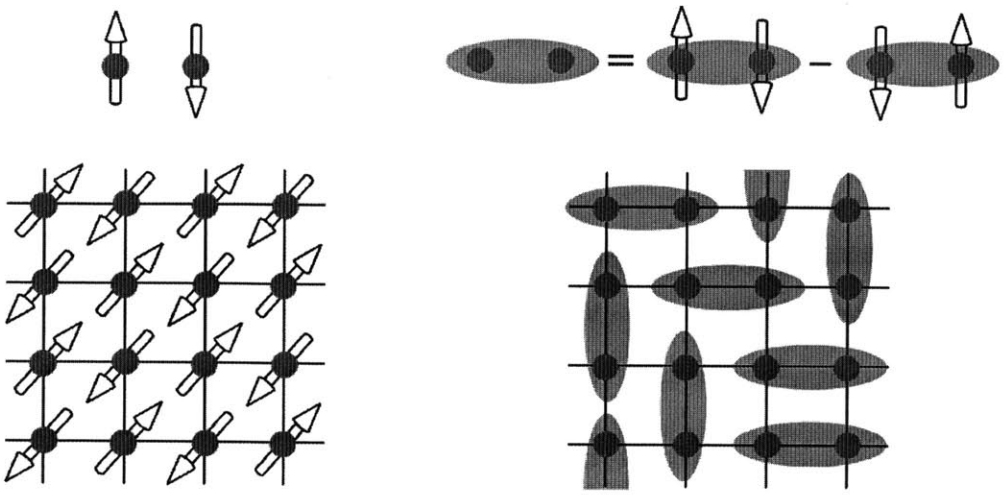

Figure 1-1: Cartoon picture of Neel and Anderson RVB state for just two spins (top row) and on a square lattice. RVB state is a superposition of all possible tilings of the lattice with nearest neighbor valence bonds.

citation with total $S = 1$. In the Neel state, such excitations, delocalized over the bulk of the lattice, would become a spin wave. Note, that despite this delocalization in real space, the spin wave carries a spin $S = 1$. In contrast to the Neel case, in the RVB state two spins excluded from singlet formation are free to move away from each other, as shown in Figure 1-2. This results in *a pair* of delocalized excitations, each carrying spin-1/2, called *spinons*. As noted earlier, spinons are absent in the Neel state shown in Figure 1-1. While the distance between spinons does not impact the energy of the RVB state, in the Neel antiferromagnet long separations between spinons produce "unhappy" bonds with their number proportional to the distance between spinons. Therefore in the Neel antiferomagnet, spinons are confined, and proper excitations are spin waves carrying spin-1 quantum number.

The resonant valence bond state discussed so far has fractional excitations, which are, however, gapped: breaking a singlet pair costs a finite amount of energy. In principle, there is no reason to restrict singlets to nearest neighbors, and one can include longer range bonds in superposition that forms the RVB state. Valence bonds formed by spins far apart are more weakly bound, thus including longer range singlets lowers

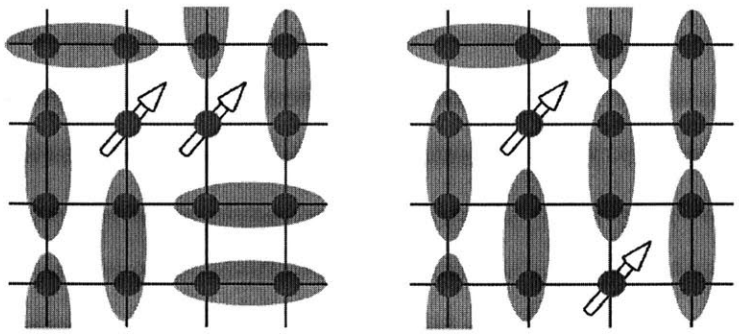

Figure 1-2: Fractionalization of a single spin-1 excitation into two spinons in a RVB state.

the minimal energy of excitations. If these longer range singlets have a substantial weight, this may result in a quantum spin liquid state with *gapless* excitations. Moreover, these excitations may possess bosonic, fermionic or even more general statistics, and, as we shall see below, are often accompanied by a gauge field, just like real electrons that carry electromagnetic charge.

The RVB construction can be used to motivate a *positive* definition of a quantum spin liquid [9]. Indeed, spin liquids cannot be classified according to broken symmetry [10] as they do not break any symmetries. The absence of symmetry breaking is a defining property of a spin liquid, which is, however, of little use. To prove that a given state is a spin liquid, within such definition one would have to rule out all possible orders.

Inspiration for a different definition of spin liquid provided by the RVB state comes from a basic block of the RVB state – the spin singlet. A singlet state of two spins is special since it has a maximum possible degree of quantum entanglement. Quantum entanglement is a notion unique to quantum mechanics, where one can prepare an entire system in a well defined state, while leaving the state of smaller constituents of the system (such as individual spins) uncertain. The commonly accepted quantitative measure of entanglement is entanglement entropy. It is equal to zero in any product state, e.g. $\uparrow\downarrow$ or $(\uparrow - \downarrow)(\uparrow + \downarrow)/2$. On the other hand, the singlet is said to be a

maximally entangled state, with an entanglement entropy equal to $\log 2$. While taken together, the two spins are in a pure quantum-mechanical state $(\uparrow\downarrow - \downarrow\uparrow)/\sqrt{2}$, each of them considered separately has a maximum possible uncertainty, pointing up or down with probability $1/2$.

The RVB state is, by construction, a "soup" of spin singlets. From the discussion of the entanglement structure of the singlet above, one may expect, that the RVB and, more generally, spin liquid states possess a special structure of entanglement. Formalizing this intuition, we define a spin liquid as a state with *non-local* entanglement [9]. Non-locality of entanglement means that it violates usual scaling laws. Depending on the nature of excitations in the spin liquid, the entanglement non-locality has different manifestations. In the next Section, we will review different types of spin liquids and discuss their entanglement structure.

1.2 Different spin liquids and their entanglement

Before discussing entanglement structure, we will introduce different type of spin liquids. The next Section will discuss the specific route to these states offered by mean field theory. According to the nature of excitations, spin liquids may be divided into *gapped* (which are often dubbed as topological) and *gapless* classes. Within the family of gapless spin liquids, one can separate states where excitations have bosonic or fermionic nature. The latter, which will be of primary interest in this thesis, can have fermionic spinons with a Fermi surface, or with a Dirac dispersion (so-called algebraic spin liquids), and are often endowed with an emergent gauge field strongly coupled to spinons.

We will begin by examining a gapped spin liquid phases, which are examples of *topological order* [11]. Generic gapped states are known to obey an area law scaling of entanglement. The entanglement entropy is always defined with respect to a particular bipartition of the system. The area law scaling of entanglement formalizes the intuition that only the degrees of freedom across the boundary are correlated: entanglement entropy scales as $S_{\text{ent}} \sim \alpha \ell^{d-1}$, where ℓ^{d-1} is a boundary area (or,

length for two spatial dimensions, $d = 2$) of the corresponding region.

Topological order is usually defined via the degeneracy of the ground state that depends on the topology of the system [11]. Another surprise of the ground state with topological order is that their entanglement is *smaller* than usual, i.e. for two dimensional systems there is a constant negative correction, $S_{\text{ent}} \sim \alpha\ell - \gamma$ in the entanglement scaling with $\ell \to \infty$, called topological entanglement entropy [12,13]. Recent advances in numerical techniques, in particular, density matrix renormalization group [14,15], allowed for the calculation of γ in specific spin models. For a gapped $\mathbb{Z}_2$ spin liquid (see discussion in Section 1.3.1), γ was calculated numerically yielding $\gamma = \log 2$ for ground states of the Heisenberg model on Kagome lattice [16,17]. This confirms the topological nature of the gapped spin liquid ground state [18].

After a brief discussion of gapped spin liquids which realize topological order, we shift to spin liquids with gapless excitations – the main subject of the present thesis. As discussed before, gapless spin liquids correspond to RVB states where longer range singlets have a significant contribution. This may lead one to expect a violation of the boundary law scaling for entanglement, in contrast to a constant subleading corrections for gapped spin liquids.

Indeed, using a Variational Monte Carlo approach (see Section 1.3.2), Refs. [19,20] demonstrated the scaling of entanglement as $S_{\text{ent}} \sim \ell \log \ell$ for the gapless spin liquid with a spinon Fermi surface, and a universal positive correction to entanglement for the Dirac spin liquid, $S_{\text{ent}} \sim \alpha\ell + \gamma$. The logarithmic correction to entanglement for the spin liquid with a spinon Fermi surface is similar to the entanglement scaling for the case of *free* fermions [21], and can be viewed as the most severe violation of the area law. We note parenthetically, that we are discussing the ground state entanglement, which should not be confused with the entanglement of highly excited states which usually scales as a volume law, $S_{\text{ent}} \sim \ell^2$ (in two dimensions).

As discussed in the above survey, for all spin liquid ground states entanglement behaves in an anomalous way, either by receiving corrections to scaling, or by violating scaling typical of ground states. Therefore, *non-local* behavior of entanglement may be viewed as a precursor of exotic properties, and a defining feature of spin liquids.

With this, we turn to considering all spin liquids briefly discussed here using the mean field approach.

1.3 Mean field approach to spin liquids

After an attempt to broadly define the spin liquid ground state, we dive into the basics of mean field description of a spin liquids. This approach will be extensively used throughout this thesis, as it provides a starting point for describing spin liquid ground states. Starting with the mean field framework described below, one can later include an emergent gauge field fluctuations, which we shall discuss in Section 1.3.1. Also, mean field can be used a starting point to build variational wave functions, as discussed in Section 1.3.2.

Although spin liquids lack any conventional order parameter, it is possible to build a mean field-type description of spin liquid ground states. As usual, in the mean field approach, one has to make an (educated) guess regarding the spin liquid state one attempts to describe. Rather than using the spin operator itself as an order parameter (recall, that $\langle\vec{S}\rangle$=0 in spin liquid), the mean field description of the spin liquid relies on the slave particle approach.

The spin operator is expressed in terms of slave bosons or fermions, subject to a constraint necessary to retain correct the Hilbert space dimension. In what follows we represent spin using fermions. In particular, a spin-1/2 operator can be represented via $f_\uparrow$, $f_\downarrow$ as:

$$\vec{S}_i = \frac{1}{2} f^\dagger_{i\alpha} \boldsymbol{\sigma}_{\alpha\beta} f_{i\beta}. \tag{1.1}$$

The mapping between Hilbert spaces is exact, provided one imposes a constraint of single occupancy,

$$f^\dagger_{i\uparrow} f_{i\uparrow} + f^\dagger_{i\downarrow} f_{i\downarrow} = 1, \tag{1.2}$$

thus excluding states with no fermions or two fermions on each site.

To do the mean field decoupling, we express the spin operator via fermions, ar-

riving at the Hamiltonian that is quartic in fermion operators:

$$H = \sum_{\langle ij \rangle} J_{ij} \vec{S}_i \cdot \vec{S}_j = -\frac{1}{2} \sum_{\langle ij \rangle} J_{ij} \left(f^\dagger_{i\alpha} f_{j\alpha} f^\dagger_{j\beta} f_{i\beta} + \frac{1}{2} f^\dagger_{i\alpha} f_{i\alpha} f^\dagger_{j\beta} f_{j\beta} \right), \qquad (1.3)$$

From here one can perform a Hubbard-Stratonovich decoupling of the quartic terms using mean field parameters in the particle-hole, and, if necessary, in particle-particle channels:

$$\chi_{ij} = \langle f^\dagger_{i\alpha} f_{j\alpha} \rangle, \qquad \Delta_{ij} = \langle f_{i\uparrow} f_{j\downarrow} \rangle. \qquad (1.4)$$

Keeping only the particle-hole channel, the resulting mean-field Hamiltonian becomes:

$$H_{\text{MF}} = -\frac{1}{2} \sum_{\langle ij \rangle} J_{ij} \left[\chi_{ij} f^\dagger_{i\alpha} f_{j\alpha} + \text{H. c.} - |\chi_{ij}|^2 \right] + \sum_i \mathrm{i}\lambda_i (f^\dagger_{i\alpha} f_{i\alpha} - 1), \qquad (1.5)$$

where we added a Lagrange multiplier to enforce the single-occupancy constraint. The specific form of mean field decoupling, χ_{ij} can be determined variationally, which is equivalent to finding a mean-field saddle point – see below. Depending on the solution for χ_{ij} one can obtain a different type of dispersion for fermionic spinons that are naturally represented by $f_{i\alpha}$ in this formalism. The ground state at the mean field level corresponds to spinons filling a corresponding band structure (note, that fulfilling constraint (1.2) on average, pins the Fermi level to a half-filling for the spin-1/2 case).

The choice of χ_{ij} in (1.5) is restricted by symmetries of the system. Naively, one may say that the fully symmetric spin liquid necessarily has uniform χ_{ij}. However, Wen [10, 22] found more that 200 symmetric spin liquids on a square lattice. It turns out that due to the presence of constraint (1.2), representation (1.1) has a *gauge symmetry*. This gauge freedom, discussed below in more detail, requires one to expand the notion of the lattice symmetry group to that of a projective symmetry group. Thus the number of different ansätze respecting all symmetries is expanded from one to a much larger number, leading to a large number of symmetric spin liquids.

Above, we described the mean field approach in the context of spin-1/2 systems. However, in Chapters 2 and 3 of this thesis we will consider spin-1 system. A gener-

alization of the slave-fermion type of mean field for spin-1 case will be described in more detail in Section 2.1.4.

1.3.1 Beyond mean field: gauge field

Upon closer examination, the representation of spin (1.1) used above has an SU(2) gauge redundancy. The U(1) subgroup of this SU(2) freedom is almost obvious: we can adjust the phase of fermions on each site independently, without changing spin operator (1.1):

$$f_{i,\uparrow(\downarrow)} \to e^{i\theta_i} f_{i,\uparrow(\downarrow)}. \tag{1.6}$$

It appears [10] that this U(1) symmetry can be further expanded to SU(2), as

$$\begin{pmatrix} f_{i\uparrow} \\ f^\dagger_{i\downarrow} \end{pmatrix} \to U_i \begin{pmatrix} f_{i\uparrow} \\ f^\dagger_{i\downarrow} \end{pmatrix}, \tag{1.7}$$

where $U_i \in \mathrm{SU}(2)$ is a position-dependent unitary matrix.

The presence of the gauge degree of freedom in the original Hamiltonian (1.3) has important consequences for the path integral formulation. Indeed, above we discussed the mean field solution for χ_{ij}. It can be viewed as a saddle point approximation for the path integral

$$Z = \int [Df_i][D\lambda_i][D\chi_{ij}] e^{iS}, \quad \text{with} \quad S = \int dt\, L; \tag{1.8}$$

$$L = \sum_i f^\dagger_{i\alpha} \partial_t f_{i\alpha} - H_{\mathrm{MF}}, \tag{1.9}$$

where mean-field Hamiltonian is given by (1.5). The presence of a gauge degree of freedom is reflected in the appearance of fluctuations around the saddle point solutions that do not cost any energy. Such degrees of freedom *cannot* be integrated out within a saddle point approximation, and have to be included into an effective theory.

Saddle points of the action (1.8)-(1.9), depending on their structure [10,22] usually break the original SU(2) symmetry (1.7), producing U(1) or $\mathbb{Z}_2$. When the remaining symmetry is U(1), the action (1.8) has a U(1) gauge field coupled to spinons. Indeed,

the Lagrange multiplier, along with the phase fluctuation of χ_{ij} may be viewed as a scalar and vector potentials of the emergent gauge field, a_i^0, and a_{ij} which live on lattice sites and links respectively:

$$H_{\mathrm{MF}} = -\frac{1}{2}\sum_{\langle ij\rangle} J_{ij}\left[|\chi_{ij}|e^{\mathrm{i}a_{ij}} f_{i\alpha}^{\dagger} f_{j\alpha} + \mathrm{H.\,c.} - |\chi_{ij}|^2\right] + \sum_i a_i^0 (f_{i\alpha}^{\dagger} f_{i\alpha} - 1). \quad (1.10)$$

The gauge transformation works as

$$f_i \to e^{\mathrm{i}\theta_i} f_i, \qquad a_i^0 \to a_i^0 + \partial_t \theta_i, \qquad a_{ij} \to a_{ij} + \theta_i - \theta_j, \quad (1.11)$$

leaving the action (1.8) invariant. Since we have a lattice version of the gauge field, it is compact, i.e. defined modulo 2π. Depending on the choice of χ_{ij}, such ansatz leads either to U(1) spin liquid with a Fermi surface, or to an algebraic spin-liquid, where spinons have a Dirac-like dispersion.

The mean field description of $\mathbb{Z}_2$ spin liquid may be understood from further breaking of U(1) symmetry. Akin to the conventional metal, where U(1) symmetry is broken by the development of superconducting order, one can have a non-zero pairing of spinons Δ_{ij}, Eq. (1.4), in the mean field solution. In such a case, the phase fluctuations become massive via the Anderson-Higgs mechanism, leaving behind a discrete $\mathbb{Z}_2$ gauge symmetry.

When gauge symmetry is broken, simultaneously the pairing may either fully gap out spinons, corresponding to a mean-field description of the short-range RVB state; or leave gapless nodal excitations, leading to a $\mathbb{Z}_2$ Dirac spin liquid. The π fluxes of the remaining $\mathbb{Z}_2$ gauge field correspond to another type of low-energy excitations, called visons. Bound states of such π-flux vortex and a spinon would have bosonic statistics. Thus, the gapped $\mathbb{Z}_2$ spin liquid has gapped bosonic and fermionic spin-1/2 excitations.

Another important aspect of breaking U(1) symmetry to $\mathbb{Z}_2$ concerns the stability of the spin liquid. The stability of a mean field construction is a non-trivial issue when a continuous compact gauge field is strongly coupled to spinons. Indeed, one may

easily imagine an onset of confinement due to strong gauge forces, which would result in $S = 1$ excitations and invalidate the mean field description. For example Hermele, *et. al.* [23] demonstrated the stability of the Dirac spin liquid coupled to a U(1) gauge field for a sufficiently large number of spinon flavors. However, when the U(1) gauge group is broken down to a discrete $\mathbb{Z}_2$, the remaining discrete gauge field is incapable of confining spinons, resulting in a stable spin liquid.

Finally, the presence of the gauge field explains the vast number of different symmetric spin liquids classified by mean field [10, 22]. Naively, only very few choices of χ_{ij} respect all the symmetry. However, once the action of the space-group symmetries can be supplemented by a gauge transform (1.11), there are many more allowed choices of χ_{ij}. Such expansion of space symmetry group by a gauge transformations is called a *projective symmetry group*, and will be extensively used in Chapter 4. Thus, the classification of spin liquids within a mean field reduces to finding different representations of a projective symmetry group, where the gauge field plays an important role.

Above we discussed the presence of an emergent gauge field which often accompanies gapless fractionalized excitations in a spin liquid. It can change physical properties of the spin liquid, and often raises concerns regarding the stability of the mean field construction. In some sense, the presence of such a gauge field strongly coupled to fermionic spinons may be viewed as another signature of spin liquid. Thus, it is interesting to consider, how one can experimentally probe the presence of not only spinons, but of the gauge field as well. This question will be addressed in the last two Chapters of this thesis, where the gauge field will be an important ingredient responsible for many physical properties. In particular, in Chapter 3 we propose how an impurity can be used as a probe of spin-1 spin liquid with spinon Fermi surface and a U(1) gauge field. Chapter 4 considers the interaction of spinons with phonons in the $S = 1/2$ spin liquid with spinons possessing Dirac dispersion.

1.3.2 Beyond mean field: projection

The mean field approach discussed above is useful to access different spin liquid phases and their properties. On the other hand, to answer a question about a ground state of a specific spin model, one has to find a state with the lowest energy. While the mean field approach is capable of accessing energies of different states, it is not reliable and often fails. Indeed, as we relax the single occupancy constraint (1.2) and impose it only on average, the resulting wave function is not a legitimate wave function of a spin system. Generically, the wave function

$$|\psi_0\rangle = \prod_{\boldsymbol{k}\in \mathrm{FS}} f^\dagger_{\boldsymbol{k}}|0\rangle, \tag{1.12}$$

describing a half-filled band of spinons, has components with double occupied/empty sites in the real space basis. These components do not have counterparts in a spin language, and thus are unphysical.

The most straightforward route to obtain a legitimate spin wave function from (1.12) is to strictly enforce single occupancy. This may be done by applying the projection operator P_G to (1.12) [24]:

$$|\psi\rangle = P_G|\psi_0\rangle = \left[\prod_i (1 - n_{i\uparrow}n_{i\downarrow})\right]|\psi_0\rangle. \tag{1.13}$$

Now, $|\psi\rangle$ can be used as a trial wave function of the spin system. Unfortunately, projection precludes analytic treatment. Therefore, one has to resort to numerical techniques to calculate the energy of the ansatz wave function $|\psi\rangle$. The standard method of choice for this uses Monte-Carlo type sampling. The energy is then minimized with respect to different mean field parameters (e.g. different choice of χ_{ij}) to yield the variational Monte Carlo (VMC) estimate for the ground state energy.

The VMC approach is a standard tool to access properties of spin-1/2 systems [24]. In this thesis, in Chapter 2 we will apply the VMC approach to study the phase diagram of different spin-1 model on a triangular lattice.

1.4 Main results of this thesis

As we discussed above, a quantum spin liquid is an exotic state of spin systems with a characteristic long range entanglement. Until recently, theoretical development of spin liquid physics was largely motivated by its relevance for the RVB theory of cuprate superconductors [25]. However, within the past decade a number of experimental materials that are likely to realize spin liquid physics, have been discovered. The most celebrated examples are organic solid [26, 27] and kagome antiferromagnet [28, 29], which both consist of two-dimensional planes. Also, a number of experiments suggest a realization of spin liquids on essentially three-dimensional lattices [30]. Finally, all of the aforementioned experiments concentrated on spin-1/2 system, as it is believed to reveal the strongest quantum fluctuations. However, recently several spin-1 spin liquids candidates were reported [31, 32].

The discovery of materials that possibly realize spin liquid ground states inspired more active theoretical research, which can be roughly classed into one of three directions:

(a) classification of possible spin liquid phases and understanding their properties;

(b) searching for the spin liquid ground state in realistic spin lattice models;

(c) studying different probes that allow for unambiguous identification of the spin liquid.

Below we discuss the contribution of the present thesis in the context of these directions. Chapter 2 touches all three outlined directions in the context of $S = 1$ spin liquids. On the other hand, Chapters 3 and 4 address issue (c), exploring different probes of the spin liquid. Chapter 3 further details spin-1 physics by looking at its interaction with a spin-half impurity. Additionally, Chapter 4 considers spinon-phonon interactions as probe of emergent Dirac spinons in an algebraic $S = 1/2$ spin liquid.

1.4.1 $S = 1$ spin liquid

As we already mentioned, most of the prospective spin liquid candidates are described by $S = 1/2$ spins on different lattices. This is not surprising [9], as quantum fluctuations that favor quantum spin liquid ground state, are typically suppressed for larger spins. However, a discovery of spin-1 spin liquid systems [31, 32] inspired a number of theoretical proposals [33–37]. In particular, the basics of slave-fermion mean field theory for spin-1 were considered in Refs. [35, 36].

Chapter 2 of this thesis considers a $S = 1$ spin liquid on a triangular lattice, covering all of the directions (a)–(c) outlined above. First, we use a mean field approach to identify a spin liquid state that has no analogue for spin-1/2 systems. Within the slave-fermion approach, representing the spin-1 operator via fermionic spinons requires at least *three* flavors of spinons (according to S_z projection of spin being 0, ± 1). This opens an interesting possibility, which is not present for spin-1/2 models, of gapping out two out of three spinons. We explore such states at the mean field level, identifying an interesting quantum spin liquid ground state with a $d + \mathrm{i}d$ pairing of spinons. This state may be roughly viewed as a spin-1 analogue of the RVB state where valence bonds are now represented by spin-one *triplets*.

We use the mean field approach, which is argued to be stable as the U(1) gauge field acquires mass due to the pairing of spinons, to deduce the physical properties of the $d+\mathrm{i}d$ paired spin liquid ground state. This state on one hand, possesses a gapless Fermi surface of spinons, which corresponds to nematic excitations, and dominates the heat capacity. On the other hand, the spin excitations are gapped, resulting in highly anisotropic spin susceptibility and a vanishing NMR relaxation rate. Finally, this state is predicted to have gapless edge modes carrying $S = 1$ quantum numbers and leading to a quantized spin Hall response.

Finally, we study the phase diagram of two different spin-1 models on a triangular lattice using the variational Monte Carlo (VMC) approach. Even though mean-field suggests a realization of the $d + \mathrm{i}d$ quantum spin liquid state in the analogue of Heisenberg model for spin-1, the more reliable VMC approach reveals a prevalence

of ordered states. However, a more complicated Hamiltonian which contains ring-exchange terms for spin-1, has a region of the phase diagram where the $d + id$ paired quantum spin liquid is a ground state.

1.4.2 Kondo physics in U(1) $S = 1$ spin liquid

Motivated by the results of Chapter 2, where we considered a $S = 1$ spin liquid state with pairing, in Chapter 3 we address physical properties of the $S = 1$ spin liquid without spinon pairing. Such a state has a U(1) gauge field strongly coupled to three fermionic species of spinons with a Fermi surface. Properties of non-Fermi-liquid (NFL) behavior induced by the gauge field coupled to fermions with a Fermi surface were a subject of intense study, as a similar problem arises in a variety of contexts [38–46].

In Chapter 3 we consider a spin-1/2 impurity embedded into $S = 1$ U(1) spin liquid state. This problems is interesting as another realization of overscreened Kondo physics: the spinons that carry spin-1 quantum numbers fail to screen the spin-1/2 impurity, leading to an NFL fixed point. However, even more intriguing is how this overscreened NFL fixed point is influenced by the presence of the U(1) gauge field, which itself leads to non-Fermi-liquid behavior.

Using a recently developed method of double expansion [45], we address how the presence of gauge field influences the NFL fixed point. Extrapolating the results of our calculations to the physical case, we discover that softening of quasiparticles due to the gauge field reduces singular exponents associated with an overscreened Kondo fixed point. Therefore, overscreened Kondo physics may serve not only as a probe of fermionic spinons with a Fermi surface, but also indicate the presence of the gauge field.

1.4.3 Spinon-phonon interactions in algebraic spin liquid

The last Chapter of this thesis, Chapter 4 studies lattice vibrations as another probe of spinons. However, contrary to previous chapters, where we address spin-1 systems,

the subject of the last Chapter is spin-1/2 spin liquid. To be more precise, we study algebraic spin liquids, where low-energy excitations are spinons with Dirac dispersion, coupled to a U(1) gauge field.

The interaction of spinons with phonons was considered for spinons with Fermi surface in Ref. [47], where a universal form of interaction was discovered. However, the treatment of Ref. [47] does not apply to the Dirac spin liquid. In Chapter 4 we demonstrate that the case of the Dirac spin liquid is drastically different from the spinons with Fermi surface.

Considering different algebraic spin liquids that have identical low-energy description in terms of U(1) gauge field and spinons with Dirac dispersion, we show that spinon-phonon interaction "remembers" the microscopic structure of the algebraic spin liquid. Intuitively, this happens because the spinor structure of Dirac particles is tied to microscopic details of the underlying lattice. More precisely, the form of the spinon-phonon interaction Hamiltonian is dictated by the specific representation of the projective symmetry group. Therefore, the spinon-phonon interaction is potentially capable of distinguishing between different types of spin liquids which are very difficult to tell otherwise.

Using the explicit form of spinon-phonon interactions, we calculate the attenuation of ultrasound from interaction with spinons. In this calculation, the presence of the gauge field plays an important role, by canceling the leading order contribution which does not depend on the projective symmetry group. Thus, we conclude that the spinon-phonon interaction can probe not only the presence of spinons, but also certain details of the underlying projective symmetry group. Finally, the symmetry classification presented in Chapter 4 may be useful for deducing coupling of other probes to the spinons.

1.5 Mean field: challenges and perspectives

The results of this thesis, summarized above address different aspects of spin liquid physics. In particular, we suggested a novel spin liquid ground state for spin-1 sys-

tems, and considered impurity physics and interaction with lattice vibrations as a probes of spin liquid physics. For all of these, a mean field approach to a spin liquid, and its extensions, were a key ingredient. Moreover, despite immense progress in developing novel numerical methods, the mean field approach still remains relevant. Rather than superseding it, the recent theoretical and experimental developments present a new challenges for the mean field approach.

One such question is inspired by numerics. Novel numerical methods like density-matrix renormalization group (DMRG) [14, 15] as well as different modifications of variational Monte Carlo enables access to ground states of specific spin models for unprecedented systems sizes. However, these novel numerical methods are similar to an experiment in that one has to interpret their results using some framework. At this point one often resorts to the mean field approach, as it is able to provide clear physical intuition, and a framework to understand the numerics. The open challenge is to go beyond and use mean field to further guide numerics, and suggest ingredients relevant for stabilizing given phases, or driving towards new states.

Another challenge for the phenomenological-type of mean field approach is coming from experiments. Most of the experimental spin liquid candidates are "contaminated" by additional ingredients that are beyond simple theoretical models. Very often these are either some type of disorder or weak additional interactions. While incorporating these ingredients into numerics may seem intractable, one can possibly address these ingredients within a mean field approach. Also, mean field and its extension with gauge fluctuations can be potentially useful for attempting to describe an extensive amount of data obtained from neutron scattering experiments on spin liquid candidates.

While the identification of spin liquid materials remains the current challenge for the field of spin liquids, the theory and experiment are moving at a fast pace towards its resolution, with a mean field approach playing an important role. An end to the drought of quantum spin liquids [48] will hopefully bring new states of matter to the laboratory and reveal many more interesting and exciting phenomena to study.

Chapter 2

$S = 1$ spin liquid on a triangular lattice

In this Chapter we investigate possible quantum spin liquid ground states in Heisenberg-type models for $S = 1$ on triangular lattice. We start with a brief introduction, where we outline experimental motivation behind our studies, introduce Hamiltonians and fermionic representation of a spin. After this, we study the phase diagram of bilinear-biquadratic Heisenberg Hamiltonian within a mean field approximation [1]. Next, in Section 2.3 we use the projection to compare energy of different competing ground states for bilinear-biquadratic Heisenberg and ring exchange models [2]. Finally, Section 2.4 consider physical properties of the spin liquid state with $d + id$ pairing of spinons. We conclude with discussion of open questions and prospective directions in Section 2.5.

2.1 Introduction

2.1.1 Motivation

As we discussed in the Chapter 1, spin liquid is a long sought exotic state of matter, where long range magnetic order is destroyed by quantum fluctuations at zero temperature. A number of materials have been discovered which are promising can-

didates for $S = 1/2$ spin liquid state [26, 28, 30, 48]. Spin systems with higher values of spin, however, usually show a strong tendency towards long-range ordering and lattice-symmetry breaking at low temperature. It is therefore not surprising that spin-liquid candidates for higher values of spin have been more scarce to find.

More recently, possible spin liquid materials with $S = 1$ have been discussed. One example is the insulating spin-1 quantum magnet on a triangular lattice, $NiGa_2S_4$, reported by Nakatsuji *et al* [31]. This material motivated a number of theoretical papers proposing different microscopic realizations of $S = 1$ spin liquid [33–37]. Another example is a two-dimensional triangular magnet $Ba_3NiSb_2O_9$ [32] produced via high pressure synthesis. This material has two new high-pressure phases which possibly realize two and three-dimensional $S = 1$ spin liquid.

In particular the 6H-B phase, described as a triangular lattice of $S = 1$ Ni^{2+} ions, shows no magnetic ordering down to $T = 350$ mK, well below the Curie-Weiss temperature scale $\theta_{CW} = -75.5$ K. Such behavior combined with the frustration of triangular lattice suggests a possibility of spin liquid phase. The spin susceptibility saturates to a constant at low temperatures; specific heat is linear in temperature over over a wide range, $T = 0.35 - 7$ K, with high coefficient and Wilson ratio $R_W = 5.6$. Such observations are highly unusual for a magnetic insulator and point to a spin liquid with *gapless fermionic excitations*. Indeed, the only other example where such behavior has been seen is the organic $S = 1/2$ spin liquid system [48]. Quantum fluctuations are less important for $S = 1$, making these data even more striking.

2.1.2 Possible spin liquid states with a Fermi surface

Experimental data discussed above motivates us to think about possibility of spin liquid states with phenomenology which would be consistent with the discussed experiment. In view of the evidence for gapless fermionic excitations, the framework of spin liquids where spin is fractionalized into fermions seems to be the most natural way to address the above question. However, even within this framework, finding a state consistent with experiment is a non-trivial problem. For example a Fermi surface of neutral spin-carrying excitations is strongly coupled to a $U(1)$ gauge field [49, 50],

and the specific heat is expected to behave as $T^{2/3}$. On the other hand paired spin liquid states in the absence of impurities will typically have $C/T \to 0$ in the $T \to 0$ limit.

Below we propose a new candidate spin liquid ground state with a Fermi surface coexisting with fermion pairing which gaps out the gauge field. We use the minimal number of spinons required to represent spin $S = 1$, that is equal to *three* [35,36]. The basis of this three-fermion representation allows to obtain an exotic quantum spin liquid state that reproduces the phenomenology of the experiment on $Ba_3NiSb_2O_9$ [32].

Our state is not the only one consistent with the experiment, as several alternative theoretical scenarios have been proposed in references [51, 52]. In particular, Ref. [51], uses a representation of the spin $S = 1$ operator in terms of *four* flavors of fermionic spinons and studies possible spin liquid states at the mean field level. Such a fractionalization into four spinon flavors is most natural in the case of a two-orbital Hubbard model with not too strong interactions (Hund coupling) between the electrons. Another proposal not involving spin-liquid states is discussed in Ref. [52], where inter-layer couplings between the Ni^{2+} spins tune the system to a quantum critical point.

Currently, the details of the effective spin model describing $Ba_3NiSb_2O_9$ are not known. Therefore, we do not attempt to propose a realistic microscopic spin model for this material. Instead, we investigate two families of promising antiferromagnetic triangular-lattice spin-one models. The aim is to determine whether, at the mean field level (Section 2.2), or, variationally (Section 2.3), the natural quantum spin-liquid candidates (involving three spinon flavors) have a chance to win over long-range ordered ground states in these microscopic models.

2.1.3 Models

Here we introduce the bilinear-biquadratic Heisenberg model with single-ion anisotropy term, and, as its extension, an SU(3) symmetric model with three-site ring-exchange terms. These models will be studied in what follows using mean-field and projection.

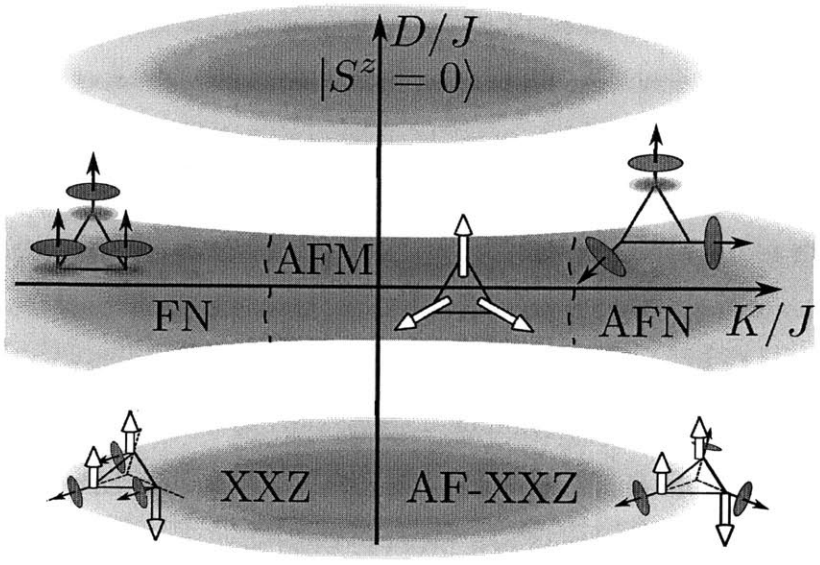

Figure 2-1: Schematic representation of the ground state in different limits of the Hamiltonian (2.1). White arrows represent average spin; arrows with discs indicate the director of the nematic order parameter. Details are discussed in the text.

Bilinear-biquadratic Heisenberg model

The bilinear-biquadratic Heisenberg model consists of quantum $S = 1$ spins forming a triangular lattice. For simplicity, we consider only nearest neighbor interactions. The general form of Hamiltonian can be written as

$$H_{KD} = \sum_{\langle ij \rangle} [J\vec{S}_i \cdot \vec{S}_j + K(\vec{S}_i \cdot \vec{S}_j)^2] + D\sum_i (S_i^z)^2, \tag{2.1}$$

where we included Heisenberg exchange interaction with coupling $J > 0$ and bi-quadratic exchange with coupling K. In addition we allow easy-plane or easy-axis type of anisotropy controlled by the parameter D, but we neglect this anisotropy in the couplings J and K since it is presumably small for transition metals. The Hamiltonian (2.1) has been considered in the literature in limits when the anisotropy is either zero or dominates over other couplings, or there are longer range competing exchange couplings. Fig. 2-1 summarizes known results for the ground state (GS) phase diagram in a schematic way. There are three different phases on the line of zero anisotropy $D = 0$ [53–56]:

1. In the range $K = -0.4J \ldots J$ GS is 120°-degree antiferromagnet (AFM).

2. For larger negative K system favors collinear ferro-nematic (FN) order, *i.e.* nematic order that does not break lattice translational symmetry. In this state the average spin vanishes $\langle \vec{S} \rangle = 0$, but full spin rotation symmetry is broken down to rotations around an axis specified by the director vector $\boldsymbol{d}$ (see Refs. [54, 55] and discussion below).

3. For positive $K > J$ the ground state is described by aniferro-nematic (AFN) order. In this state director vectors $\boldsymbol{d_i}$ on three different sublattices are orthogonal to each other (see Fig. 2-1), thus breaking lattice translation symmetry.

In addition, the ground state is understood in the limits of large positive (easy-plane) and negative (easy-axis) anisotropy, D. In the extreme case of easy-plane anisotropy ($D \gg J, |K|$), the GS is a trivial product of states of $|S^z = 0\rangle$ on all sites, corresponding to the trivial single-site FN order.

For large but negative D, implying extreme easy axis anisotropy, only two states with $S^z = \pm 1$ on each site survive. This system can be described by a spin-1/2 XXZ model with all exchange couplings being antiferromagnetic if $2J > K > 0$ or with J^z being frustrating and $J^\perp$ ferromagnetic if $K < 0$. In both cases there is spin density wave ordering of the z-component of the spin in the GS, supplemented by planar AFN order in former and collinear nematic order in the latter case [57].

In what follows we study the phase diagram of Hamiltonian (2.1) for both signs of D and K but will assume $|D|, |K| < J$. Except of very small $|D|$, this is outside of the regions of known GS's shown in Fig. 2-1.

SU(3) ring-exchange model

To motivate our second choice of the spin-one model, let us consider an SU(3) symmetric Hubbard model for three flavors of fermions f_a,

$$H_{SU(3)} = -t \sum_{\langle i,j \rangle} f^\dagger_{ai} f_{aj} + U \sum_j n_j^2 , \tag{2.2}$$

where $n_j = \sum_a n_{aj} = \sum_a f^\dagger_{aj} f_{aj}$. Let us consider the case when each flavor is at 1/3-filling ($\sum_j n_{aj}/N = 1/3$). For $U \gg |t|$, the low-energy subspace of this model corresponds to the spin-one Hilbert space. Similar to Refs. [58,59], we can derive a low-energy effective spin-one Hamiltonian for (2.2). To lowest order in t, we find the exchange term

$$\sum_{\langle i,j \rangle} f^\dagger_{ai} f_{bi} f^\dagger_{bj} f_{aj} \,. \tag{2.3}$$

To next order, the following three-site term is expected to arise:

$$\sum_{\langle i,j,k \rangle} \{ f^\dagger_{ai} f_{bi} f^\dagger_{bj} f_{cj} f^\dagger_{ck} f_{ak} + \text{h.c.} \} \,, \tag{2.4}$$

where the sum $\langle i,j,k \rangle$ is over elementary triangles of the lattice. Let us write the flavor exchange operators in (2.3) as $\mathcal{P}_{ij} = \sum_{ab} f^\dagger_{ai} f_{bi} f^\dagger_{bj} f_{aj}$. The three-site terms in (2.4) correspond to $\mathcal{P}_{ij}\mathcal{P}_{jk} + \mathcal{P}_{jk}\mathcal{P}_{ij}$. These operators move the local states clock- and anticlockwise around the triangles of the lattice.

In the case of a similar Hubbard model with *two* fermion flavors (spin $S = 1/2$), the exchange operator $\mathcal{P}_{ij}$ appearing in the low-energy model corresponds to the Heisenberg term in spin language, $\mathcal{P}_{ij} = 2\vec{S}_i \cdot \vec{S}_j + 1/2$. In this case, a three-site term $\mathcal{P}_{ij}\mathcal{P}_{jk} + \text{h.c.}$ is trivial in the sense that it can be reduced to a sum of two-site terms. For three flavors, however, the situation is different. In that case and spin $S = 1$, one finds [60]:

$$\mathcal{P}_{ij} = \vec{S}_i \cdot \vec{S}_j + (\vec{S}_i \cdot \vec{S}_j)^2 - 1 \,. \tag{2.5}$$

Therefore, the lowest-order term (2.3) corresponds to the bilinear-biquadratic model (2.1) with $K = 1$ and $D = 0$. The next-order ring-exchange term (2.4) is a nontrivial perturbation since it cannot be reduced to two-site terms. Ring-exchange models for spin 1/2 with nontrivial four-site plaquette terms [61] are believed to exhibit spin-liquid ground states [49,62,63].

Motivated by the three-flavor Hubbard model, we propose to study the SU(3)

symmetric ring-exchange model,

$$H_\alpha = \cos\alpha \sum_{\langle i,j\rangle} \mathcal{P}_{ij} + \sin\alpha \sum_{\langle i,j,k\rangle} \{\mathcal{P}_{ij}\mathcal{P}_{jk} + \text{h.c.}\}\,. \tag{2.6}$$

The sum in (2.6) goes over nearest-neighbor links $\langle i,j\rangle$ and elementary triangles $\langle i,j,k\rangle$ of the lattice. The parameter of this model is $\alpha \in [-\pi,\pi]$.

The mean field analysis of the ring exchange Hamiltonian (2.6), reveals the same ordering patterns as we found in the case of the KD-model. Indeed, using uncorrelated three-sublattice product states, one gets a ferromagnetic phase in the parameter range $\alpha < -\arctan(3/4) \simeq -0.2\pi$ and $\alpha > \pi - \arctan(1/2) \simeq 0.85\pi$. Any uniform product state $\prod_j |a\rangle_j$ is an exact eigenstate with energy $\epsilon(\alpha) = 3\cos\alpha + 4\sin\alpha$, and it is the lowest-energy three-sublattice product state in this parameter range. For $-\arctan(3/4) < \alpha < \arctan(3/2) \simeq 0.31\pi$ the 120° antiferromagnetic product state is stabilized. Finally, in the range $\arctan(3/2) < \alpha < \pi - \arctan(1/2)$, the antiferronematic order develops, with three nematic directors order in a common plane at an angle of 120° to each other on nearest-neighbor sites (see also Fig. 2-5).

2.1.4 Representation of spin-1 via fermionic spinons

Below we consider *fermionic* quantum spin liquid wave functions for spin $S = 1$. The most straightforward route to such states is to decompose spin operator in terms of fermionic spinons, as we discussed in Section 1.3. Below we outline the basic details of the mean field construction for spin-1.

To construct spin liquid states for spin $S = 1$, we follow an approach similar to Ref. [36]. We write the spin operators in terms of three flavors of fermionic spinons, f_a, in the following way:

$$S_a = -\mathrm{i}\varepsilon_{abc} f_b^\dagger f_c\,, \tag{2.7}$$

where $a \in \{x,y,z\}$, and repeated indices are always summed over in what follows. We choose to work with operators f_a that create spin states $|a\rangle$ in the time-reversal

invariant basis, i.e.,

$$\begin{aligned} |x\rangle &= \frac{1}{\sqrt{2}}(|1\rangle + |\bar{1}\rangle), \\ |y\rangle &= \frac{\mathrm{i}}{\sqrt{2}}(|1\rangle - |\bar{1}\rangle), \\ |z\rangle &= -\mathrm{i}|0\rangle\,, \end{aligned} \tag{2.8}$$

where $|1\rangle$, $|\bar{1}\rangle$, and $|0\rangle$ are S_z-eigenstates with eigenvalues ± 1 and 0, respectively.

By representing spin in terms of fermions, we have enlarged the Hilbert space. The fermion operators act in the eight-dimensional Fock space while the original spin space is three dimensional. In order to recover the physical subspace, a local constraint on the fermionic occupation number has to be enforced,

$$n = \sum_a f_a^\dagger f_a \equiv N_f\,. \tag{2.9}$$

Both particle ($N_f = 1$) or hole ($N_f = 2$) subspaces can be chosen, in contrast to the case of $S = 1/2$, where we had a single choice. Nevertheless, they can be mapped into each other by particle-hole transformation discussed below, supplemented by a change of the sign of hopping. Therefore we consider only particle representation but do not restrict hopping to be positive to include the hole representation[1].

The spin operator remains invariant under the following transformations of the fermionic operators

$$f_a \mapsto e^{\mathrm{i}\phi} f_a \tag{2.10}$$

and

$$f_a \mapsto f_a^\dagger\,. \tag{2.11}$$

Equation (2.11) is a *particle-hole* transformation and the constraint (2.9) is changed according to $N_f \mapsto 3 - N_f$. Hence, the local symmetry group for this representation of spin $S = 1$ operators is the semi–direct product $\mathrm{U}(1) \rtimes \mathbb{Z}_2$ [36].

[1]This is different from Ref. [35], where authors use combination of particle and hole constraints in order to preserve particle-hole symmetry. Our treatment violates particle-hole symmetry from the very beginning.

In the time-reversal-invariant basis (2.8), the quadrupolar operators, defined as

$$Q_{ab} = (S_a S_b + S_b S_a)/2 - 2/3\,\delta_{ab}, \tag{2.12}$$

acquire a particularly simple form [64]. In the particle representation ($N_f = 1$), we have

$$S_a S_b = \delta_{ab} - f_a^\dagger f_b\,, \qquad Q_{ab} = \delta_{ab}/3 - (f_a^\dagger f_b + f_b^\dagger f_a)/2. \tag{2.13}$$

2.2 Mean-field treatment of bilinear-biquadratic Heisenberg model

Here we analyze a bilinear-biquadratic Heisenberg spin Hamiltonian, Eq. (2.1) using mean field treatment. Although the phase diagram obtained within this section will be superseded by the phase diagram resulting from variational Monte Carlo approach, Section 2.3, we will use the formalism developed here to address the physical properties of the $d + \mathrm{i}d$ paired spin liquid state.

2.2.1 Expressing Hamiltonian via fermionic operators

We employ representation (2.7) to express Hamiltonian, Eq. (2.1) via fermionic operators. The bilinear term is expressed via fermions as

$$\vec{S}_i \cdot \vec{S}_j = (\vec{f}_i^\dagger \cdot \vec{f}_j^\dagger)(\vec{f}_i \cdot \vec{f}_j) + \vec{f}_i^\dagger (\vec{f}_i \cdot \vec{f}_j^\dagger)\vec{f}_j, \tag{2.14}$$

where we introduced a short-hand vector notation $\vec{f} = (f_x, f_y, f_z)$ and $\vec{f}_i \cdot \vec{f}_j$ denotes the scalar product. Using the constraint, which in new notations becomes $\vec{f}_i^\dagger \cdot \vec{f}_i = 1$, the biquadratic term also can be expressed as a product of four fermion operators [53],

$$(\vec{S}_i \cdot \vec{S}_j)^2 = 1 - (\vec{f}_i^\dagger \cdot \vec{f}_j^\dagger)(\vec{f}_i \cdot \vec{f}_j). \tag{2.15}$$

Adding a Lagrange multiplier μ to enforce the single occupancy constraint (2.9) on average, we have

$$H = \sum_{\langle ij \rangle} [J \vec{f}_i^\dagger (\vec{f}_i \cdot \vec{f}_j^\dagger) \vec{f}_j + (J-K)(\vec{f}_i^\dagger \cdot \vec{f}_j^\dagger)(\vec{f}_i \cdot \vec{f}_j) + K] + \sum_i [\mu(1 - \vec{f}_i^\dagger \cdot \vec{f}_i) + D(1 - f_{iz}^\dagger f_{iz})]. \quad (2.16)$$

2.2.2 Mean field equations from variational principle

Having expressed the Hamiltonian via fermion operators we study the mean field phase diagram of our model. To unambiguously decouple quartic fermion terms, we use the Feynman variational principle [65, 66] which is equivalent to the trial wave functions approach. We define an action based on the Hamiltonian (2.16),

$$S = \int_0^\beta d\tau \left[\sum_i f_{ai}^\dagger (\partial_\tau - \mu) f_{ai} + H \right], \quad (2.17)$$

as well as the trial quadratic action, $\tilde{S}$, with the Hamiltonian H, which is quartic in fermionic operators, replaced by $\tilde{H}$ that is quadratic:

$$\tilde{H} = \sum_{\langle ij \rangle} [\vec{f}_i^\dagger T_{ij} \vec{f}_j + \vec{f}_i^\dagger A_{ij} \vec{f}_j^\dagger + \text{H.c.}] + \sum_i \vec{f}_i^\dagger t_i \vec{f}_i. \quad (2.18)$$

The mean field parameters T_{ij}, A_{ij}, and t_i are determined from the stationary points of the functional $\Psi[\tilde{S}] = \langle S - \tilde{S} \rangle_{\tilde{S}} - \log \tilde{Z}$,

$$\begin{aligned} T_{ij}^{ab} &= -J\, \delta_{ab} \langle f_{jc}^\dagger f_{ic} \rangle + (J-K) \langle f_{ja}^\dagger f_{ib} \rangle, \\ A_{ij}^{ab} &= -J \langle f_{ib} f_{ja} \rangle + (J-K)\, \delta_{ab} \langle f_{ic} f_{jc} \rangle, \\ t_i^{ab} &= \sum_{\langle ij \rangle} [J \langle f_{jb}^\dagger f_{ja} \rangle - (J-K) \langle f_{ja}^\dagger f_{jb} \rangle] - D \delta_{ab} \delta_{az}. \end{aligned}$$

At zero temperature, $T = 0$, we get the estimate for the ground state energy, $E_{\text{g.s.}} \leq \tilde{E}_{\text{g.s.}} = \langle H \rangle_{\tilde{G}}$, where

$$\tilde{E}_{\text{g.s.}} = \sum_{\langle ij \rangle} [T_{ij}^{ab} \langle f_{ia}^{\dagger} f_{jb} \rangle + A_{ij}^{ab} \langle f_{ia}^{\dagger} f_{jb}^{\dagger} \rangle] + \frac{1}{2} \sum_{i} [t_i^{ab} \langle f_{ia}^{\dagger} f_{ib} \rangle - D \langle f_{iz}^{\dagger} f_{iz} \rangle + 6K + 2D]. \quad (2.20)$$

We search for self-consistent solutions to the mean field equations that do not break any additional symmetries other than $\mathcal{T}$-reversal. When the full spin rotation symmetry is present, the only possible pairing order parameter is $\Delta_{\text{s}} \sim \langle \vec{f}_i \cdot \vec{f}_j \rangle$. Such pairing preserves full rotational symmetry in spin space, the resulting state being a spin singlet. We call this pairing singlet, since the total spin of the cooper pairs is zero (see below). Singlet pairing is possible only with odd orbital momentum of the cooper pairs, *i.e.* p, f-wave pairing. Since in Hamiltonian (2.1), only *in-plane* rotational symmetry is present for $D \neq 0$, the triplet pairing with order parameter $\Delta_{\text{t}} \sim \langle (\vec{f}_i \times \vec{f}_j)_z \rangle = \langle f_{ix} f_{jy} - f_{iy} f_{jx} \rangle$ is allowed. However, the presence of two order parameters simultaneously violates the symmetry with respect to rotations of π around the x or y axis.

Both aforementioned types of pairing were considered by Liu *et al.* [36] in a similar system, however without anisotropy but with competing third nearest neighbor J. Their treatment of biquadratic exchange also differs from ours. The result of [36] was that singlet pairing always wins. Below, after discussing different types of pairing and their symmetry, we derive the mean field equations for each type of pairing. In Section 2.2.6 we identify the region in phase space where triplet pairing has lower energy within mean field. This result does not survive more rigorous treatment using Gutzwiller projection. However, later, in Section 2.3, we find a region of the phase diagram for the SU(3) spin model, where the triplet pairing has the lowest energy among all considered states.

2.2.3 Different pairings and their symmetry properties

Using notation $\Delta_{ij}^{ab} = \langle f_{ai} f_{bj} \rangle$, two types of pairing discussed above are written as

(i) equal-flavor singlet pairing where $\Delta_{ij}^{zz} \neq 0$, $\Delta_{ij}^{xx} = \Delta_{ij}^{yy} \neq 0$, $\Delta_{ij}^{ab} = 0$ otherwise.

(ii) x-y triplet pairing: $\Delta_{ij}^{xy} = -\Delta_{ij}^{yx} \neq 0$, $\Delta_{ij}^{ab} = 0$ otherwise.

On the one hand, for $\Delta_{ij}^{xx} = \Delta_{ij}^{yy} = \Delta_{ij}^{zz}$, equal-flavor pairing (i) corresponds to spin-one *singlet* pairing. The pairing term $\Delta_{ij}^{ab} f_{ai}^{\dagger} f_{bj}^{\dagger}$ creates a state $(\vec{f}_i^{\dagger} \cdot \vec{f}_j^{\dagger})|\bar{0}\rangle$ that is invariant under spin rotation; hence, it is a singlet. In general, for $\Delta_{ij}^{xx} = \Delta_{ij}^{yy} \neq \Delta_{ij}^{zz}$, the state is not an eigenstate of $(\vec{S}_{ij}^{\rm tot})^2 = (\vec{S}_i + \vec{S}_j)^2$. However, for $\Delta_{ij}^{xx} = \Delta_{ij}^{yy} = -\Delta_{ij}^{zz}/2$ one can check that $(\vec{S}_{ij}^{\rm tot})^2 = 6$; therefore, this bond operator creates a spin-one *quintuplet.*

On the other hand, the x-y pairing bond operator $\Delta_{ij}^{ab} f_{ai}^{\dagger} f_{bj}^{\dagger}$, (ii), creates a spin-one *triplet.* To see this, let us denote the state created by such operator as

$$|1\rangle_{ij} = (|xy\rangle_{ij} - |yx\rangle_{ij}) \propto (|1\bar{1}\rangle_{ij} - |\bar{1}1\rangle_{ij}).$$

Since $(\vec{S}_{ij}^{\rm tot})^2 = 4 + 2\vec{S}_i \cdot \vec{S}_j$, and $[\vec{S}_i \cdot \vec{S}_j + 1]|1\rangle_{ij} = 0$, we have the expectation value

$${}_{ij}\langle 1|(\vec{S}_{ij}^{\rm tot})^2|1\rangle_{ij} = 2,$$

which corresponds to a triplet state.

Due to the anticommuting spinon operators, the pairing parameters Δ_{ij}^{ab} must have particular symmetry properties under inversion of the link direction $\langle i, j \rangle$: For equal-flavor pairing (i), we have $\Delta_{ij}^{aa} = -\Delta_{ji}^{aa}$; i.e., the pairing is *odd* under space inversion, e.g. it can have only odd orbital momenta (p-wave, f-wave,...). For x-y pairing (iii), we have $\Delta_{ij}^{xy} = \Delta_{ji}^{xy}$; *i.e.*, the pairing is *even* under space inversion and requires the orbital momentum of cooper pair to be even (s, d-wave,...). This is in contrast to $S = 1/2$ spin liquids, where singlet pairing is even while triplet pairing is odd under space inversion.

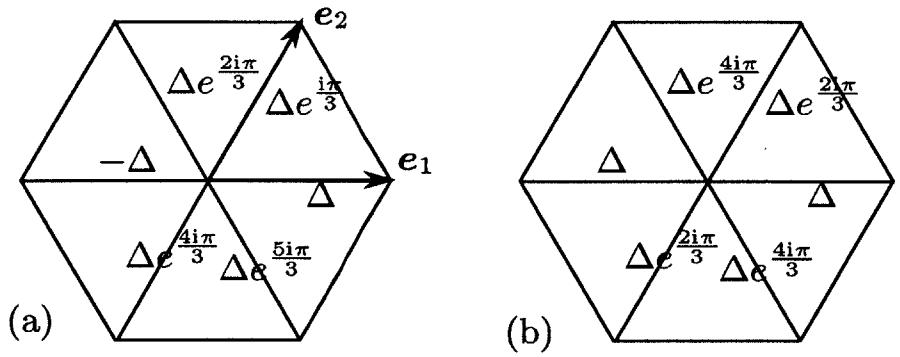

Figure 2-2: Relative phase of the nearest neighbor pairing for $p + ip$-wave (a) and $d + id$ wave pairing (b) correspondingly. $\boldsymbol{e}_1$ and $\boldsymbol{e}_2$ are basis vectors of triangular lattice.

Angular momentum of the pairing specifies the phases of the order parameter on different links of the lattice. Denoting nearest-neighbor links of the triangular lattice by $\boldsymbol{e}_1 = (1, 0)$, and $\boldsymbol{e}_2, \boldsymbol{e}_2 = (\pm 1, \sqrt{3})/2$, we can write explicit form of order parameter for singlet pairing (i), which can happen with p or f-wave orbital momentum. In particular, $p_x + ip_y$-wave $(p + ip)$ pairing corresponds to [see Fig. 2-2(a)]

$$\Delta^{aa}_{\boldsymbol{e}_1} = \Delta^{aa}_{\boldsymbol{e}_2} e^{i\pi/3} = \Delta^{aa}_{\boldsymbol{e}_3} e^{i2\pi/3},$$

whereas real f-wave pairing implies

$$\Delta^{aa}_{\boldsymbol{e}_1} = -\Delta^{aa}_{\boldsymbol{e}_2} = \Delta^{aa}_{\boldsymbol{e}_3}.$$

Note, that real p, d-wave pairings break lattice symmetry and are not considered.

For triplet x-y pairing (ii), the possible pairing symmetries are extended s-wave

$$\Delta^{xy}_{\boldsymbol{e}_1} = \Delta^{xy}_{\boldsymbol{e}_2} = \Delta^{xy}_{\boldsymbol{e}_3},$$

and $d_x + id_y$-wave $(d + id)$ with [Fig 2-2(b)]

$$\Delta^{xy}_{\boldsymbol{e}_1} = \Delta^{xy}_{\boldsymbol{e}_2} e^{i2\pi/3} = \Delta^{xy}_{\boldsymbol{e}_3} e^{i4\pi/3}.$$

Higher angular momenta would require spinon pairing between farther-neighbor sites, which we choose to exclude from the present study.[2]

Symmetry of the quantum spin liquid states (2.29) under lattice rotations forbids mixing of different types of pairing symmetries in the Hamiltonian (2.28). For example, lattice rotation symmetry is broken in a state where the f_z spinon is paired with f-wave, and f_x, f_y are paired with $p+ip$ pairing symmetry. Similarly, in the x-y paired quantum spin liquid (ii), f_z must remain unpaired unless lattice rotation symmetries are broken. The reason is the following: After performing a lattice rotation on the mean-field Hamiltonian (2.28), one would like to find a gauge transformation (2.10) that brings it back to the original form. If such a gauge transformation exists, then the corresponding spin wave function (2.29) is unchanged by the rotation (provided the single occupancy constraint is fulfilled, and up to a phase). However, since all three spinon flavors transform with the same U(1) phase, such a gauge transformation [22] can only exist when all spinon flavors have identical pairing symmetries.[3]

The quantum spin liquid states with extended s-wave and f-wave states respect parity P (reflection on a symmetry axis of the lattice) and time-reversal symmetry Θ. The $p+ip$ and the $d+id$ states, however, break both P and Θ, but conserve the product ΘP. In this sense, they can be termed chiral spin liquids [67], albeit for spin $S=1$. The $p+ip$ state is fully gapped and, therefore, a conventional topological state of matter. The $d+id$ state, on the other hand, represents a new class of paired chiral states in two dimensions that exhibit both P- and Θ-symmetry breaking *and* a gapless bulk Fermi surface at the same time. These exotic properties will be discussed in more detail in Section 2.4.

[2]The case of x-y pairing also allows for *on-site* s-wave pairing with a term $\Delta^{xy} f^\dagger_{xj} f^\dagger_{yj}$. However, we found that such a pairing term does not gain any variational energy in the models we consider.

[3]In this work, we also considered quantum spin liquid wave functions with mixed pairing symmetries, *i.e.*, states that break lattice rotation symmetry. However, we find that such quantum spin liquid states are always higher in energy than the rotation-invariant quantum spin liquid states for the models we consider.

2.2.4 Mean field equations for singlet pairing

We introduce the mean field parameters χ^a, n^a, and $\Delta_{\rm s}^a$, $a = x, y, z$ defined as

$$\chi^a = \langle f_{ia}^\dagger f_{i+e_1 a}\rangle, \quad n^a = \langle f_{ia}^\dagger f_{ia}\rangle, \quad \Delta_{\rm s}^a = \langle f_{ia} f_{i+e_1 a}\rangle. \tag{2.21}$$

The hopping is the same on all links, whereas the pairings for the remaining two orientations are $\langle f_{ia} f_{i+e_2 a}\rangle = \Delta_{\rm s}^a e^{\frac{i\pi l}{3}}$, $\langle f_{ia} f_{i+e_3 a}\rangle = \Delta_{\rm s}^a e^{\frac{2i\pi l}{3}}$, where the pair angular momentum $l = 1, 2, 3$ for $p + ip$, $d + id$, and f-wave pairing respectively, see Section 2.2.3 and Fig. 2-2 above. Spin rotation symmetry in the xy-plane requires $\chi^x = \chi^y$, $n^x = n^y$, $\Delta_{\rm s}^x = \Delta_{\rm s}^y$. The Hamiltonian in momentum space (modulus non-essential constant terms) can be rewritten as

$$\tilde{H} = \sum_{\boldsymbol{k},a} \chi_{\boldsymbol{k}}^a f_{\boldsymbol{k}a}^\dagger f_{\boldsymbol{k}a} + \Delta_{\boldsymbol{k}}^a f_{\boldsymbol{k}a}^\dagger f_{-\boldsymbol{k}a}^\dagger + \Delta_{\boldsymbol{k}}^{a*} f_{-\boldsymbol{k}a} f_{\boldsymbol{k}a}, \tag{2.22}$$

with mean field parameters

$$\chi_{\boldsymbol{k}}^a = 2\gamma(\boldsymbol{k})[(J-K)\chi^a - J(\chi^x + \chi^y + \chi^z)] + 6Kn^a - \mu - \delta_{a,z}D, \tag{2.23}$$

$$\Delta_{\boldsymbol{k}}^a = \psi(\boldsymbol{k})[(J-K)(\Delta_{\rm s}^x + \Delta_{\rm s}^y + \Delta_{\rm s}^z) - J\Delta_{\rm s}^a]. \tag{2.24}$$

The function $\gamma(\boldsymbol{k})$ is a sum over nearest neighbors, $\gamma(\boldsymbol{k}) = \cos\boldsymbol{k}\cdot\boldsymbol{e}_1 + \cos\boldsymbol{k}\cdot\boldsymbol{e}_2 + \cos\boldsymbol{k}\cdot\boldsymbol{e}_3$.On the other hand, $\psi(\boldsymbol{k})$ depends on the type of pairing under consideration. For $p + ip$-wave and f-wave pairings:

$$\begin{aligned}
\psi^f(\boldsymbol{k}) &= i(\sin\boldsymbol{k}\cdot\boldsymbol{e}_1 - \sin\boldsymbol{k}\cdot\boldsymbol{e}_2 + \sin\boldsymbol{k}\cdot\boldsymbol{e}_3),\\
\psi^{pip}(\boldsymbol{k}) &= i(\sin\boldsymbol{k}\cdot\boldsymbol{e}_1 + e^{i\pi/3}\sin\boldsymbol{k}\cdot\boldsymbol{e}_2 + e^{2i\pi/3}\sin\boldsymbol{k}\cdot\boldsymbol{e}_3).
\end{aligned}$$

Hamiltonian (2.22) is diagonalized with Bogoluybov transformation acting separately on each fermion species. This results in the spectrum $E_{\boldsymbol{k}}^a = \sqrt{(\chi_{\boldsymbol{k}}^a/2)^2 + |\Delta_{\boldsymbol{k}}^a|^2}$, and

mean field equations:

$$\chi^a = \frac{1}{N}\sum_{\boldsymbol{k}} \frac{1}{6}\gamma(\boldsymbol{k})\left[1 - \frac{\chi^a_{\boldsymbol{k}}}{2E^a_{\boldsymbol{k}}}\right], \tag{2.25a}$$

$$\Delta^a_{\rm s} = \frac{1}{N}\sum_{\boldsymbol{k}} \frac{1}{3}\psi^*(\boldsymbol{k})\frac{\Delta^a_{\boldsymbol{k}}}{2E^a_{\boldsymbol{k}}}, \tag{2.25b}$$

$$n^a = \frac{1}{N}\sum_{\boldsymbol{k}} \frac{1}{2}\left[1 - \frac{\chi^a_{\boldsymbol{k}}}{2E^a_{\boldsymbol{k}}}\right], \tag{2.25c}$$

supplemented by the constraint equation $\langle \vec{f}^\dagger_{\boldsymbol{i}} \cdot \vec{f}_{\boldsymbol{i}} \rangle = 1$.

2.2.5 Mean field equations for triplet pairing

For pairing with even orbital momentum hoppings are defined as in (2.21), whereas pairing is $\Delta^{xy}_{\rm t} = 1/2\langle f_{\boldsymbol{i}x} f_{\boldsymbol{i}+\boldsymbol{e}_1 y} - f_{\boldsymbol{i}y} f_{\boldsymbol{i}+\boldsymbol{e}_1 x}\rangle$. The Hamiltonian is:

$$\tilde{H} = \sum_{\boldsymbol{k},a} \chi^a_{\boldsymbol{k}} f^\dagger_{\boldsymbol{k}a} f_{\boldsymbol{k}a} + \Delta^{xy}_{\boldsymbol{k}} f^\dagger_{\boldsymbol{k}x} f^\dagger_{-\boldsymbol{k}y} + \Delta^{xy*}_{\boldsymbol{k}} f_{-\boldsymbol{k}y} f_{\boldsymbol{k}x},$$

with $\chi^a_{\boldsymbol{k}}$ given by Eq. (2.23), and

$$\Delta^{xy}_{\boldsymbol{k}} = 2J\psi(\boldsymbol{k})\Delta^{xy}_{\rm t}. \tag{2.26}$$

Note, that the f_z *band is unpaired and retains its Fermi surface.* We consider s-wave and $d + {\rm i}d$-wave pairings (as we discussed above, d-wave violates lattice symmetry and higher orbital momentum pairing requires inclusion of further neighbors). For the case of s-wave pairing, the function $\psi^s(\boldsymbol{k}) = \gamma(\boldsymbol{k})$. For $d + {\rm i}d$-wave pairing we have $\psi^{did}(\boldsymbol{k}) = \cos \boldsymbol{k}\cdot\boldsymbol{e}_1 + e^{2{\rm i}\pi/3}\cos \boldsymbol{k}\cdot\boldsymbol{e}_2 + e^{-2{\rm i}\pi/3}\cos \boldsymbol{k}\cdot\boldsymbol{e}_3$. The Bogolyubov spectrum is

$$E^x_{\boldsymbol{k}} = E^y_{\boldsymbol{k}} = \sqrt{(\chi^{x,y}_{\boldsymbol{k}})^2 + |\Delta^{xy}_{\boldsymbol{k}}|^2}, \qquad E^z_{\boldsymbol{k}} = \chi^z_{\boldsymbol{k}}. \tag{2.27}$$

Self-consistent mean field equations for x and y-components are given by Eq. (2.25) with the new expressions for the spectrum (2.27) and gap function (2.26). For the z

component we have

$$\chi^z = \frac{1}{N}\sum_{\boldsymbol{k}} \frac{1}{3}\gamma(\boldsymbol{k}) n_F(\chi^z_{\boldsymbol{k}}), \qquad n^z = \frac{1}{N}\sum_{\boldsymbol{k}} n_F(\chi^z_{\boldsymbol{k}}).$$

Our mean field approach includes on-site FN order automatically. The on-site nematic order is described by the order parameter tensor, $Q^{ab} = 1/2\langle \vec{S}^a\vec{S}^b + \vec{S}^b\vec{S}^a\rangle - 2/3\delta^{ab}$. For a single site with $S = 1$ all states with zero average spin $\langle\vec{S}\rangle = 0$ can be characterized by the unit director vector $\boldsymbol{d}$ [54], in the basis defined earlier, $|\boldsymbol{d}\rangle = d_x|x\rangle + d_y|y\rangle + d_z|z\rangle$. For this state Q^{ab} is expressed via $\boldsymbol{d}$ as $Q^{ab} = 1/3\delta_{ab} - d_a d_b$. For example, $\boldsymbol{d}\|\hat{z}$ corresponds to the state $|S^z = 0\rangle$, and the nematic order is diagonal, $Q^{ab} = \mathrm{diag}(1/3, 1/3, -2/3)$. In our model we also have states with vanishing spin order and diagonal on-site nematic order. However, since our ground state is RVB-like with long-range entanglement, Q^{ab} cannot be described by the above simple form. We have to introduce the magnitude q, $Q^{ab} = q(1/3\delta_{ab} - d_a d_b)$. Calculating the nematic order parameter tensor in our model we have $Q^{ab}_i = \delta_{ab}[1/3 - n^a]$, where n^a is the average occupation of corresponding fermion. Since $n^x = n^y$, we have nematic order with $\boldsymbol{d}\|\hat{z}$, with a magnitude given by $q = n^z - n^x$, varying from 1 for $n^z = 1$ (state $|S^z = 0\rangle$) to $-1/2$ for $n^z = 0$. Non-zero anisotropy $D \neq 0$ causes n^a to be different from $1/3$, and therefore directly couples to FN order along the z-axis.

2.2.6 Phase diagram

Having studied the energies of all aforementioned states using Eq. (2.20), we found that, *among spin liquid states,* the main competition is between states with $p + \mathrm{i}p$ and $d + \mathrm{i}d$-wave pairings, all other states being higher in energy. As one increases K, the effective coupling for the odd-channel pairing decreases, whereas for even pairing it remains the same. Finally for $K \approx 0.45J$ singlet pairing wins. The resulting phase diagram is shown in Fig. 2-3. The boundary between two states appears to be weakly dependent on D.

Note, that while obtaining this phase diagram we did not consider any ordered states. Inclusion of such states in the next section shows that the Hamiltonian (2.1)

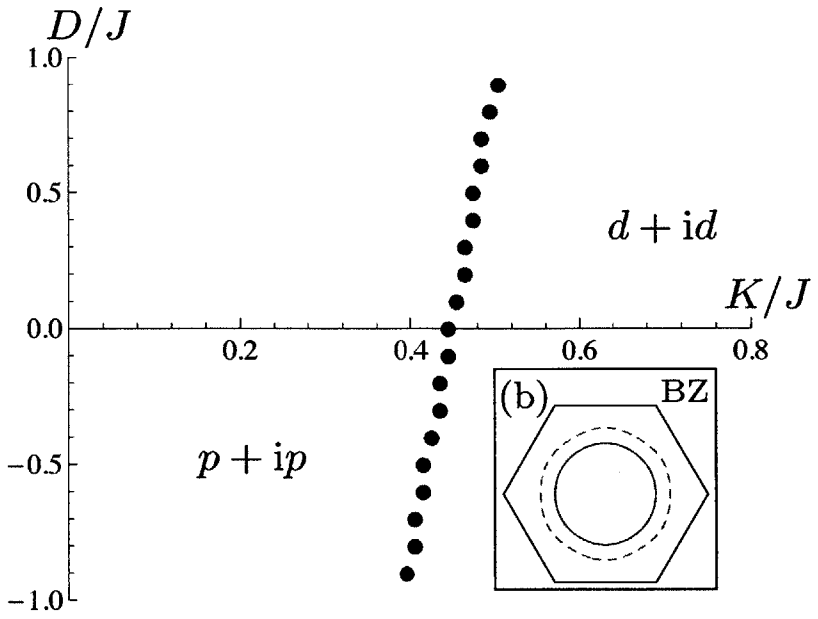

Figure 2-3: The phase boundary between spin liquid ground states with $p + ip$ and $d + id$ pairing. Panel (b) Gapped (dashed red line) and ungapped (blue line) Fermi surfaces of x, y, and z-fermions for $K/J = 0.55$, $D/J = 0.8$.

does not have a spin liquid ground state in the considered range of parameters. However, we do find the $d + id$ paired spin liquid state in more generic SU(3) spin model (2.6).

2.3 Phase diagram from variational Monte-Carlo

In the previous Section we presented mean-field treatment of the bilinear-biquadratic Hamiltonian. This approach relaxes the single-occupancy constraint so that it holds only on average. This procedure enables derivation of a low-energy effective theory for possible spin liquid phases but is generically not reliable for addressing microscopic stability of a particular ground states. Better suited for this purpose is a variational wave function approach, that was discussed in Section 1.3.2.

In this approach, unphysical states are removed by hand from wave functions that correspond to possible low-temperature phases of the theory. Thus, the single-occupancy constraint is fulfilled exactly, and the resulting wave functions are genuine

microscopic variational wave functions for spin-one models. Determining the best variational state for a spin model then provides guiding information about the low-temperature phase of the model. In this Section we present variational results for the phase diagram of Hamiltonians introduced in Eqs. (2.1) and (2.6).

Below we introduce microscopic variational wave functions for spin $S = 1$ on the triangular lattice. First, we describe quantum spin liquid wave functions that do not break the space group symmetries of the lattice. Second, we outline a general approach for constructing competitive long-range ordered states that have an enlarged unit cell. Using these variational functions we determine the phase diagram of both bilinear-biquadratic Heisenberg Hamiltonian, Eq. (2.1), and of the ring exchange model, Eq. (2.6).

2.3.1 Variational wave functions for spin liquid ground states

We again start by writing down quadratic mean field (or "trial") Hamiltonian in terms of the spinon operators,

$$H_{\rm qsl} = \sum_{\langle i,j\rangle} (s f^\dagger_{ai} f_{aj} + \Delta^{ab}_{ij} f_{ai} f_{bj} + \text{h.c.}) - \mu_a \sum_j f^\dagger_{aj} f_{aj} \,. \tag{2.28}$$

The sum $\langle i, j\rangle$ goes over the nearest-neighbor links of the triangular lattice. In this trial Hamiltonian, the emergent gauge fields that would be present in the corresponding low-energy theory are omitted. Particular values for the mean-field parameters $s = \pm 1$, Δ^{ab}_{ij}, and μ_a represent possible low-temperature quantum spin liquid phases. Parameter $s = \pm 1$ corresponds to flux of π or zero through all triangles of the lattice, and implements the change in the sign of hopping which is equivalent to switching between particle and hole representation. Next, we assume unbroken spin-rotation symmetry around the z axis, and we focus on $S^{\rm tot}_z$ eigenstates with $S^{\rm tot}_z = 0$. Note that under spin rotations, $\vec{f}_j = (f_x, f_y, f_z)_j$ transform as real vectors [i.e., $\vec{f}_j$ transform in the adjoint representation of SU(2)]. Furthermore, we restrict ourselves to states

that have a single site per unit cell and that do not break the space group symmetries of the lattice (translations, rotations, and inversion). In this situation, the following cases exhaust the possible quantum spin liquid candidates on the triangular lattice:

(i) Equal-flavor singlet pairing: $\Delta_{ij}^{zz} \neq 0$, $\Delta_{ij}^{xx} = \Delta_{ij}^{yy} \neq 0$, $\Delta_{ij}^{ab} = 0$ otherwise.

(ii) x-y triplet pairing: $\Delta_{ij}^{xy} = -\Delta_{ij}^{yx} \neq 0$, $\Delta_{ij}^{ab} = 0$ otherwise.

(iii) U(1) state: $\Delta_{ij}^{ab} = 0$.

The chemical potentials for x and y fermions are chosen to be identical, $\mu_x = \mu_y$. Other possible pairings Δ_{ij}^{ab} than the ones considered in (i) or (ii) violate our symmetry requirements, see discussion in Section 2.2.3. We also note that although we consider triplet pairing among variational wave functions, the total spin per site for all considered states is small in the thermodynamic limit. We have $\sqrt{\langle(\vec{S}^{\text{tot}})^2\rangle}/N \sim 1/\sqrt{N}$ where N is the number of sites and $\vec{S}^{\text{tot}} = \sum_j \vec{S}_j$.

Let us briefly discuss the intuition behind states (i)-(iii). In the "parent" U(1) spin liquid ($\Delta^{ab} = 0$) state, all three spinon flavors have a Fermi surface. This corresponds to the Coulomb phase of the emergent U(1) gauge theory where the photons are massless. The paired states with $\Delta^{ab} \neq 0$ correspond to "Higgs" phases where the global U(1) symmetry is spontaneously broken and the photon acquires a mass [68]. Among the equal-flavor pairing states, the state with pairing in f-wave channel has gapless nodal points in the spectrum while the $p + ip$ spin liquid is fully gapped. In the x-y paired spin liquid, the spin excitations are gapped. However, the f_z spinons correspond to nematic ($S_z = 0$) excitations which form a gapless Fermi surface and are weakly interacting (and therefore deconfined). We expect the Fermi surface to survive after Gutzwiller projection because the other fermion flavors are gapped and the U(1) gauge field is also gapped due to the Higgs mechanism.

In order to obtain a microscopic variational quantum spin liquid wave function, we take the ground state $|\psi_0\rangle$ of (2.28) and apply the Gutzwiller projector $P_G(n_j = 1)$, enforcing single occupancy on each site and thereby removing unphysical components. In this way we construct a genuine spin-one RVB spin-liquid wave function, generalizing similar approaches to $S = 1/2$ spin liquids [69]. Here, we choose to work in the

microcanonical formalism where the fermion number is held fixed; *i.e.*, we project the wave function to a fixed total number of spinon flavors, $N_a = \sum_j n_{aj}$,

$$|\boldsymbol{N}\rangle = P_{\boldsymbol{N}} P_G (n_j = 1) |\psi_0\rangle \,, \tag{2.29}$$

with $\boldsymbol{N} = (N_x, N_y, N_z)$. Since $N_x = N_y$ (to maintain spin-rotation symmetry around the z-axis) and from the local constraint we have $2N_x + N_z = N$, where N is the number of lattice sites ($N = 12 \times 12$ in most of our calculations). Expectation values in RVB wave functions (2.29) can be calculated numerically within Variational Monte Carlo (VMC) techniques [24]. More technical details on our numerical scheme are given in Appendix A.

The variational parameters we are using for the microscopic quantum spin liquid wave functions are the amplitudes $|\Delta^{ab}|$ for all pairing symmetries discussed above and the chemical potentials μ_x and μ_z. Furthermore, we consider the cases $s = \pm 1$ in (2.28), corresponding to the presence or the absence of π flux through the triangles of the lattice, and effectively switching between particle and hole representations of spin. For the paired states, N_z is used as an additional variational parameter (independent of μ_z; see Appendix A.1 for more details).

2.3.2 Long-range ordered states

In order to make reliable statements about the low-temperature phase of a spin model, the energies of quantum spin liquid wave functions have to be compared with competitive long-range ordered states. We consider natural ordering patterns that are suggested within a simple product-state ansatz (e.g., a 120° magnetic ordering in the case of the antiferromagnetic Heisenberg model on the triangular lattice). The quantum spin liquid wave functions (2.29) are highly correlated states. To be able to compare the variational energies, we also need to introduce nontrivial quantum correlations to the ordered states.

We use the following two complementary schemes to introduce quantum corrections on top of long-range ordered product states. The first approach builds on the

fermionic representation and gauge theory description of the spin model. Long-range ordered phases can be captured within the following quadratic trial Hamiltonian,

$$H_{\rm ord} = s\sum_{\langle i,j\rangle} f_{ai}^\dagger f_{aj} - h\sum_j d_j^{a*} d_j^b f_{aj}^\dagger f_{bj} - \mu_a \sum_j f_{aj}^\dagger f_{aj}\,. \tag{2.30}$$

Similar to the quantum spin liquid wave functions (2.29), the Gutzwiller-projected ground state of (2.30) serves as a variational state. The normalized complex vectors $\boldsymbol{d}_j$ specify a particular spin-one ordering pattern. The variational parameter h interpolates from the U(1) spin liquid ($h = 0$) to the product state $|\psi_{\rm p}\rangle = \prod_j \sum_a d_j^a |a\rangle_j$ when $h \to \infty$. As before, we set $\mu_x = \mu_y$; $\mu_x - \mu_z$ is taken as a variational parameter and we consider π- and 0-flux states by $s = \pm 1$.

Another route to constructing correlated long-range ordered wave functions is to apply spin Jastrow factors to a product state. The analysis of such wave functions for the spin-1/2 antiferromagnetic Heisenberg model on the triangular lattice was pioneered by Huse and Elser in Ref. [70]. For that model, Huse-Elser wave functions were found to give low variational energies, comparable to exact energies on small clusters. A generalization of the Huse-Elser wave function to the case of spin $S = 1$ can be written as

$$|\mathcal{J}\rangle = \exp(-\sum_{\langle i,j\rangle}\{\beta(S_{zi}S_{zj}) + \gamma(S_{zi}S_{zj})^2\})|\psi_{\rm p}\rangle\,. \tag{2.31}$$

Here, $|\psi_{\rm p}\rangle$ is a product state of spin one. In this paper, we restrict ourselves to nearest-neighbor Jastrow factors, and take β, γ to be real variational parameters.

A general spin-one product state can be written as

$$|\psi_{\rm p}\rangle = \prod_j \sum_a d_j^a |a\rangle_j\,, \tag{2.32}$$

where $|a\rangle \in \{|x\rangle, |y\rangle, |z\rangle\}$ span the local Hilbert space; see Eq. (2.8). Let us write $\boldsymbol{d} = \boldsymbol{u} + \mathrm{i}\boldsymbol{v}$, where $\boldsymbol{u}$ and $\boldsymbol{v}$ are real vectors, and consider the single-site state $|\psi\rangle = \sum_a d^a|a\rangle$. We can always take $\boldsymbol{d} = (d^x, d^y, d^z)$ to be normalized and $\boldsymbol{u}\cdot\boldsymbol{v} = 0$ (choice

of phase). The spin expectation value in this state is given by

$$\langle \boldsymbol{S} \rangle = 2\,\boldsymbol{u} \times \boldsymbol{v}\,. \tag{2.33}$$

If $\boldsymbol{d}$ is real, the corresponding state is a *spin nematic* with $\langle \vec{S} \rangle = 0$. In this case, $\boldsymbol{d}$ is called the *director* and we have

$$\langle S_a^2 \rangle = 1 - (d^a)^2\,. \tag{2.34}$$

On the other hand, $\boldsymbol{u}^2 = \boldsymbol{v}^2 = 1/2$ corresponds to a *spin coherent* state where $|\langle \vec{S} \rangle| = 1$ is maximal [64].

The fermionic states (2.30) and the Huse-Elser wave functions (2.31) are two general and complementary ways to introduce nontrivial quantum fluctuations on top of spin-one product states (2.32). Although additional variational parameters can be built into the product state itself, we need to choose a suitable (family of) product states (specified by $\boldsymbol{d}_j$) to start with. As the example by Huse and Elser [70] suggested, good ground-states energies can be obtained by choosing the product states that minimize the energy of the spin model. Below we will use a similar choice guided by a variational study of the model (2.1) at the level of product states. Such study, performed in Ref. [55], suggested a three-sublattice ordering pattern, generalizing the ordering pattern of Ref. [34] to $D \neq 0$. Motivated by these results, we choose the antiferromagnetic and nematic ordered states as an input to our correlated ordered states discussed above.

Antiferromagnetic ordered state

First, we consider an antiferromagnetic (AFM) state where the spins $\langle \psi_{\rm p} | \vec{S}_j | \psi_{\rm p} \rangle$ have a constant length and lie in a common plane at an angle of 120° to each other on nearest-neighbor sites. The average spin length, $|\langle \psi_{\rm p} | \vec{S}_j | \psi_{\rm p} \rangle|$, is taken as a variational parameter. In the notation of Eqs. (2.30) and (2.32), the spin states on sublattices

A, B, and C of the triangular lattice are written as

$$\begin{aligned} \boldsymbol{d}_{j\in A} &= (0, -\mathrm{i}\sin\eta, \cos\eta)\,, \\ \boldsymbol{d}_{j\in B,C} &= (\pm\frac{\sqrt{3}\mathrm{i}}{2}\sin\eta, \frac{\mathrm{i}}{2}\sin\eta, \cos\eta)\,, \end{aligned} \tag{2.35}$$

where $\eta \in [0, \pi/2]$ is a variational parameter. Using Eq. (2.33), one may check that this state corresponds to 120° antiferromagnetic ordering in the x-y plane with $|\langle\psi_{\mathrm{p}}|\vec{S}_j|\psi_{\mathrm{p}}\rangle| = \sin 2\eta$. We also consider the same ordering in the x-z plane.[4] For $\eta = \pi/4$, each site is in a spin-coherent state; i.e., $|\langle\vec{S}_j\rangle| = 1$. The values $\eta \in \{0, \pi/2\}$ correspond to spin-nematic states with $\langle\vec{S}_j\rangle = 0$. For $\eta = 0$, all directors point along the z axis (ferro-nematic state), whereas for $\eta = \pi/2$, the directors on nearest-neighbor sites lie in a common plane at an angle of 120° (120° nematic state).

Spin-nematic ordered states

As a second ordering pattern, we consider spin-nematic (NEM) states with $\langle\psi_{\mathrm{p}}|\vec{S}_j|\psi_{\mathrm{p}}\rangle = 0$. The angle between the directors on different sublattices is constant and taken as a variational parameter ("umbrella" configuration). More precisely, we take the following family of spin-nematic states,

$$\begin{aligned} \boldsymbol{d}_{j\in A} &= (0, -\sin\eta, \cos\eta), \\ \boldsymbol{d}_{j\in B,C} &= (\mp\frac{\sqrt{3}}{2}\sin\eta, \frac{1}{2}\sin\eta, \cos\eta)\,, \end{aligned} \tag{2.36}$$

where the variational parameter η controls the angle between the nematic directors on different sublattices. As before, the special value $\eta = 0$ corresponds to a ferro-nematic, while $\eta = \pi/2$ is a 120° nematic state. At the intermediate value $\sin\eta = \sqrt{2/3}$, the directors are perpendicular to each other on neighboring sites (90° antiferro-nematic state [34]).

[4] We always choose the spin Jastrow factors in the 120°-AFM Huse-Elser wave function (2.31) to lie *perpendicular* to the ordering plane of the spins. That is, for $D < 0$ (when the spins order in the x-z plane) the Jastrow factor in Eq. (2.31) should read $\exp\{-\beta S_{yi}S_{yj} - \gamma(S_{yi}S_{yj})^2\}$.

2.3.3 Phase diagram of bilinear-biquadratic Heisenberg model

We start by considering the bilinear-biquadratic model introduced in Eq. (2.1),

$$H_{KD} = \sum_{\langle i,j \rangle} \{ \vec{S}_i \cdot \vec{S}_j + K(\vec{S}_i \cdot \vec{S}_j)^2 \} + D \sum_j S_{zj}^2 , \tag{2.37}$$

where we set the Heisenberg exchange energy $J = 1$. Below, we restrict ourselves to the parameter range $|K| \leq 1.5$ and $|D| \leq 1.5$.

For intermediate values of D, one may expect an x-y paired quantum spin liquid to be stabilized in this model. Since $S_{zj}^2 = 1 - n_{zj}$, the single-ion anisotropy D acts as a chemical potential for the f_z spinon. For nonzero D, the Fermi surfaces of f_z and of f_x, f_y in the U(1) state are expected to mismatch, and it is conceivable that f_x and f_y pair while leaving f_z with a spinon Fermi surface. Indeed, in Section 2.2 mean-field theory found that for $K \lesssim 0.5$, the $p + ip$ quantum spin liquid wins, while for $K \gtrsim 0.5$, the $d + id$ state with a spinon Fermi surface is the most stable quantum spin liquid candidate [1]. Below we discover that the variational energy of ordered states is always lower than the one of the quantum spin liquid states when the local constraint (2.9) is taken into account exactly.

Our variational results confirm the known phase diagram at $D = 0$ discussed in Section 2.1.3. Furthermore, we find that the three-sublattice ordering of the ground state persists for nonzero values of D; i.e., all spin liquid states are higher in energy than the three-sublattice ordered states we considered.[5]

A typical plot of the variational energies (for $D = -0.4$) is shown in Fig. 2-4. For $K \lesssim 0.3$, the magnetic Huse-Elser wave function ($\mathcal{J}$-AFM), Eq. (2.31), is the best variational state. For $0.3 \lesssim K \leq 1$, the fermionic antiferromagnetic state (f-AFM), Eq. (2.30), is the state with the lowest energy. As discussed above, the corresponding product states [specified in Eq. (2.35)] are magnetically ordered with partially developed spins at 120° angles between sublattices. For $D > 0$, the ordered spins lie in the x-y plane while for $D < 0$, the spins order in a plane that contains

[5] We investigate the range $|D| < 1.5$ in detail. But even greater values of D do not seem to stabilize the quantum spin liquid states.

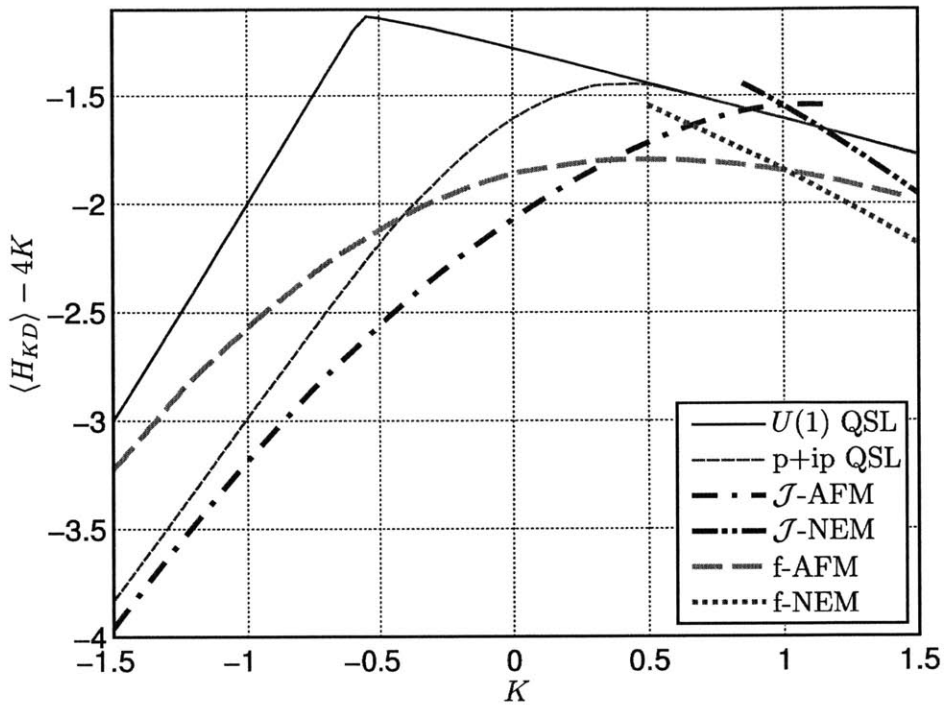

Figure 2-4: Variational energies (per site) for the bilinear-biquadratic model, Eq. (2.37), as a function of K, for $D = -0.4$. The system is $N = 12 \times 12$ lattice sites.

the z axis. For $K \geq 1$, the fermionic nematic state (f-NEM) with directors specified in Eq. (2.36) is the one with the lowest energy. For $D = 0$, the best state is the 90° antiferro-nematic state [34], and for $D \neq 0$, the three nematic directors close ($D > 0$) or open up ($D < 0$) relative to the z axis, depending on the sign of the single-ion anisotropy. In the fermionic long-range ordered states (2.30), the optimal variational parameter is $h \simeq 1.5$. For this parameter value, the spinon excitations are fully gapped. Therefore, the low-energy spinons are absent at the mean field level, and we expect that bosonic spin-wave excitations for these ordered states capture the low-energy physics of this model [34].

The energetically best quantum spin liquid states are the $p + ip$-state for $K \lesssim -1$ and $D \simeq 0$, and the unpaired U(1) state for $K \simeq 1$, both having zero flux through the triangles ($s = -1$). All the other spin liquid states show very small or no condensation energies with respect to the U(1) state. It is remarkable that for $K \simeq 1$, the U(1) state with three spinon Fermi surfaces is actually lower in energy than the optimized

Variational state	Heisenberg energy
Huse-Elser $\mathcal{J}$-AFM	-1.783(1)
Fermionic f-AFM	-1.570(2)
p+ip spin liquid	-1.33(0)
U(1) spin liquid	-1.00(3)

Table 2.1: Variational energies (per site) for the spin-one triangular-lattice Heisenberg antiferromagnet, (2.37), for $K = D = 0$; $N = 144$ sites.

Huse-Elser wave function. We do not find any pairing instability of the U(1) spin liquid on the line $K \simeq 1$ for $D \gtrsim -0.8$. For $D \lesssim -0.8$, there is a small energy gain from pairing in the $d + \mathrm{i}d$ channel. However, the ordered fermionic states are still lower in energy. When $D = 0$, the three spinon Fermi surfaces match exactly. For $D > 0$, the f_z Fermi surface expands while f_x and f_y Fermi surfaces shrink. The opposite happens for negative D. The kink in the U(1) energy in Fig. 2-4 marks the polarization to a ferro-nematic state with $\langle S_{zj}^2 \rangle = 0$, for $K \lesssim -0.6$. That is, the spinon Fermi surface of f_z spinons disappear at this point.

The variational energies for the spin-one Heisenberg antiferromagnet ($K = D = 0$) are displayed in Table 2.1. Note that the Heisenberg energy for the optimal product state of fully developed (coherent) spins ordered at 120° is -1.5. At the Heisenberg point, the spin liquids are even higher in energy than this uncorrelated product state.

At the point $K = 1$ and $D = 0$, the model (2.37) acquired SU(3) symmetry [64]. On the line $D = 0$ and arbitrary K, the remaining symmetry is SO(3) spin-rotation. This symmetry is broken to U(1) (generated by S_z) when $D \neq 0$. However, on the line $K = 1$ and arbitrary D, the model possesses an SU(2) symmetry generated by the operators S_z, $S_x^2 - S_y^2$, and $S_x S_y + S_y S_x$. The generator $S_x^2 - S_y^2$ allows rotation of the antiferromagnetic and the nematic ordered states [specified in Eqs. (2.35) and (2.36)] into each other and they are degenerate. This property of the product states remains valid after the introduction of quantum fluctuations via (2.30) or (2.31), and it explains the degenerate crossings for the ordered states seen in Fig. 2-4 at $K = 1$. See Appendix A.3 for a more detailed discussion of these symmetries.

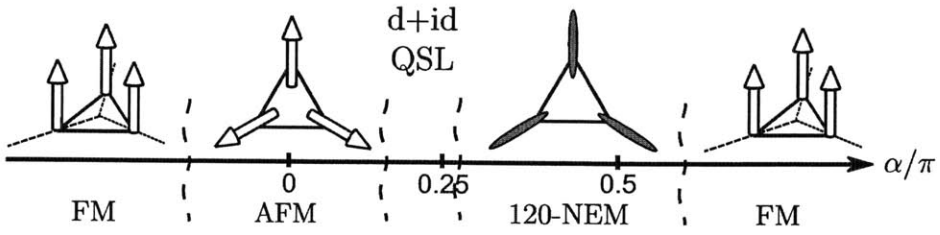

Figure 2-5: Pictorial presentation of the variational phase diagram that we find for the SU(3) ring-exchange model (2.6).

2.3.4 Phase diagram of SU(3) ring-exchange model

We recall that analysis of Section 2.1.3 revealed the same ordering patterns for the SU(3) ring exchange model, as one we found in the case of the KD-model. Therefore in what follows we use the same trial wave functions specified in Eqs. (2.35) and (2.36) to construct correlated ordered states for the ring-exchange model.

We calculate the variational energies of the quantum spin liquid states (2.28) as

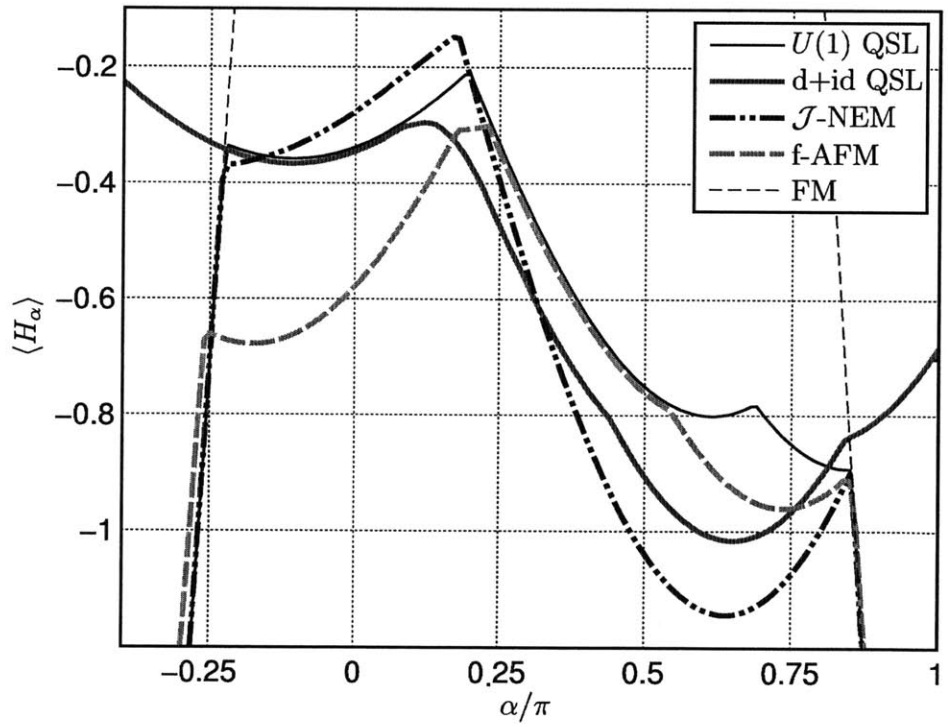

Figure 2-6: Variational energies (per site) of the SU(3) ring-exchange model, Eq. (2.6), as a function of α/π. $N = 12 \times 12$ lattice sites.

well as the energies of correlated three-sublattice ordered states (2.30) and (2.31) for the ring-exchange model specified in Eq. (2.6). The scheme of the phase diagram is shown in Fig. 2-5, and energies of different ground states are compared in Fig. 2-6. We see that the conclusions we draw from the simple product state calculation in Section 2.1.3 agree with the result using correlated wave functions in most of the parameter range: the phase diagram has domains of FM, AFM and nematic ordered states.

However, in the region between the AFM and the 120°-nematic phase, around $\alpha \simeq \pi/4$, we find an extended region where the $d + id$ quantum spin liquid has the lowest energy. The optimal $d+id$ variational parameter $|\Delta^{xy}|$ along with $\langle S_z^2 \rangle - 2/3 = 1/3 - N_z/N$ are shown in Fig. 2-7. The ring-exchange term favors a π-flux $d+id$ state with $s = 1$: As α increases, the 0-flux state with a large pairing term ($|\Delta^{xy}| \simeq 4$) changes to a π-flux state with $|\Delta^{xy}| \simeq 0.5$ at $\alpha \simeq 0.22\pi$.

Note that the $d+id$ quantum spin liquid phase in Fig. 2-5, as well as the adjacent 120° nematic phase, exhibit a ferro-quadrupolar order. For the $d + id$ state this is apparent from Fig. 2-7 since $\langle S_z^2 \rangle > 2/3$. In contrast, lattice rotation symmetry is unbroken in the $d + id$ quantum spin liquid while both adjacent ordered phases spontaneously break lattice rotation.[6]

As discussed above, for $\alpha = 0$ and up to a constant, (2.6) corresponds to the model (2.37) with $K = 1$ and $D = 0$. The ground state of this model was recently approached with density matrix renormalization group (DMRG) calculations in Ref. [71]. In this work, the authors found a three-sublattice ordering pattern that is consistent with our result. The DMRG energy is displayed in Table 2.2 along with the variational energies of the lowest-energy states used in the present paper.

[6] Note that the 120° nematic state only involves two out of three flavors. Therefore, in this phase, the SU(3) symmetry of the model is spontanously broken to SU(2). As a result, the three-site ring exchange term merely renormalizes the two-site Heisenberg term, and the ground state is the SU(2) Néel state on the triangular lattice. We thank A. Läuchli for this remark.

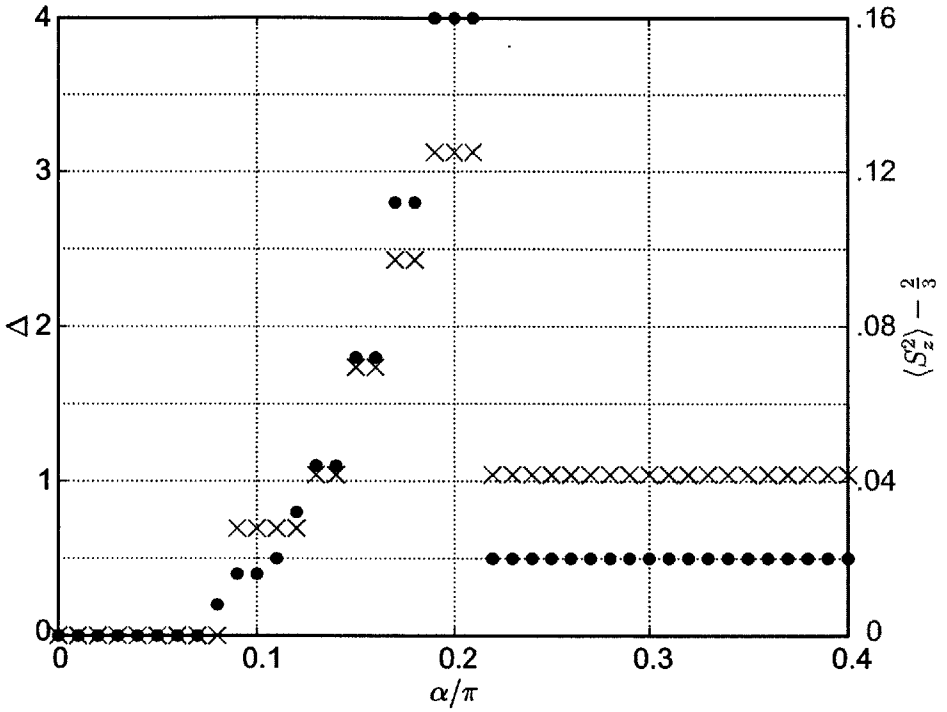

Figure 2-7: Optimized variational parameters $\Delta = |\Delta^{xy}|$ (dot symbols, left scale) and $\langle S_z^2 \rangle - 2/3$ (x symbols, right scale) for the $d + id$ quantum spin liquid state in the ring-exchange model (2.6). Among the states we consider, the $d + id$ state has the lowest energy in the range $0.17\pi \lesssim \alpha \lesssim 0.33\pi$. For $0.17\pi \lesssim \alpha \lesssim 0.22\pi$, the optimal state is a 0-flux state with $s = -1$; for $0.22\pi \lesssim \alpha \lesssim 0.33\pi$, we find a π-flux state with $\Delta \simeq 0.5$ and $s = 1$.

State	SU(3) energy
Fermionic f-AFM	-0.57(8)
Huse-Elser $\mathcal{J}$-AFM	-0.27(7)
U(1) spin liquid	-0.34(3)
DMRG [71] ($N = 8 \times 10$)	-0.678

Table 2.2: Variational energies for the SU(3) model, Eq. (2.6), at $\alpha = 0$ on $N = 12 \times 12$ sites.

Phases of perturbed ring exchange model

We also consider additional perturbations to the ring-exchange model (2.6) in order to assess the effect of such terms on possible low-temperature quantum spin liquid phases. First, we add a single-ion anisotropy term $D \sum_j S_{zj}^2$. As discussed in the previous section, such a term breaks the SU(3) symmetry of the model to SU(2).

For small D, the ordering plane is explicitly chosen. Large D deforms the three-sublattice ordering pattern in a way similar to the bilinear-biquadratic Heisenberg model (2.37). However, we find that the phase boundaries of the $d+\mathrm{i}d$ state with the adjacent ordered states are barely affected by D (we investigate the range $|D| \lesssim 1.5$).

Second, we add a next-neighbor exchange term $J_2 \sum_{\langle\langle i,j \rangle\rangle} \mathcal{P}_{ij}$ to (2.6). Such a term strongly frustrates three-sublattice ordering. At $\alpha = 0$, we find that the three-sublattice ordering is destroyed for J_2 as small as $J_2 \simeq 0.25$, and the U(1) quantum spin liquid has the lowest energy among our ansatz wave functions. However, an analysis of this model in terms of product states reveals that the competing ordering pattern is *spiral*. So far, we have not included spiral states into our variational analysis and this is an interesting open question.

2.4 Physical properties of $d + \mathrm{i}d$ state.

In this Section we discuss the physical properties of the $d+\mathrm{i}d$ paired spin liquid state. We start by reviewing the gauge theory of this state, and then consider the physics of the edge modes, as well as thermodynamic functions and response properties of the above state.

2.4.1 Gauge theory for the $d + \mathrm{i}d$ quantum spin liquid

In this section, we discuss the low-energy gauge theory description of the $d + \mathrm{i}d$ spin liquid and some of its properties. In order to impose the local particle-number constraint (2.9), the Lagrange multiplier λ_j is introduced in the Euclidean path integral for the spinon partition function, [69]

$$Z = \int D\lambda \prod_a [Df_a^\dagger Df_a]\, e^{-S}\,. \tag{2.38}$$

The action is given by

$$S = \sum_j \int_0^\beta d\tau \left\{ f_{aj}^\dagger (\partial_\tau - \mathrm{i}\lambda_j) f_{aj} + \mathrm{i}\lambda_j z_j + H \right\}. \tag{2.39}$$

The Ising variables $z_j \in \{1,2\}$ specify whether site j is constraint to the particle ($N_f = 1$) or hole ($N_f = 2$) representation. The Lagrange multiplier λ_j turns out to be the temporal component of the emergent U(1) gauge field. H is the microscopic spin-one Hamiltonian under consideration, written in terms of the spinon variables f_{aj}. As already stated in Eqs. (2.10) and (2.11), a local transformation that leaves the spin operator (2.7) invariant is given by an element $g_j \in \mathrm{U}(1) \rtimes \mathbb{Z}_2$. Under the transformation $g_j = (e^{\mathrm{i}\phi_j}, \chi_j = \pm)$, the fields transform as

$$f_{aj} \mapsto e^{\mathrm{i}\phi_j} \left(\frac{1+\chi_j}{2} f_{aj} + \frac{1-\chi_j}{2} f_{aj}^\dagger \right) , \tag{2.40a}$$

$$z_j \mapsto 3\frac{1-\chi_j}{2} + \chi_j z_j , \tag{2.40b}$$

$$\lambda_j \mapsto \chi_j \lambda_j + \partial_\tau \phi_j . \tag{2.40c}$$

Note that the action (2.39) is not invariant under time-dependent particle-hole transformations χ_j. Therefore, the particle-hole part of the local symmetry group is not a genuine gauge symmetry of the action. In the following, we can simply choose a particular *static* $\mathbb{Z}_2$ configuration, e.g. $z_j = 1$, in (2.39). Furthermore, generic mean-field decouplings break this local particle-hole symmetry.

In a next step, the spinon interaction terms in H can be decoupled by appropriate Hubbard-Stratonovich fields as is done in the usual slave particle formalism [69]. To maintain the gauge invariance of the action, we need to introduce link variables a_{ij} that are the space components of the U(1) lattice gauge field. The gauge field (λ_j, a_{ij}) mediates the interaction between the fermionic spinons. So far, all manipulations are formal transformations that do not change the physical content of the action. The question remains whether the resulting U(1) lattice gauge theory exhibits a phase with deconfined spinons. Possible low-temperature phases of the gauge theory are specified at the mean-field level by quadratic Hamiltonians (2.28) and (2.30).

Let us now specialize to the $d + \mathrm{i}d$ phase that we found previously in the SU(3) ring-exchange model (2.6). This is a Higgs phase where particle-number conservation is spontaneously broken and the U(1) gauge field acquires a mass $m_0 \propto |\Delta^{xy}|$. At the same time, the fermions f_x and f_y are gapped and can safely be integrated out

in the path integral. This generally leads to a Maxwell term for the U(1) gauge field in the low-energy effective action. Another low-energy term is a Chern-Simons term $\epsilon^{\mu\nu\lambda}a_\mu\partial_\nu a_\lambda$. The Chern-Simons term violates time reversal Θ and parity P. Therefore, its coefficient σ_h cannot vanish in the chiral $d+id$ spin liquid [67]. Hence, in the continuum limit, we arrive at the following effective action

$$\begin{aligned} S_{\text{eff}} = \int d\tau d^2x \{ f_z^\dagger [\partial_\tau - ia_0 - \mu_z + \frac{(\boldsymbol{\nabla} - i\boldsymbol{a})^2}{2m}] f_z \\ + \frac{m_0}{2}a_\mu^2 + \frac{\sigma_h}{2}\epsilon^{\mu\nu\lambda}a_\mu\partial_\nu a_\lambda + \ldots \}, \end{aligned} \tag{2.41}$$

where the ellipsis denotes higher-order terms in derivatives and gauge fields. In this theory, the f_z spinon maintains its Fermi surface, and it is only weakly interacting via the massive photon. The excitations corresponding to f_z are therefore deconfined in this phase.

2.4.2 Chiral edge modes for the $d+id$ quantum spin liquid

In Ref. [72] it was shown that the $d+id$ superconductor is a topological state with Chern number equal to two. From the bulk-edge correspondence, this indicates the presence of two chiral edge modes. A semiclassical argument [73] supports this conclusion. Here we recapitulate this semiclassical argument and generalize it to chiral topological superconductors. After this, we specialize to the $d+id$ quantum spin liquid state. We calculate its energy spectrum on a triangular-lattice strip, and we discuss the corresponding low-energy edge theory.

Edge modes in chiral superconductors

In the bulk of a superconductor involving *two* fermion flavors, writing $\psi = (c_1, c_2^\dagger)$, the Bogolubov equations are

$$\begin{pmatrix} \xi_{\boldsymbol{k}} - E_{\boldsymbol{k}} & \Delta(\boldsymbol{k}) \\ \Delta^*(\boldsymbol{k}) & -\xi_{\boldsymbol{k}} - E_{\boldsymbol{k}} \end{pmatrix} \psi_{\boldsymbol{k}} = 0\,. \tag{2.42}$$

Here, we consider fully gapped superconductors with $|\Delta(\boldsymbol{k})| > 0$. The spectrum is given by $E_{\boldsymbol{k}} = \pm\sqrt{\xi_{\boldsymbol{k}}^2 + |\Delta(\boldsymbol{k})|^2}$.

Next, consider a superconductor with a boundary along the x-direction. Asymptotically (i.e., for $|\boldsymbol{k}|y \gg 1$), an incident bulk wave packet $\psi_{\boldsymbol{k}} e^{\mathrm{i}\boldsymbol{k}\cdot\boldsymbol{r}}$ with $\boldsymbol{k} = (k_x, k_y)$ is reflected at the boundary to an outgoing wave packet $\psi_{\boldsymbol{k}'} e^{\mathrm{i}\boldsymbol{k}'\cdot\boldsymbol{r}}$ with wave vector $\boldsymbol{k}' = (k_x, -k_y)$. The two wave packets "see" the gap functions $\Delta(\boldsymbol{k})$ and $\Delta(\boldsymbol{k}')$, respectively. For a given incident wave vector $\boldsymbol{k}$, it seems therefore possible to map this problem on the half plane to a one-dimensional scattering problem where the order parameter $\Delta(y)$ interpolates from $\Delta(\boldsymbol{k})$ as $y \to -\infty$ to $\Delta(\boldsymbol{k}')$ as $y \to +\infty$:

$$\begin{pmatrix} -\mathrm{i}\partial_y - E & \Delta(y) \\ \Delta^*(y) & \mathrm{i}\partial_y - E \end{pmatrix} \psi_{k_x}(y) = 0\,. \tag{2.43}$$

This one-dimensional problem can now be solved in the usual way [74, 75]. For simplicity, let us choose a bulk potential of the form $\Delta(\boldsymbol{k}) = \Delta e^{\mathrm{i}l\theta(\boldsymbol{k})}$ where $l \in \mathbb{Z}$ is the winding of the phase of the order parameter around the Fermi surface, and $\cos\theta(\boldsymbol{k}) = k_x/|\boldsymbol{k}|$. A scattering state with incident angle θ results in an outgoing angle $\theta' = \pi - \theta$. The asymptotic potentials can therefore be chosen as $\Delta(\boldsymbol{k}) = \Delta e^{\mathrm{i}l(\theta-\pi/2)}$ and $\Delta(\boldsymbol{k}') = \Delta e^{-\mathrm{i}l(\theta-\pi/2)}$. Accordingly, the order parameter $\Delta(y)$ in (2.43) has a constant real part $\Delta\cos l(\theta - \pi/2)$, and an imaginary part $\Delta\sin l(\theta - \pi/2)$ that changes sign across the boundary. This problem can be solved exactly for certain special cases of the interpolating gap profiles [74,76]. For example, a kink profile with $\Delta(y) = \Delta[\cos l(\theta - \pi/2) - \mathrm{i}\tanh(y)\sin l(\theta - \pi/2)]$ yields the bound-state spectrum

$$E_\theta = \Delta\cos[l(\theta - \frac{\pi}{2})]\,\mathrm{sgn}[\sin l(\theta - \frac{\pi}{2})]\,, \tag{2.44}$$

with corresponding eigenvectors

$$\psi_\theta(y) = \frac{1}{2\cosh(y)}\,(1, \mathrm{sgn}[\sin l(\theta - \frac{\pi}{2})])\,. \tag{2.45}$$

We observe that E_θ as a function of θ vanishes exactly $|l|$ times. Therefore, there are

$|l|$ gapless edge modes. Using $\cos\theta \simeq k_x/k_f$ and expanding Eq. (2.44) around a node at momentum k_x^n, we get $E_\theta \simeq -l(k_x - k_x^n)\Delta/k_f + \ldots$. The edge modes are chiral and propagate with the velocity $v_n = -l\Delta/k_f$. In the simplest nontrivial and well-known case of a p+ip-superconductor [74, 75, 77] ($l = 1$), a single chiral edge mode is located at $k_x^n = 0$. Higher angular momenta have chiral modes at $k_x^n \neq 0$. Since the phase winding of the order parameter around the Fermi surface is a topological property, we expect that the number of chiral edge modes is a robust feature of the state, too. The precise location of the nodes $\{k_x^n\}$ and the corresponding propagation speeds $|v_n|$, however, depend on further microscopic details.

Low energy edge theory for the $d + \mathrm{i}d$ quantum spin liquid state

According to the above semiclassical argument, the $d + \mathrm{i}d$ quantum spin liquid state ($l = 2$) is expected to exhibit two chiral edge modes located at wave vectors $k_x^n \simeq \pm k_f/\sqrt{2}$. To substantiate this claim, we calculate the spectrum of the $d + \mathrm{i}d$ state (2.28) on an triangular-lattice strip of infinite length [here, we neglect the local constraint (2.9) and work in the fermionic Fock space]. The four lowest energy levels are shown in Fig. 2-8 as a function of wave vector k_x along the strip. The triangular-lattice $d + \mathrm{i}d$ state indeed exhibits two gapless left movers localized on the lower boundary and two right movers localized on the upper boundary. The spectrum of f_z spinons with a bulk Fermi surface is omitted in Fig. 2-8.

As discussed above, the low-energy degrees of freedom localized on the edge for the $d + \mathrm{i}d$ quantum spin liquid state are two chiral Dirac fermions. To discuss the physics of these edge states, it is convenient to go to the spinon basis creating S_z eigenstates. We have

$$f_\sigma = \frac{1}{\sqrt{2}}(f_x - \mathrm{i}\sigma f_y)\,, \tag{2.46}$$

with $\sigma = \pm 1$. We also denote $f_{\bar{1}} = f_{-1}$. The x-y (triplet) pairing term of the $d + \mathrm{i}d$ state is $f_{xi}f_{yj} - f_{yi}f_{xj} = \mathrm{i}(f_{1i}f_{\bar{1}j} - f_{\bar{1}i}f_{1j})$. Let us consider an edge along the x direction and denote the momentum along the edge by $k = k_x \in [-\pi, \pi]$. The two

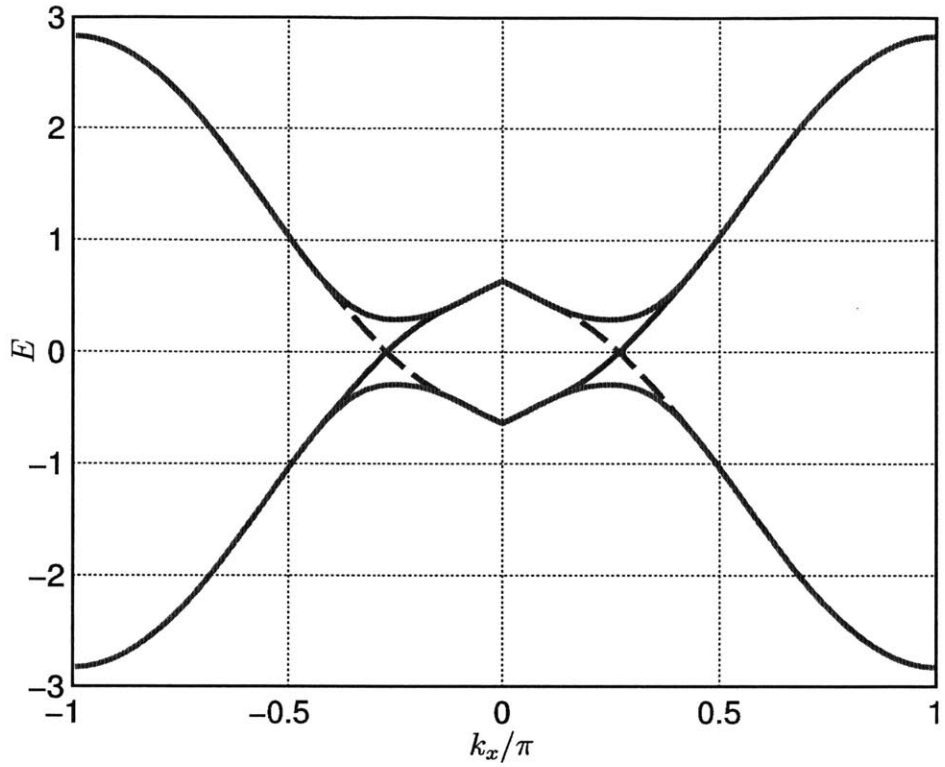

Figure 2-8: The four lowest energy levels of the $d + \mathrm{i}d$ mean-field state (2.28) on an infinite triangular-lattice strip as a function of wave vector k_x along the strip. The width of the strip is 200 sites. The boundaries are chosen to be parallel to one lattice direction and we use open boundary conditions. The spectrum of the f_z spinon with a bulk Fermi surface is omitted. The gapless states (blue online) are localized on the lower boundary for left movers (dashed line), and on the upper boundary for right movers. The higher states (red online) are delocalized and the energy levels above them are "dense".

gapless points in the boundary spectrum are denoted by $k_x^n = \pm k^0$ with $k^0 > 0$.

Using the semiclassical expression (2.45), the edge states are created by operators

$$\chi_\sigma(k) \sim f_{\sigma k} + \sigma \mathrm{sgn}(k) f^\dagger_{\bar{\sigma} - k}\,, \tag{2.47}$$

for $|k| \simeq k^0$. The excitations $\chi_1(k)$ and $\chi_{\bar{1}}(k)$ carry spin $S_z = \pm 1$, respectively. Note that the edge states at positive and negative momenta k are not independent: We have $\chi^\dagger_\sigma(k) = \sigma \mathrm{sgn}(k)\, \chi_{\bar{\sigma}}(-k)$. The low-energy effective edge Hamiltonian is therefore

given by

$$\mathcal{H} = v_0 \sum_{k \simeq k^0, \sigma} (k - k^0)\, \chi^\dagger_\sigma(k) \chi_\sigma(k)\,, \tag{2.48}$$

where the sum over k is restricted to the vicinity of the node at momentum $+k_0$ to avoid double counting of states.

Similar to the ordinary quantum Hall effect, the chiral edge modes are expected to be robust with respect to disorder and impurities because no backscattering is possible [78]. Furthermore, due to S_z conservation, hybridization terms such as $f_z^\dagger \chi_\sigma$ cannot appear in the low-energy Hamiltonian. In a mean-field decoupling, interaction terms such as $f_z^\dagger f_z \chi_\sigma^\dagger \chi_\sigma$ only shift the chemical potentials of bulk and edge gapless modes, and do not significantly alter the edge physics. The presence of protected chiral edge modes carrying spin $S_z = \pm 1$ implies a quantized spin Hall conductivity. We also expect a thermal Hall conductivity in the $d + \mathrm{i}d$ quantum spin liquid state.

In the $d + \mathrm{i}d$ quantum spin liquid phase with unbroken lattice symmetries, f_z must necessarily form a spinon Fermi surface (see Sec. 2.3.1). However, this argument becomes invalid when the lattice symmetries are explicitly broken. For example, close to the boundary of the sample, symmetry allows a pairing term for f_z. Similarly, we expect the spinon to acquire a local gap in the vicinity of bulk impurities. This property makes the Fermi surface of f_z spinons hard to detect in any experiment that involves local probes.

2.4.3 Thermodynamic properties and response functions of $d + \mathrm{i}d$ spin liquid

After reviewing the gauge theory description and physics of the edge mode, here we release the local constraint (2.9) in order to analyze the spectral properties of the $d + \mathrm{i}d$ mean field state. This can be justified from the point of view of the U(1) gauge theory since we are in a Higgs phase where gauge fluctuations can be neglected. In this case, the f_z spinon can be treated as a weakly interacting Fermi liquid.

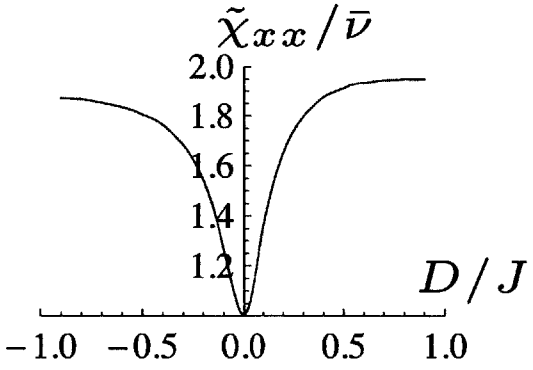

Figure 2-9: The spin susceptibility $\tilde{\chi}_{xx} = \chi_{xx}/(\mu_B g)^2$ in the $d+id$ phase as a function of D/J for $K/J = 0.55$. The susceptibility is normalized by the average density of states, $\bar{\nu} = (\nu_x + \nu_z)/2$, where ν_x is calculated without the gap.

Static spin susceptibility and NMR relaxation rate

The response function, $R_{aa}(\mathrm{i}\omega) = \sum_{ij} \int_0^\beta d\tau\, e^{\mathrm{i}\omega\tau} \langle S_{ai}(\tau) S_{aj} \rangle$, in the $d + \mathrm{i}d$ state has the following properties: Since f_x and f_y fermions are paired, we have $R_{zz}(\mathrm{i}\omega) = 0$, and χ_{zz} vanishes. However, $R_{xx}(\mathrm{i}\omega) = R_{yy}(\mathrm{i}\omega)$ do not vanish at low temperature. In the low-frequency, low-temperature limit, $|\omega| \ll T \to 0$, we find

$$\chi_{xx} = \mathrm{Re}[R_{xx}(0)] = \int_{\mathrm{BZ}} \frac{d^2k}{2\pi} \frac{E_{\boldsymbol{k}} - \mathrm{sgn}(\xi^z_{\boldsymbol{k}})\xi^x_{\boldsymbol{k}}}{E_{\boldsymbol{k}}(E_{\boldsymbol{k}} + |\xi^z_{\boldsymbol{k}}|)} \tag{2.49}$$

where $\xi^a_{\boldsymbol{k}} = 2s[\cos(\boldsymbol{e}_1 \cdot \boldsymbol{k}) + \cos(\boldsymbol{e}_2 \cdot \boldsymbol{k}) + \cos(\boldsymbol{e}_3 \cdot \boldsymbol{k})] - \mu_a$ is the dispersion of the x- and z-fermions. $E_{\boldsymbol{k}} = \sqrt{(\xi^x_{\boldsymbol{k}})^2 + |\Delta^{xy}_{\boldsymbol{k}}|^2}$, and the $d + \mathrm{i}d$ gap function is $\Delta^{xy}_{\boldsymbol{k}} = \Delta[\cos(\boldsymbol{e}_1 \cdot \boldsymbol{k}) + e^{2\pi\mathrm{i}/3}\cos(\boldsymbol{e}_2 \cdot \boldsymbol{k}) + e^{-2\pi\mathrm{i}/3}\cos(\boldsymbol{e}_3 \cdot \boldsymbol{k})]$. As before, $\boldsymbol{e}_{1,2,3}$ are vectors of nearest-neighbor links on the triangular lattice.

We find that the static spin susceptibility χ_{xx} takes a nonzero value given by the integral over the Brillouin zone (BZ), Eq. (2.49). Its numerical value depends on the parameters Δ, μ_x, μ_z, and on $s = \pm 1$. In the limit when gap is much smaller than anisotropy of chemical potentials, $\Delta \lesssim |\mu_x - \mu_z| \ll 1$, χ_{xx} approaches the Pauli susceptibility of two unpaired Fermions, $\chi_{xx} \simeq 2\nu_z$, where $\nu_z = \int_{\mathrm{BZ}} d^2k/(2\pi)\, \delta(\xi^z_{\boldsymbol{k}})$ is the density of states at the Fermi surface. In the opposite limit, $|\mu_x - \mu_z| \ll \Delta \ll 1$, the susceptibility approaches approximately half this value, $\chi_{xx} \simeq \nu_z$. The full curve

of $\chi_{xx}/(\mu_B g)^2$ normalized by the density of states at intermediate values of Δ as a function of $\mu_x - \mu_z$ is plotted in Fig. 2-9.

The nuclear spin relaxation rate is given by $T_1^{-1} \sim T\mathrm{Im}[R_{aa}(\mathrm{i}\omega \to 0)]$. Since two out of three fermions are gapped, $\mathrm{Im}[R_{aa}(\mathrm{i}\omega \to 0)]$ vanishes for temperatures and frequencies smaller than the gap for all α. This implies the NMR relaxation $1/(T_1 T)$ is exponentially small for temperatures below the pairing scale. These results tell us that the Fermi surface associated with f_z [see Fig. 2-3 (b)] should be viewed very differently than the spinon Fermi surface in the $S = 1/2$ spin liquid which carries spin-1/2 quantum numbers and leads to gapless spin-1 excitations. In our case $S^z = 1$ excitations are gapped even though the static spin susceptibility $\chi_{xx}, \chi_{yy} \neq 0$ and the specific heat has linear T dependence.

Specific heat and Wilson ratio

In the $d + \mathrm{i}d$ spin liquid, the magnetic specific heat at low temperature is linear in temperature due to the f_z spinon Fermi surface. The coefficient is given by

$$\gamma = \frac{C_M}{T} = \frac{\pi^2 \nu_z}{3}. \tag{2.50}$$

The Wilson ratio is defined as

$$R_W = \frac{4\pi^2}{3}\frac{\bar{\chi}_0}{\gamma}. \tag{2.51}$$

For the case of powder samples, a directional average should be used in this expression for comparison with experiment, $\bar{\chi} = 2\chi_{xx}/3$.

The Wilson ratio, $R_W = 8\chi_{xx}/(3\nu_z)$, for the $d + \mathrm{i}d$ state is plotted as a function of $\mu_z - \mu_z^0$ in Fig. 2-10. The choices of parameters ($\Delta = 0.5$ and 2.6 for the 0-flux state, and $\Delta = 0.5$ for the π-flux state) are examples of lowest energy $d + \mathrm{i}d$ states in the ring-exchange model, (2.6), at $\alpha \simeq \pi/4$. Note that, in this plot, we adjust the chemical potential $\mu_x = \mu_y$ such that the constraint is satisfied *on average*, $\sum_a \langle n_a \rangle = 1$. The shift μ_z^0 is the optimized chemical potential for the ring-exchange

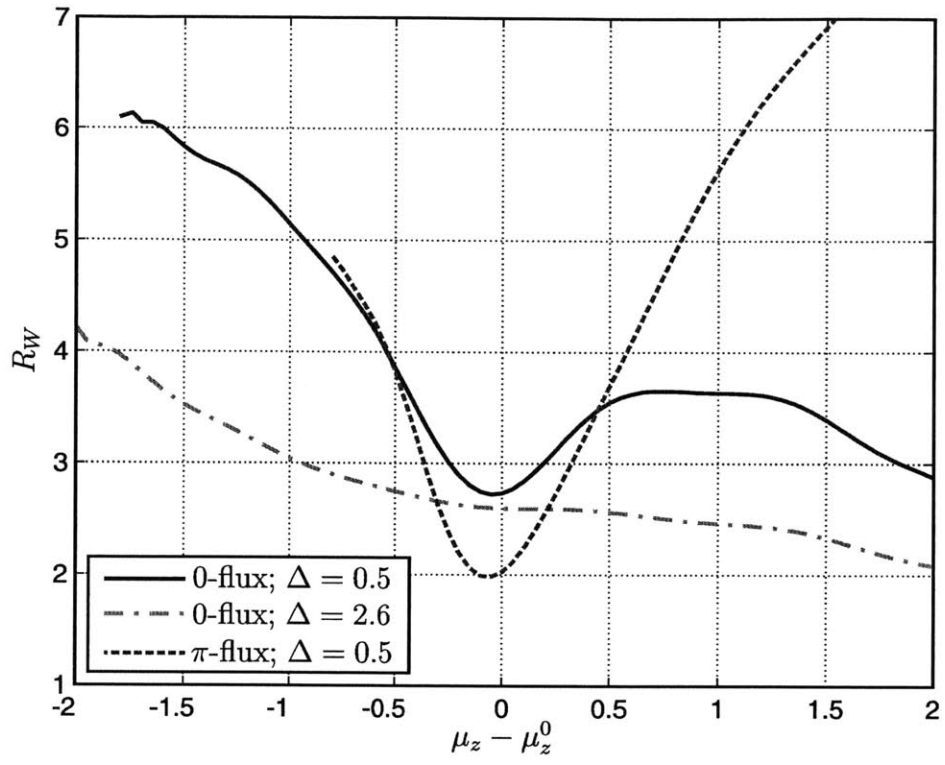

Figure 2-10: Wilson ratio, (2.51), for the $d + \mathrm{i}d$ state as a function of the spinon chemical potential, $\mu_z - \mu_z^0$. The shift μ_z^0 corresponds to the optimal value of the chemical potential in the ring exchange model (2.6) at $\alpha = \pi/4$ (without single-ion anisotropy).

model, i.e., for $D = 0$. In Fig. 2-10, we see that the Wilson ratio is enhanced in the $d + \mathrm{i}d$ state with respect to a metal (where $R_W = 4/3$) by a factor of approximately two at $\mu_z = \mu_z^0$. This can be attributed to the fact that only a *single* fermion flavor contributes to the coefficient of specific heat in the quantum spin liquid state. Since $S_z^2 = 1 - f_z^\dagger f_z$, a single-ion anisotropy term in the Hamiltonian acts as a chemical potential for the f_z spinon. We have $D \propto (\mu_z - \mu_z^0)$, and R_W can be further enhanced by a non-zero D. An easy-plane anisotropy ($D < 0$) shrinks the spinon Fermi surface, resulting in enhancement of R_W. For an easy-axis anisotropy ($D > 0$), the Wilson ratio is enhanced due to an increase in magnetic susceptibility in the case of the π-flux state.

Thermal Hall effect

Due to the spinon Fermi surface of f_z, the $d + id$ quantum spin liquid state exhibits a longitudinal heat conductivity [79]. According to the Wiedemann-Franz law, it is of the form

$$\kappa^{xx} = \frac{\tau\ \varepsilon_f}{\hbar}\, g_0\,, \tag{2.52}$$

where $g_0 = \pi^2 T/(3h)$ is the thermal conductance quantum, ϵ_f is the Fermi energy of the f_z spinon, and τ is its lifetime. However, no longitudinal spin current will flow since the spin excitations are fully gapped in the bulk. Nevertheless, we expect a thermal (and spin) Hall conductivity due to the chiral edge modes [80,81]:

$$\kappa^{xy} \simeq 2g_0\,. \tag{2.53}$$

Since the state is compressible, κ^{xy} is not expected to be exactly quantized. The f_z spinon with a bulk Fermi surface also contributes to κ^{xy} due to a classical Hall effect in the chiral spin liquid. On the other hand, the spin Hall conductivity is expected to be exactly quantized.

2.5 Conclusion and outlook

In this Chapter, we constructed all natural quantum spin liquid states with three flavors of fermionic spinons for spin $S = 1$ Heisenberg and ring exchange models on the triangular lattice. We compare their variational energies with the ones of various long-range ordered states. We find that for large biquadratic and ring-exchange terms (of the order of the Heisenberg exchange $J > 0$), an exotic chiral quantum spin liquid with a spinon Fermi surface is stabilized.

The $d + id$ spin liquid state has a number of exotic physical properties, such as coexistence of spinon Fermi surface with gapped spin excitations, edge modes and quantized spin Hall response. It is instructive to contrast these properties to different $\mathbb{Z}_4$ spin liquid state proposed by Xu *et al.* [51] for spin-1 models. The $\mathbb{Z}_4$ state from Ref. [51] has gapless fermionic spinon excitations with quadratic band touching. This

leads to a T-linear specific heat and a constant spin susceptibility at low temperature. However, in contrast to the $d + \mathrm{i}d$ state, the bulk spin excitations are gapless in the $\mathbb{Z}_4$ state, and no chiral edge modes are expected. This leads to a finite spin relaxation rate at low temperature as well as absence of thermal and spin Hall effects in this state.

Another interesting state is the U(1) state has Fermi surfaces for all three spinon flavors. However, since this state is in a Coulomb phase, the U(1) gauge fluctuations are expected to be relevant leading to non-Fermi-liquid behavior. Physics of this state will be a subject of the next Chapter.

The natural open question is if the considered spin-1 ring exchange model can describe the relevant magnetic interactions in magnetic materials. A perturbative expansion in t/U of a two-band Hubbard model with an additional orbital degree of freedom and strong Hund coupling would produce a spin $S = 1$ Heisenberg term $\vec{S}_i \cdot \vec{S}_j$ to order t^2. Only to next order, t^4, one expects biquadratic terms $(\vec{S}_i \cdot \vec{S}_j)^2$ as well as three-site terms $(\vec{S}_i \cdot \vec{S}_j)(\vec{S}_j \cdot \vec{S}_k)$ [82, 83]. Those three-site terms has to be of the same order as the Heisenberg term to realize the ring-exchange model. We found that a dominant nearest-neighbor Heisenberg term disfavors the $d + \mathrm{i}d$ quantum spin liquid ground state.

While it is unclear, at present, whether the ring-exchange model (2.6) can realistically describe the magnetic materials such as $Ba_3NiSb_2O_9$, it is a very natural model to study if one starts from an integer-filled three-band Hubbard model. Such three- (and higher-) band Hubbard models are currently of great interest, both theoretically and experimentally, in the cold-atom community; see, *e.g.*, Refs. [71,84].

Chapter 3

Kondo physics in $S = 1$ spin liquid with emergent Fermi surface

In this Chapter we study the behavior of Kondo $s = 1/2$ impurity embedded in a two-dimensional $S = 1$ U(1) spin liquid with a Fermi surface [3]. This problem contains an interesting interplay between non-Fermi-liquid behavior induced by a U(1) gauge field coupled to fermions and a non-Fermi-liquid fixed point in the overscreened Kondo problem. Using a large-N expansion together with an expansion in the dynamical exponent of the gauge field, we find that the coupling to the gauge field leads to weak but observable changes in the physical properties of the system at the overscreened Kondo fixed point. We discuss the extrapolation of this result to a physical case and argue that the realization of overscreened Kondo physics could lead to observations of effects due to gauge fields.

3.1 Introduction

Impurity models constitute an important chapter in modern condensed matter physics. Since the original paper by Kondo [85] considering electron sea screening a single impurity spin, this problem has attracted significant theoretical and experimental attention [86–109]. More recently, impurity physics has been studied in the context of strongly interacting systems. Numerous examples include [110] an impurity in

systems with vanishing density of states [111–116] high temperature superconductors [117–121], and quantum magnets [122–132]. Quantum magnets are particularly versatile as a host system, having a large number of possible ground states with different low energy excitations.

In this Chapter we consider a spin-half impurity embedded in a spin-1 quantum paramagnet with a spin liquid ground state [8, 25]. We consider the situation where the low energy excitations of the paramagnet are described by emergent fermionic excitations with a Fermi surface, coupled to a U(1) gauge field. This study is motivated by the recent appearance of several $S = 1$ spin liquid candidate materials [32, 133]. Theoretically, a number of spin liquid ground states for spin-1 system have been proposed [2, 33, 134–140]. One possible scenario described in Chater 2 above, involves emergence of three fermionic excitations carrying spin-1 quantum numbers [2, 136, 139]. In the previous Chapter we considered different scenarios of (partially) gapping out the Fermi surfaces of three spinons. Assuming that Fermi surfaces of these excitations are not destroyed by a pairing instability, we obtain the U(1) spin-1 spin liquid that is considered below as a host system for the impurity.

Impurity physics in a spin-1/2 spin liquids has been considered in the context of bosonic spin liquids [127], algebraic spin liquids [129, 130], and spin liquids with a Fermi surface [132]. In particular, Ribeiro and Lee in Ref. 132 concluded that physics of a spin-1/2 impurity embedded in a spin liquid with $S = 1/2$ fermionic excitations is similar to that of the conventional Kondo problem [101]. In what follows we argue that a spin-1/2 impurity in a $S = 1$ spin liquid with a Fermi surface realizes overscreened Kondo physics. Although our results are qualitatively similar to the overscreened Kondo effect in conventional systems, there are observable differences due to the presence of an emergent gauge field coupled to spinons.

Our findings suggest that an impurity in a $S = 1$ spin liquid can be used to probe fermionic excitations. As discussed in Section 1.4, experimental detection of spinons is an open problem. Different experimental probes have been suggested in the context of spin-1/2 spin liquids [47, 141–145]. We suggest that the realization of overscreened Kondo physics is a possible way to unravel physics of spin-one spin liquid, allowing

probes of fermionic excitations, as well as the presence of an emergent gauge field.

Overscreened Kondo physics is realized in multichannel Kondo models, where a single spin is coupled to N copies (flavors) of itinerant electrons [88]. On the one hand, such a generalization of original Kondo model may be seen as merely a theoretical tool, allowing a perturbative expansion in $1/N$. On the other hand, the physics changes drastically depending on the interrelation between impurity spin length, s, and the number of flavors coupled to the impurity. When the number of flavors, N, is just enough or less than needed to screen the impurity spin, $N \leq 2s$, antiferromagnetic coupling between the impurity and electrons flows to infinity in the infrared, meaning that at low temperatures impurity spin is screened to the maximum possible extent by electrons. For the case of perfect screening, $N = 2s$, this results in Fermi-liquid behavior [89, 101]. In the underscreened case residual ferromagnetic interaction leads to a singular Fermi liquid [146, 147]. However, in the overscreened regime, $N > 2s$, *i.e.* when there are more channels than required to screen the impurity spin, the system has a non-Fermi-liquid fixed point [91, 93, 95, 97]. This state is characterized by singularities in different physical observables, such as impurity spin susceptibility, specific heat, *etc.* It is particularly interesting as a solvable example of a system with a non-Fermi-liquid fixed point [91]. Despite the rich and interesting physics, the overscreened regime of Kondo model has only few realizations (in particular quantum dots and two levels systems [100, 102, 103, 148, 149]). Hence our system is also interesting as a possible implementation of overscreened Kondo physics.

Qualitatively, the problem of a spin-half impurity hosted by isotropic $S = 1$ spin liquid looks similar to the conventional overscreened Kondo impurity model. When coupled antiferromagneticaly, itinerant excitations carrying spin-1 quantum numbers cannot screen the impurity. However, the presence of emergent coupled to fermionic excitations (see Section 1.3.1), makes these two problems different. Even without the impurity, fermions are in a non-Fermi-liquid regime [39–45] due to the gauge field. The fermion propagator is dressed by a singular self-energy, so there are no well defined quasiparticle excitations in the system. This is manifested, for example, in the singular behavior of the specific heat $C \propto T^{2/3}$ in two dimensions at low

temperatures [39, 43].

Coupling the impurity to fermions with non-Fermi-liquid behavior allows us to study the interplay between the gauge field induced non-Fermi-liquid behavior and the Kondo non-Fermi-liquid fixed point. The conventional approach to the Kondo problem is either an exact solution by mapping it onto one-dimensional problem [90, 108], or $1/N$ expansion. Both methods are not directly applicable in our case. The presence of gauge field impedes the mapping of our model to a one dimensional problem in the radial channel. On the other hand, a rigorous $1/N$ expansion is not possible, due to singular self-energy corrections [44, 150]. The latter issue has been recently resolved in the paper by Mross *et. al.* [45], where a controlled double expansion scheme has been provided. It combines the $1/N$ expansion with an expansion in another small parameter (related to the dynamical critical exponent of the gauge field).

We adopt the recently developed double expansion method [45] to our problem. Since the double expansion includes the large N limit, we expect to have a perturbatively accessible fixed point. At leading order, the gauge field does not affect the position of this non-Fermi-liquid Kondo fixed point. However, it leads to corrections to the scaling dimension of the Kondo coupling. Assuming that the results obtained using the double expansion interpolate to the physical case, we conclude that physical properties such as impurity spin susceptibility, specific heat, *etc.* are still characterized by singular behavior. Unlike the case of the Kondo model in the regime of perfect screening [132], where the coupling to the gauge field has no consequences to leading order in $1/N$, in our case the gauge field influences Kondo physics.

This Chapter is organized as follows. In the remainder of this Section, we introduce the basics of our model, diagram technique and briefly explain the idea behind double expansion. In Section 3.2 we first review known results for the β-function in the overscreened Kondo problem without the gauge field. Afterwards, we calculate the β-function with the gauge field and study the changes in scaling behavior of different physical quantities. Finally, in Section 3.3 we discuss the extrapolation of our findings beyond the double expansion, and comment on possible experimental realizations and experiments to detect Kondo physics. Details regarding the calculation of corrections

to the β-function due to gauge field are given in the Appendix B.

3.1.1 Spin liquid with fermionic excitations and impurity

Let us consider a spin Hamiltonian on a lattice consisting of spin-1 sites,

$$H_{\text{spin}} = \sum_{ij} \left[J_{ij} \vec{S}_i \cdot \vec{S}_j + K_{ij} (\vec{S}_i \cdot \vec{S}_j)^2 \right] + \ldots, \tag{3.1}$$

where ellipses denote other possible terms such as ring exchange. We are motivated by results of Chapter 2 [2] which shows evidence of stabilizing a spin liquid phase with spinon Fermi surface on a triangular lattice with nearest neighbors bilinear, and biquadratic spin interactions along with ring exchange terms. The low energy description of such a state is a theory of fermions strongly coupled to a U(1) gauge field. From now we assume that such a spin liquid state exists and work only with the low energy effective theory described below.

Let us briefly summarize results for the effective theory [10] of U(1) spin liquid. A spin-1 operator at a given site is represented using *three* fermion operators, $\tilde{f}_\lambda$, $\lambda = 1, 2, 3$ as in Section 2.1.4:

$$\vec{S}_i = \sum_{\lambda,\rho=1}^{3} \tilde{f}^\dagger_{i\lambda} \boldsymbol{I}^{\lambda\rho} \tilde{f}_{i\rho}, \tag{3.2}$$

with $\boldsymbol{I}^{\lambda\rho}$ being the set of three spin-1 matrices (generators of SU(2) in spin-1 representation) [136]. The explicit form of $\boldsymbol{I}^{\lambda\rho}$ may be chosen as in Eq. (2.7), but it is not important to us. In order to remove unphysical states from the Hilbert space, introduced by the representation in Eq. (3.2), one has to enforce a single occupancy constraint on each site. Fermionic $\tilde{f}_\lambda$ are the low energy excitations of the spin liquid, carrying spin-1 quantum numbers. In addition, the low energy description contains a U(1) gauge field, that is coupled to fermions $\tilde{f}_{i\lambda}$ and enforces the single occupancy constraint.

Before proceeding further, let us reiterate the question of interest. We want to understand if the non-Fermi-liquid fixed point of a conventional overscreened Kondo

model is changed by the presence of the gauge field in the bulk. The model outlined above provides us with a particular setup to study the influence of the non-Fermi-liquid bulk on the overscreened Kondo fixed point. However, in order to have control over calculations we need to resort to the large-N limit.

There is a freedom in the implementation of the large-N limit, constrained by the crucial requirement for the generalization procedure to retain the presence of the overscreened Kondo fixed point. We choose a model with N species of *spin-half* fermions, $f_{i\alpha m}$ with $\alpha = \uparrow, \downarrow$, and $m = 1 \ldots N$ as a large-N generalization. This is the simplest model which allows for controllable calculations.

The corresponding Lagrangian for our generalized model may be split into a fermionic part (including coupling to gauge field and impurity spin), and a gauge field Lagrangian,

$$L = L_{\text{fermion}} + L_{\text{gauge}}. \tag{3.3}$$

The generalized fermion Lagrangian becomes:

$$L_{\text{fermion}} = \int d\tau \sum_{\boldsymbol{k},m,\alpha} \Big(\bar{f}_{\boldsymbol{k}\alpha m}(\partial_\tau - \varepsilon_{\boldsymbol{k}}) f_{\boldsymbol{k}\alpha m} - \frac{e}{\sqrt{N}} \sum_{\boldsymbol{q}} f^\dagger_{\boldsymbol{k}+\frac{\boldsymbol{q}}{2}\alpha m} \boldsymbol{v}(\boldsymbol{k}) \cdot \boldsymbol{a}_{\boldsymbol{q}} f_{\boldsymbol{k}-\frac{\boldsymbol{q}}{2}\alpha m} - \frac{J_K}{N} \vec{S}(0) \cdot \boldsymbol{s} \Big), \tag{3.4}$$

where we use imaginary time. In accordance with the discussion above, fermion operators $f_{i\alpha m}$ now carry spin-1/2 quantum numbers ($\alpha = \uparrow, \downarrow$). We omit the time component of gauge field from the coupling, since it is screened [42], and do not write the diamagnetic term, including it in the gauge field propagator. The fermion spin at $\boldsymbol{r} = 0$ is

$$\vec{S}(0) = \frac{1}{\mathcal{N}} \sum_{\boldsymbol{k},\boldsymbol{p},\alpha,\beta,m} f^\dagger_{\boldsymbol{k}\alpha m} \frac{\boldsymbol{\sigma}^{\alpha\beta}}{2} f_{\boldsymbol{p}\beta m}, \tag{3.5}$$

with $\boldsymbol{\sigma} = (\sigma^x, \sigma^y, \sigma^z)$ being the set of three Pauli matrices, and $\mathcal{N}$ being a number of sites in the lattice. In what follows, Greek indices label spin projection, $\alpha, \beta, \ldots = \uparrow, \downarrow$, whereas Latin indices $m, n, \ldots = 1 \ldots N$ label channels. The coupling to the impurity, J_K, is assumed to be antiferromagnetic, $J_K > 0$.

The gauge field Lagrangian is

$$L_{\text{gauge}} = \frac{1}{2}\int \frac{d\boldsymbol{q}\, d\omega}{(2\pi^3)} a_i^*(\boldsymbol{q},\omega) D_{ij}^{-1}(\boldsymbol{q}, i\omega) a_j(\boldsymbol{q},\omega), \tag{3.6}$$

where the time component of the gauge field is excluded. The bare gauge field propagator is zero, since the gauge field is not dynamical but rather represents fluctuations around the mean field ansatz. However, nontrivial dynamics are generated if one accounts for coupling to fermions, leading to a non-zero $D_{ij}^{-1}(\boldsymbol{q}, i\omega)$, discussed in Section 3.1.3.

3.1.2 Diagram technique

The impurity spin is conveniently represented via fermionic operators,

$$\boldsymbol{s} = \sum_{\alpha,\beta} c_\alpha^\dagger \frac{\boldsymbol{\sigma}^{\alpha\beta}}{2} c_\beta, \tag{3.7}$$

where $c_{\uparrow,\downarrow}^\dagger$ ($c_{\uparrow,\downarrow}$) are creation (annihilation) operators of spin up or down pseudofermions [86]. In what follows we use the term "pseudofermions" to distinguish the operators c_α from the operators $f_{k\alpha m}$, which describe low energy excitations in the spin liquid. A faithful representation of spin via fermion operators requires an additional constraint to exclude doubly occupied and empty states from the Hilbert space. However, in the case of a single spin-1/2 operator, $\boldsymbol{s}$, in Eq. (3.7), gives zero when acting on unphysical states in the Hilbert space. Therefore, one can ignore the constraint in this case [86], writing the impurity Lagrangian as

$$L_{\text{imp}} = \int d\tau\, \bar{c}_m(\partial_\tau - \mu_{\text{imp}}) c_m, \tag{3.8}$$

where μ_{imp} is the large positive energy corresponding to the chemical potential for impurity pseudofermions (see discussion in Ref. [86]).

The rules for diagram technique, following from Eqs. (3.4)-(3.8) are summarized in Fig. 3-1. Propagators for fermions and pseudofermions along with interaction vertices

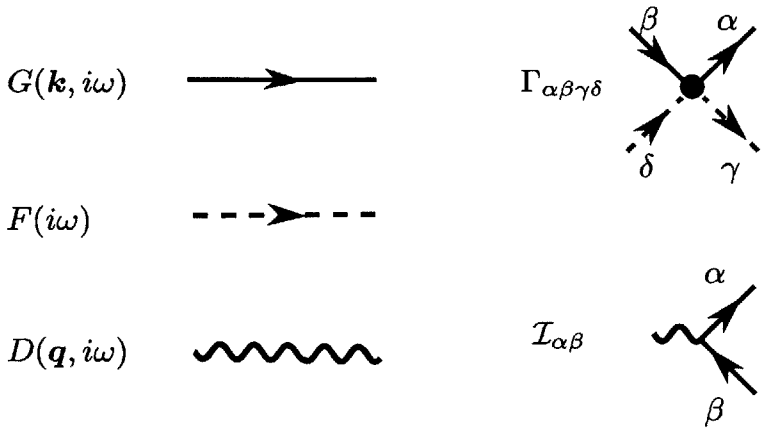

Figure 3-1: Summary of rules for diagram technique. Solid, dashed and wavy lines represent fermion, pseudofermion and gauge field propagator respectively. Also, interaction vertices of fermions with gauge field, $\mathcal{I}_{\alpha\beta}$, and fermions with impurity pseudofermions, $\Gamma_{\alpha\beta\gamma\delta}$, are shown. All objects are diagonal in flavor indices, which are thus suppressed.

are given by

$$G^{mn}_{\alpha\beta}(\boldsymbol{k}, \mathrm{i}\omega) = \frac{\delta_{\alpha\beta}\delta_{mn}}{\mathrm{i}\omega - \xi_{\boldsymbol{k}} - \Sigma(i\omega)}, \tag{3.9a}$$

$$F_{\alpha\beta}(\mathrm{i}\omega) = \frac{\delta_{\alpha\beta}}{\mathrm{i}\omega - \mu_{\mathrm{imp}}}, \tag{3.9b}$$

$$\Gamma^{mn}_{\alpha\beta\gamma\delta} = -\frac{J_K}{4}\boldsymbol{\sigma}_{\alpha\beta}\cdot\boldsymbol{\sigma}_{\gamma\delta}\delta_{mn}, \tag{3.9c}$$

$$\mathcal{I}^{mn}_{\alpha\beta} = -\frac{e}{\sqrt{N}}\boldsymbol{v}_{\boldsymbol{k}}\delta_{\alpha\beta}\delta_{mn}, \tag{3.9d}$$

where $\xi_{\boldsymbol{k}} = \varepsilon_{\boldsymbol{k}} - \mu$ is the fermion energy relative to the Fermi surface. The self-energy, included in fermion Greens function [Eq. (3.9a)] is discussed below. We note that interaction between fermions and the impurity is local in real space. Therefore, in Fourier space, the momenta of two fermion operators in the impurity interaction vertex [Eq. (3.9c)] are unrelated. Fermion propagator and interaction vertices are diagonal in flavor indices. Thus the only contribution of flavor indices is an extra factor N for every loop of fermions, and they will be suppressed in the remainder of this Chapter.

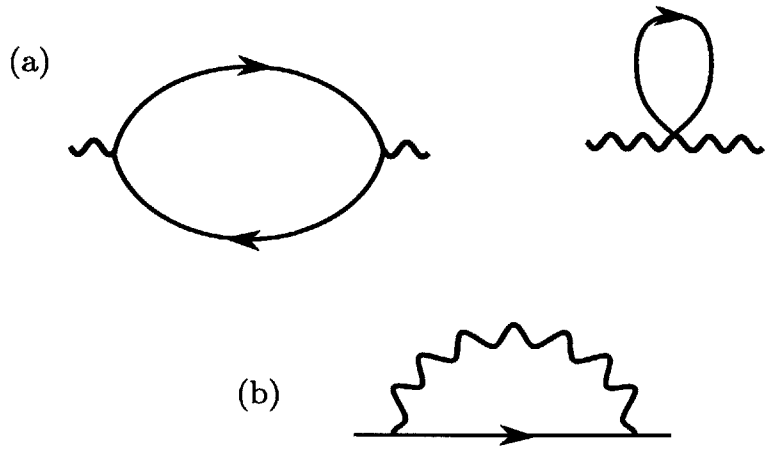

Figure 3-2: (a) Self-energy of the gauge field due to interaction with fermions. Second diagram describes diamagnetic contribution. (b) Self-energy of fermions due to interactions with gauge field in the leading order in $1/N$.

3.1.3 Double expansion

We briefly review the double expansion framework introduced in Ref. [45]. First, we specify dynamically generated propagator of the gauge field. To leading order, the propagator is given by the fermion bubble with current vertices along with diamagnetic term shown in Fig. 3-2 (a). In the Coulomb gauge, $\nabla \cdot \boldsymbol{a} = 0$, the propagator is transverse and can be written as [40, 42, 45]

$$D_{ij}^{-1}(\boldsymbol{q}, \mathrm{i}\omega) = \left(\delta_{ij} - \frac{q_i q_j}{q^2}\right) D_0^{-1}(\boldsymbol{q}, \omega), \tag{3.10a}$$

$$D_0^{-1}(\boldsymbol{q}, \mathrm{i}\omega) = \gamma \frac{|\omega|}{q} + \chi_0 q^{z_b - 1}, \tag{3.10b}$$

with $z_b = 3$ and $\gamma = 2n/k_F$, $\chi_0 = 1/(24\pi m)$ for fermions with quadratic dispersion. Note that the Landau damping term is non-zero only for $|\omega| < v_F q$. We assume z_b takes general value $z_b < 3$ and use it as a control parameter. This approach is consistent because terms $q^{z_b - 1}$ for $z_b < 3$ are non-local. Since z_b is not going to be renormalized within perturbation theory, it is a valid control parameter.

The singular form of the gauge propagator [Eq. (3.10)] leads to a singular self-energy correction for fermions. In the leading order in $1/N$, the diagram in Fig. 3-2(b)

gives us [42, 44, 45]:

$$\Sigma(\mathrm{i}\omega) = -\mathrm{i}\lambda\,|\omega|^{2/z_b}\,\mathrm{sign}\,\omega, \tag{3.11a}$$

$$\lambda = \frac{e^2}{N}\frac{v_F}{\gamma}\frac{1}{4\pi\sin\frac{2\pi}{z_b}}\left(\frac{\gamma}{\chi_0}\right)^{2/z_b}. \tag{3.11b}$$

For $z_b > 2$, the self-energy is more important than the bare $\mathrm{i}\omega$ term in Greens function [Eq. (3.9a)], when $|\omega| < \omega_0$. The energy scale ω_0 is set by a combination parameters γ, χ_0 and v_F [see Eq. (3.14)] and is of order of Fermi energy, the only energy scale related to fermions.

When the self-energy, Eq. (3.11), is singular compared to the bare frequency dependence of the fermions' Greens function, a factor of $1/N$ in the fermion self-energy leads to an extra power of N in the *numerator* of the Greens function. This spoils naive power counting in the $1/N$ expansion [44, 150] requiring a summation of an infinite series of diagrams of a particular topology (genus) at any given order in $1/N$. However, if we assume a gauge field dynamical exponent,[1] $z_b = 2 + \varepsilon$, and take the double scaling limit [45]:

$$\varepsilon \to 0, \qquad N \to \infty, \qquad \varepsilon N = \mathrm{const}, \tag{3.12}$$

we obtain finite $\lambda \propto 1/(N\varepsilon)$ in Eq. (3.11b), rather than $\lambda \propto 1/N \to 0$. The absence of the factor $1/N$ in front of the self-energy restores naive power counting, where the gauge field interaction vertex contributes $1/\sqrt{N}$ and each fermion loop gives a factor of N.

Finally, before proceeding further, we rewrite $\Sigma(\mathrm{i}\omega)$ in a simplified form, valid in the double scaling limit,

$$\Sigma(\mathrm{i}\omega) = -\mathrm{i}\frac{1}{N\varepsilon}\omega\left|\frac{\omega_0}{\omega}\right|^{\varepsilon/2}, \tag{3.13}$$

where scale ω_0 is explicitly given by

$$\omega_0 = \frac{\chi_0}{\gamma}\left(\frac{e^2}{2\pi^2}\frac{v_F}{\chi_0}\right)^{2/\varepsilon}. \tag{3.14}$$

[1] In notations adopted in Ref. [42], $\eta = z_b - 1 = 1 + \varepsilon$

3.2 Perturbatively accessible fixed point

The renormalization group (RG) approach in conjunction with $1/N$ expansion has been proven to be fruitful when applied to the conventional Kondo impurity problem [86–88, 97, 98, 151]. The renormalization procedure is defined with respect to the fermion bandwidth, D. Eliminating states far away from the Fermi surface, one studies the induced flow in the dimensionless coupling $g = \nu J_K$ (ν is the density of states per spin per channel assumed to be constant within the whole band). The corresponding β-function is defined as

$$\beta(g) = \frac{d \log g}{d \log D}, \tag{3.15}$$

and can be calculated perturbatively in g. This simplification is brought by the $1/N$ expansion and is justified in vicinity of fixed point located at small $g^* \propto O(1/N)$.

When there is a gauge field coupled to fermions, the RG approach still can be applied. However, it requires some modifications. The usual $1/N$ expansion has to be replaced by the double expansion discussed above, but the RG flow is still defined with respect to bandwidth, D. Coupling of the fermions to the gauge field, e^2, is treated as a constant, since a single impurity can not change its flow under RG. Likewise in the conventional Kondo problem, there exists a perturbatively accessible fixed point. After briefly reviewing the calculation for RG flow in conventional Kondo problem, we calculate the β-function in the presence of the gauge field and obtain physical properties in the vicinity of the fixed point.

3.2.1 β-function in conventional Kondo problem

While reviewing the RG procedure for the usual Kondo impurity problem we mostly follow Refs. [86, 87]. Renormalization of the dimensionless coupling g in the leading order is given by diagrams shown in Fig. 3-3. Diagrams (a) and (b) in Fig. 3-3 represent corrections to the bare interaction vertex in the second and third orders of perturbation theory. These are the only diagrams up to the third order, which

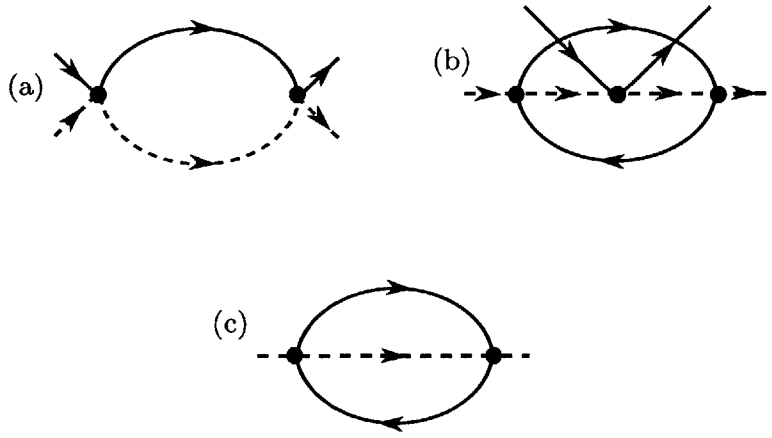

Figure 3-3: Diagrams contributing to the β-function in the leading order in $1/N$. Diagrams (a) and (b) describe corrections to the vertex in the second and third orders of perturbation theory (symmetric counterpart of diagram (a) with direction of one of the fermion line changed is not shown). Diagram (c) is the correction to the self-energy of pseudofermions, contributing to β-function via renormalization of Z-factor.

are logarithmically divergent and thus renormalize the coupling. Note, that diagrams (a) and (b) describe the contributions of the same order, since the latter diagram in addition to extra power of $g \propto 1/N$ has a factor of N from the fermion loop. Diagram (c) in Fig. 3-3 describes renormalization of Z-factor of pseudofermions and also contributes to the β-function.

Calculation of the diagrams in Fig. 3-3 gives the β-function:

$$\beta(g) = \frac{d\log g}{d\log D} = -g^2 + \frac{N}{2}g^3 + \ldots, \tag{3.16}$$

where ellipses denote terms $C_1 N g^4 + C_2 N^2 g^5$ from higher order diagrams. The coefficients $C_{1,2}$ are readily available in the literature [91,97,98,152] and are listed below in Eq. (3.20). As we shall see, these extra terms are subleading in vicinity of fixed point. One can easily solve for a stable non-Fermi-liquid fixed point of this β-function:

$$g^* = \frac{2}{N} + \ldots, \tag{3.17}$$

$$\Delta_0 = \beta'(g^*) = \frac{2}{N} + \ldots, \tag{3.18}$$

where Δ_0 is the negative slope of the β function at this fixed point. Ellipses here stand for terms $O(1/N^2)$. We see that g^* is indeed small in $1/N$, justifying the use of perturbation theory.

3.2.2 Correction to β-function due to gauge field

As we shall see, within the double expansion framework, the gauge field produces a small correction to the regular β-function. Therefore, it suffices to consider the effect of the gauge field to leading order.

There are two types of effects related to the gauge field. First, the gauge field destroys well-defined quasiparticle, leading to non-Fermi-liquid behavior. This is manifested by the singular self-energy due to the gauge field in the fermion propagator [Eq. (3.13)]. Therefore, one has to recalculate diagrams in Fig. 3-3 using the fermion propagator which contains the self-energy. A lengthy but straightforward calculation (see Appendix B.1 for details) yields an answer identical to the case without gauge field, however, with a modified divergent logarithm. Namely, the standard log-divergent contributions are replaced by

$$\log \frac{D}{\omega} \to \log \frac{D}{\omega^{1-\kappa}\omega_0^{\kappa}}, \qquad \kappa = \frac{1}{2N}\frac{1}{1+(N\varepsilon)^{-1}}, \tag{3.19}$$

where energy scale $\omega_0 \propto D$ was defined in Eq. (3.14).

Another effect of the gauge field is the appearance of vertex corrections. All diagrams describing vertex corrections can be split into two classes with representatives of each class depicted in Fig. 3-4 (a) and (b) respectively. Diagrams belonging to the first class have at least one of the ends of the gauge field propagator connected to the internal fermion line. In Appendix B.2 we show that due to the transverse character of the gauge field propagator and the locality of interaction with the impurity, all diagrams of this type with single gauge propagator exactly vanish [132].

In the vertex correction diagrams attributed to the second class, the gauge field propagator connects two external lines. One can think about these diagrams as describing a new interaction vertex [first diagram in Fig. 3-4 (b)] and its renormal-

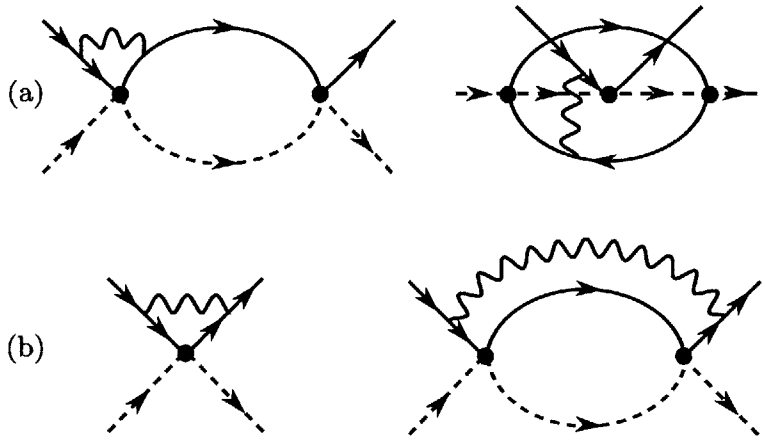

Figure 3-4: Two types of vertex corrections in the leading order in $1/N$ due to gauge field. (a) Example of vanishing diagrams with a single gauge propagator connected by at least one end to the internal line. (b) Non-vanishing corrections, representing a new non-local vertex (first diagram) and example of diagram leading to its renormalization (second diagram).

ization [all other diagrams of this type]. This new vertex contains an additional small factor $1/N$, compared to the original impurity interaction vertex. However, it is non-local, since it depends strongly on the relation between outgoing and incoming fermion momenta, $\boldsymbol{k}$ and $\boldsymbol{p}$ respectively. The vertex is logarithmically divergent when the transferred momentum $|\boldsymbol{k}-\boldsymbol{p}|$ is close to $2k_F$ and is small otherwise [40, 42, 45]. The flow of this vertex to leading order in $1/N$ is identical to the flow of the standard vertex. Thus it does not influence the scaling in the vicinity of the fixed point. The effect of this vertex is to provide subleading corrections to different observables (due to the extra factor $1/N$). Therefore, in what follows we do not consider this vertex.

As we demonstrated, no new diagrams contribute to the β-function up to order $1/N^3$. Calculation of diagrams in Fig. 3-3 with self-energy included into fermionic propagator gives us

$$\beta(g) = (1-\kappa)\left(-g^2 + \frac{N}{2}g^3\right) + \frac{N}{2}(1+\log 2)g^4 - \frac{N^2}{4}g^5, \tag{3.20}$$

where terms in the second line come from higher order diagrams and are $O(1/N^3)$ in vicinity of fixed point. The terms in the first line are universal w.r.t. the reparametriza-

tion of the coupling constant g [108]. These terms have to be included for consistency, since $\kappa \propto 1/N$, but are identical to those in the β-function without gauge field, Eq. (3.16) [account for gauge field in these terms will produce corrections $O(1/N^4)$].

The obtained β-function, Eq. (3.20), differs from the β-function without gauge field, Eq. (3.16), by terms $O(1/N^3)$. This correction does not shift the fixed point g^* even at order $1/N^2$, compared to fixed point[2] Eq. (3.17). However, it modifies the slope of $\beta(g)$ at the fixed point,

$$\Delta_1 = \frac{2}{N}(1-\kappa) + \ldots = (1-\kappa)\Delta_0, \tag{3.21}$$

compared to the slope for the case of the conventional Kondo problem, Δ_0 [Eq. (3.18)]. Below, the slope of the β-function, Δ_1 will be used to determine the flow of the coupling in the vicinity of the fixed point, as well as the singular behavior of different measurable quantities [97,98]. Therefore, the difference between Δ_0 and Δ_1 modifies the behavior of different observables compared to conventional Kondo problem.

3.2.3 Observables

In order to understand how the non-Fermi-liquid fixed point manifests itself in observables, we first find the dependence of the running coupling constant $g_R(\omega)$ on ω. It can be determined from the flow equation $dg_R(\omega)/d\log\omega = -\beta(g_R)$, by employing results for β-function and its slope at the fixed point. Denoting the bare value of coupling at $\omega = D$, as $g_R(D) = g$, we have [97,98]:

$$g_R(\omega) = g^* - \zeta\left(\frac{\omega}{T_K}\right)^{\Delta}, \tag{3.22}$$

where Δ is the slope of the β-function which depends on the presence of the coupling to the gauge field. The position of the fixed point, g^*, Eq. (3.17) is not influenced by the gauge field. The Kondo temperature is $T_K = D(T_K^{(0)}/D)^{\Delta_0/\Delta}$, where $T_K^{(0)} =$

[2]The fact that g^* does not change up to $O(1/N^2)$ becomes clear if we multiply the second line of Eq. (3.20) by the $(1-\kappa)$ as well. Such operation is allowed, as it leaves intact all terms up to $O(1/N^3)$.

$Dg^{N/2}\exp(-1/g)$ is the Kondo scale for the case without a gauge field, and $\zeta = (g^*)^2/e$. We assumed here that $\omega < T_K$ and that the initial value of coupling, g, is small.

The power law behavior of the running coupling leads to a similar behavior in different physical quantities. Corrections to different measurable properties within perturbation theory can be expressed as a series in coupling g. Applying the renormalization group to this series results in singular behavior as a function of frequency or temperature with exponent proportional to Δ. For the case when there is no gauge field present, this program has been implemented in Refs. [97,98]. Generalization of this procedure to the case with the gauge field is straightforward.

The main effect of the gauge field is always related to the different values of slope of β-function, Δ. Without a gauge field $\Delta = \Delta_0$ is given by Eq. (3.18). When there is a gauge field, we have $\Delta = \Delta_1$, specified in Eq. (3.21). While for thermodynamical quantities this is the only effect, transport properties and other quantities acquire small corrections to prefactors which are not given here.

Calculating the contribution of impurity to the imaginary part of self-energy of fermions gives the scattering rate due to the impurity. As a function of frequency, it acquires a cusp at $\omega = 0$,

$$\nu\tau_{\rm imp}^{-1}(\omega) = \frac{3\pi n_{\rm imp}}{2N^2}\left[1 - N\zeta\left(\frac{\omega}{T_K}\right)^{\Delta}\right], \tag{3.23}$$

which has to be contrasted with a Lorentzian shape of $\nu\tau_{\rm imp}^{-1}(\omega)$ for a Fermi liquid fixed point. The correction to the resistivity due to Kondo interaction has a similar form, however, it is of little interest due to neutral character of fermionic excitations in spin liquid. The correction to the heat conductivity is potentially more interesting. Using Eq. (3.23) and assuming that impurity scattering time $\tau_{\rm imp}$ is much longer that the relaxation time without impurity, τ_0, we find the correction to the inverse two-dimensional thermal conductivity

$$\delta[\kappa_{\rm th}^{-1}] = \frac{9}{N^2}\frac{\hbar}{k_B^2 T}\frac{n_{\rm imp}}{n}\left[1 - N\zeta\left(\frac{T}{T_K}\right)^{\Delta}\right], \tag{3.24}$$

where we restored $\hbar$, and k_B is the Boltzmann constant.

Also one can calculate corrections to different thermodynamic properties. A rigorous calculations of the self-energy allows us to find impurity specific heat with a critical exponent $\alpha = 2\Delta$:

$$C_{\text{imp}} = \frac{3\pi^2}{2}\zeta^2\Delta\left(\frac{T}{T_K}\right)^{2\Delta}. \tag{3.25}$$

Magnetic properties, such as the impurity susceptibility as temperature $T \to 0$ and dependence of magnetization on the field $h = \mu_B H$ at $T = 0$ are given by

$$\chi_{\text{imp}} = \left(\frac{N\zeta}{2}\right)^2 \frac{1}{T}\left(\frac{T}{T_K}\right)^{2\Delta}, \tag{3.26}$$

$$M = \frac{N\zeta}{2}\left(\frac{h}{T_K}\right)^{\Delta}. \tag{3.27}$$

Likewise, it is possible to find an expression for fermion-fermion, fermion-impurity and impurity-impurity susceptibilities [97]. Lastly, we list results for $\chi''_{\text{imp}}(\omega, T)/\omega$ which is a contribution to the NMR relaxation rate due to the impurity. Its behavior is again specified by Δ, and for $\omega \ll T$

$$\frac{\chi''_{\text{imp}}(\omega, T)}{\omega} \propto T^{2\Delta-2}. \tag{3.28}$$

3.3 Discussion

We have investigated the effect of the gauge field strongly coupled to fermions at a non-Fermi liquid overscreened Kondo fixed point. Using the double expansion framework, we demonstrated that the gauge field does not alter the position of the perturbatively accessible non-Fermi-liquid fixed point, but leads to corrections to exponents characterizing the behavior of different physical properties in the vicinity of the fixed point. In particular, it "softens" the non-analytic behavior of specific heat, magnetization, spin susceptibility, compared to those for a Kondo problem without the gauge field. The physical origin of this effect is the "smearing" of the sharp

quasiparticles by the gauge field.

Let us discuss the extrapolation to the physical case. In order to have a control over calculations, we worked in the double expansion limit, Eq. (3.12), with N species of spin-half fermions. We note, that if the coupling to gauge field was absent, the considered model for $N = 4$ corresponds to the one channel of spin-one itinerant moments coupled to impurity [95, 99]. The same equivalence was checked to hold in our perturbative calculations of β-function for the case when there is a coupling to the gauge field.

Thus, we expect that the physical case corresponds to $N = 4$, $\varepsilon = 1$. Assuming that our results can be extrapolated to these values of N and ε, we can argue that the non-Fermi-liquid Kondo fixed point is not destroyed by the presence of a gauge field. However, we expect singularities in different physical properties related to the non-Fermi-liquid fixed point to be weakened compared to their values without gauge field. In such a case, the realization of overscreened Kondo physics in $S = 1$ spin liquid may be used not only to observe neutral fermionic excitations, but as evidence for the presence of a gauge field. Indeed, non-Fermi-liquid behavior may be used as an indication of fermionic excitations present in the system. At the same time, the difference of observed scalings from those for the case without a gauge field [91,99] may be used as a litmus test for the presence of a gauge field coupled to fermions. From an experimental point of view, specific heat (proportional to impurity concentration), as well as spin susceptibility and NRM relaxation rate are the most promising probes.

It is instructive to compare the role of the gauge field in our case to the case of the Kondo model in the regime of perfect screening, Ref. [132]. In the latter case, the system flows to the infinite coupling fixed point, and the results of Ref. [132] show no changes in impurity specific heat and spin susceptibility due to the presence of the gauge field.

Finally, we discuss possible experimental realizations of our proposal. In a recent experiments [32, 133] materials that could possibly realize the spin liquid with fermionic excitations [2, 136, 139] has been found. One can speculate on the possible stabilization of U(1) spin liquid phase in the same or similar type of materials. The

presence of spin-half impurities in such a phase would realize the scenario considered in our work. Another way to implement the discussed physics is to go to lower dimensions. A gapless phase for spin-1 with bilinear and biquadratic interaction has been established for a certain range of couplings. [153–157]. A spin-half impurity in such a chain is expected to realize overscreened Kondo physics. A detailed consideration of this problem is an interesting and open question.

Chapter 4

Spinon-phonon interaction in algebraic spin liquid

In this Chapter following Ref. [4] we study the interaction of spinons with lattice vibrations. This study is motivated by a search for experimental probes to access the physics of fractionalized excitations called spinons in a spin liquids, We consider the case of algebraic spin liquid, when spinons have fermionic statistics and a Dirac-like dispersion. We establish the general procedure for deriving spinon-phonon interactions which is based on a symmetry considerations. The procedure is illustrated for four different algebraic spin liquids: π-flux and staggered-flux phases on a square lattice, π-flux phase on a kagome lattice, and zero flux phase on a honeycomb lattice. Although the low energy description is similar for all these phases, different underlying symmetry group leads to a distinct form of spinon-phonon interaction Hamiltonian. The explicit form of the spinon-phonon interaction is used to estimate the attenuation of ultrasound in an algebraic spin liquid. The prospectives of the sound attenuation as probe of spinons are discussed.

4.1 Introduction

Unambiguous experimental identification of a spin liquid [8, 25], an exotic ground state of a spin system in a dimension larger than one without a magnetic order

remains an open question [48]. A number of theoretical scenarios leads to a ground state with charge-neutral excitations, which carry spin-1/2 quantum number and have fermionic statistics. These excitations, called spinons, may have a Fermi surface or a Dirac spectrum [9, 48], and are usually strongly coupled to a gauge field. The latter case, so-called Dirac spin liquid phase, will be the primary subject of attention in the present paper.

Naively, one would expect that the presence of fermionic excitations in the system could be easily tested experimentally. However, measurements of different thermodynamic quantities, such as spin susceptibility or specific heat, often require subtraction and extrapolation to zero temperature, which can be ambiguous. Transport measurements are limited to a heat conductivity due to neutral character of spinons. The heat transport measurements are difficult to perform at low temperature. Finally, neutron scattering, potentially a direct probe of spinons [29,158], requires large single crystals which are not always available. The difficulties with experimental detection of spin liquid phases has lead to a number of theoretical proposals. These include but are not limited to Raman scattering [143], inelastic X-rays scattering [144], Friedel oscillations [145], electron spin resonance [159], impurity physics [3, 130, 132], and optical conductivity [160, 161].

Coupling between spinons and phonons can open another channel of decay for phonons, and change the attenuation of ultrasound. Thus, the sound attenuation is another potential probe of spinons.[1] The case of spin liquid with spinon Fermi surface has been recently considered by Zhou and one of us in Ref. [47]. The spinon-phonon interaction in the long wavelength limit was deduced from hydrodynamical arguments [47,162,163]. Assuming that electrons stay in equilibrium with lattice (due to presence of impurities) and making canonical transformation to the moving frame one can easily derive interaction Hamiltonian. The same interaction Hamiltonian can be reproduced from microscopical considerations using so-called deformable ions model [164, 165].

[1]Also, optical phonons has been suggested as a possible mean for detection of VBS order in Ref. [6].

However, as was pointed out in Ref. [47], spinons with a Dirac spectrum require a different treatment. Here we address this problem and consider the contribution of spinons to the attenuation of ultrasound in a Dirac spin liquid. In contrary to the case of electrons [163–165] or spinons with Fermi surface [47], it appears that there is no universal form for the interaction of spinons with acoustic phonons in Dirac spin liquid. This is related to the spinor nature of spinons with Dirac dispersion. Similarly to graphene, spinor structure describes the character of wave function on different sublattices, i.e. on the microscopic scale. Consequently, one possible route of deducing the form of spinon-phonon interaction would be to find the change of the Hamiltonian of electronic subsystem induced by the long wave modulation of the lattice parameters, starting from a microscopic Hamiltonian. This procedure, although giving explicit values of coupling constants is not universal. It depends on the microscopic implementation of a different spin liquid phase. Moreover, it is difficult to guarantee that one finds all possible terms in the interaction Hamiltonian.

We adopt a different approach and use symmetry considerations to find a spinon-phonon interaction Hamiltonian. Similar route has been recently used to deduce electron-phonon interaction in graphene [7, 166]. There, representations of the lattice symmetry group of the honeycomb lattice on continuous Dirac fields were used to find all possible symmetry allowed electron-phonon couplings [7]. However, in a Dirac spin liquid, also referred to as an algebraic spin liquid, the notion of symmetry group has to be extended to the projective symmetry group [10, 22].

In this paper we generalize the derivation of spinon-phonon interaction Hamiltonian to the case of projective representation of lattice symmetry group. The procedure is straightforward, and it requires studying the representation of symmetry group on spin-singlet fermionic bilinears. We consider four different realizations of the Dirac spin liquid: π-flux [23] and staggered-flux [5] phases on a square lattice, as well as π-flux phase on a kagome lattice [6] and a Dirac spin liquid phase on a honeycomb lattice. Within low energy effective field theory, all these phases can be described in terms of a Dirac excitations, coupled to a gauge field [5, 6, 23, 167–170]. Nevertheless, these phases retain the information about their microscopic origin. This information

is encoded in the projective representation of spinon operators under the action of the corresponding symmetry group.

As we will see below, the projective character of the representation of symmetry group has a profound consequences on a spinon-phonon interaction. For all algebraic spin liquid phases considered here except for the Dirac spin liquid on a honeycomb lattice, only the coupling to the density of spinons is allowed by symmetry at the leading order. However, we find that this coupling is screened due to the gauge field. The sound attenuation coming from the next order terms is suppressed by an extra factor and behaves as T^3 at low temperatures. In contrast, the Dirac spin liquid on a honeycomb lattice has a sound attenuation $\propto T$. Although the sound attenuation in all cases is suppressed compared to the case of a spin liquid with a Fermi surface, the spinon contribution is still the dominant process at low temperature and experimental observation of the attenuation of ultrasound due to spinons may be possible.

This Chapter is organized as follows. Section 4.2 introduces the low energy description of Dirac spin liquid and projective symmetry group. We use the π-flux phase on a square lattice as an example. Next, we discuss interaction of spinons with phonons in Section 4.3. We describe the general procedure of obtaining spinon-phonon interaction Hamiltonian from symmetry considerations. It is later illustrated in more details for the π-flux phase on a square lattice. Having found the interaction Hamiltonian, in Section 4.4 we study the sound attenuation, concentrating on attenuation of longitudinal sound. Finally, in Section 4.5 we summarize and discuss our results. Basic facts from the representation theory of finite groups and details on the calculation of sound attenuation are given in Appendix C.

4.2 Low energy description of algebraic spin liquids

We review the description of algebraic spin liquid fixed point using language of low energy effective field theory [5, 6, 23, 167–170]. This description suits our purposes since we are interested in coupling between acoustic phonons in the low energy limit. In addition, it provides universal framework applicable to a variety of different alge-

braic spin liquid phases. In short, three ingredients are needed in order to specify low energy field description of a given algebraic spin liquid phase. These are low energy Hamiltonian for continuous fields, gauge group and representation of projective symmetry group specified by its action on fields. Below we review these ingredients for the general case, as well as illustrate them for the π-flux phase on a square lattice (πF$\square$ phase). We do not list details for the staggered flux phase on a square lattice (sF$\square$), π-flux on kagome lattice (πF$\hexagon$), and Dirac spin liquid phase on honeycomb lattice (0F$\bigcirc$). The reader is referred to Refs. [5, 6, 23] for more details, specific for these phases.

4.2.1 Effective field theory and projective symmetry group

The starting point is the spin $S = 1/2$ model on some (not necessary Bravais) two-dimensional lattice. The symmetries of spin Hamiltonian are assumed to include SU(2) spin rotations, time reversal and the full lattice group of a given lattice. We write Hamiltonian as

$$H = \sum_{\langle \boldsymbol{ij} \rangle} J_{\boldsymbol{ij}} \vec{S}_{\boldsymbol{i}} \cdot \vec{S}_{\boldsymbol{j}} + \ldots, \tag{4.1}$$

where bold indices $\boldsymbol{i}, \boldsymbol{j}$ denote lattice sites and sum goes over nearest neighbor pairs of sites. Ellipses denotes other short-range interaction terms required to stabilize required spin liquid phase.

In order to get access to phases with no spin order, we use slave-fermion mean field theory. As discussed in Chapter 1, we represent spin operators using spinon operators $f_{\boldsymbol{i},\alpha}$, $\alpha = \uparrow, \downarrow$:

$$\vec{S}_{\boldsymbol{i}} = \frac{1}{2} f^{\dagger}_{\boldsymbol{i}\alpha} \boldsymbol{\sigma}_{\alpha\beta} f_{\boldsymbol{i}\beta}. \tag{4.2}$$

The mapping between Hilbert spaces is exact, provided one imposes a constraint of no double occupancy, $f^{\dagger}_{\boldsymbol{i}\alpha} f_{\boldsymbol{i}\alpha} = 1$, where summation over repeating indices is implied. Such representation of spin has SU(2) gauge redundancy. Therefore, mean field decoupling of spin interaction has to include SU(2) gauge field on the links of the lattice. Saddle points of the mean field theory, depending on their structure [10,22] may break

this SU(2) symmetry down to U(1) or $\mathbb{Z}_2$.

We will be mostly interested in phases with U(1) gauge symmetry (the only SU(2)-symmetric algebraic spin liquid phase considered here is the πF$\square$ phase [10]). General lattice gauge theory Hamiltonian at the saddle point is

$$H_{\mathrm{U}(1)} = \frac{h}{2}\sum_{\langle ij\rangle} e_{ij}^2 - K\sum_{\text{plaq.}} \cos(\phi_{\square}) + \sum_{\langle ij\rangle}[\chi_{ji}e^{-\mathrm{i}a_{ji}} f_{i\alpha}^{\dagger} f_{j\alpha} + \text{H. c.}], \tag{4.3}$$

where we assume that the choice of χ_{ij} leads to a Dirac spectrum. The gauge redundancy lead to appearance of a_{ij}, a compact U(1) vector potential living on the bonds of the lattice, and e_{ij} which is canonically conjugate electric field taking integer values. We also defined $\phi_{\square}$, living on the dual lattice, as the lattice version of curl of gauge field a_{ij}. Gauge constraint is $(\mathrm{div}\, e)_i + f_{i\alpha}^{\dagger} f_{i\alpha} = 1$. Although initially vector potential does not have any kinetic terms, these will be generated due to coupling with fermions and are written in (4.3) with coefficient K. For $K = 0$, $h \gg |\chi_{ij}|$, one recovers spin model from Eq. (4.3). Mean field is a good approximation when $K \gg |\chi_{ij}| \gg h$ and describes the algebraic spin liquid phase. It has been argued that this phase is stable [5, 23]. Monopoles are irrelevant, leading to the gauge group becoming non-compact in the low energy limit. Therefore it should be accessible starting from the spin Hamiltonian in Eq. (4.1) for some range of initial parameters. More detailed discussion of stability of algebraic spin liquid phase is presented in Refs. [5, 23].

Provided that choice of χ_{ij} leads to a Dirac spectrum, we use continuous fermionic fields to write low-energy Hamiltonian. In the momentum space it reads

$$H = v_F \int \frac{d^2\boldsymbol{k}}{(2\pi)^2} \psi_{\sigma a\alpha}^{\dagger}[(\boldsymbol{k} - \boldsymbol{a})\cdot \boldsymbol{\tau}_{\alpha\beta}]\psi_{\sigma a\beta}. \tag{4.4}$$

The indices σ, a and α in continuous eight-component fermion field $\psi_{\sigma a\alpha}$ label spin, Dirac valley and sublattice respectively. In what follows, we will use three different sets of Pauli matrices acting in different spaces. Pauli matrices acting on the spin indices are denoted as $\{\sigma^x, \sigma^y, \sigma^z\}$. The second index distinguishes between different

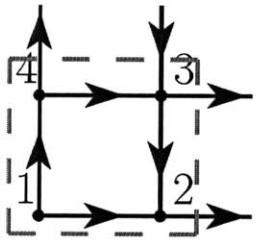

Figure 4-1: Choice of the anzats for the πF$\square$ phase. Red dashed line encloses the unit cell. Numbers indicate the labeling of sites, used in the main text. Hopping in the direction of arrows is proportional to +i.

Dirac points (valleys) and we label Pauli matrices acting in this space as $\{\mu^x, \mu^y, \mu^z\}$. Finally, Eq. (4.4) involves Pauli matrices $\{\tau^x, \tau^y, \tau^z\}$ acting on spinor (sublattice) indices. Below we will omit the sign of the tensor product implying *e.g.* $\sigma^y\tau^x = \sigma^y \otimes \mathbb{1} \otimes \tau^x$.

A particular choice of anzatz χ_{ij} naively violates some symmetries of the original Hamiltonian. However, representation Eq. (4.2) is invariant under the gauge transformations

$$f_i \to f_i e^{i\theta_i}, \qquad a_{ij} \to a_{ij} + \theta_i - \theta_j. \tag{4.5}$$

Consequently, there is a freedom in the choice of the action of different symmetries: one can supplement them with some gauge transformation. Requiring mean field Hamiltonian (4.3) to remain invariant we can fix this freedom and show that all symmetries of original spin Hamiltonian remain unbroken.

The fact that the action of symmetries on fermionic fields is supplemented by gauge transform has a deep consequences. Rather than forming usual representation of lattice symmetry group, fermions are said to realize *projective representation* of lattice symmetry group [10,22]. This representation is fully specified by the action of the lattice symmetry group generators on the fermionic fields. Knowing the mapping from the lattice fields $f_{i\alpha}$ to ψ, one can easily find the action of generators on the continuous fermionic field. Below, we will demonstrate this procedure for the πF$\square$ phase.

4.2.2 Example: π-flux spin liquid on a square lattice

We use the the πF$\square$ phase [23] to illustrate the abstract construction presented above. The starting point is the choice specific values of χ_{ij} in Eq. (4.3) to fix the mean field anzats. Our notations are different from those in Ref. [23]. We quadruple our unit cell, so it includes four sites. Sites within the new unit cell are labeled by an index $m = 1 \ldots 4$ as in Fig. 4-1. The χ_{ij} and a_i^0 are chosen as

$$\chi_{ii+\hat{x}} = \mathrm{i}, \qquad \chi_{ii+\hat{y}} = (-)^{i_x}\mathrm{i}; \qquad a_i^0 = 0. \tag{4.6}$$

Resulting mean field Hamiltonian with the spin index and gauge field omitted is:

$$H_{\mathrm{mf}} = -\frac{1}{2}J\sum_{r}[\mathrm{i}(f_{r2}^\dagger + f_{r4}^\dagger)f_{r1} + \mathrm{i}(f_{r3}^\dagger + f_{r+a_21}^\dagger)f_{r4} + \mathrm{i}(f_{r+a_11}^\dagger - f_{r3}^\dagger)f_{r2} + \mathrm{i}(f_{r+a_14}^\dagger - f_{r+a_22}^\dagger)f_{r3} + \mathrm{H.\,c.}], \tag{4.7}$$

where Bravais lattice vector $\boldsymbol{r} = n_1\boldsymbol{a}_1 + n_2\boldsymbol{a}_2$ with n_1, n_2 integers labels unit cells, and $\boldsymbol{a}_1 = 2\hat{\boldsymbol{x}}$, $\boldsymbol{a}_2 = 2\hat{\boldsymbol{y}}$. Making Fourier transform

$$f_{rm} = \frac{1}{\sqrt{N}}\sum_{\boldsymbol{k}} e^{\mathrm{i}\boldsymbol{k}\cdot\boldsymbol{r}} f_{km}, \tag{4.8}$$

where N is the number of unit cells, we obtain the Hamiltonian in momentum space

$$H_{\mathrm{mf}} = -\frac{J}{2}\sum_{\boldsymbol{k}} f_{km}^\dagger H_{mn}(\boldsymbol{k}) f_{kn}, \tag{4.9}$$

$$H_{mn}(\boldsymbol{k}) = \mathrm{i}\begin{pmatrix} 0 & -1+K_1^* & 0 & -1+K_2^* \\ 1-K_1 & 0 & 1-K_2^* & 0 \\ 0 & -1+K_2 & 0 & 1-K_1 \\ 1-K_2 & 0 & -1+K_1^* & 0 \end{pmatrix}, \tag{4.10}$$

with the notation $K_{1,2} = e^{\mathrm{i}\boldsymbol{k}\cdot\boldsymbol{a}_{1,2}}$. The momentum is measured in the units of the inverse lattice constant of the original lattice (i.e. before enlarging the unit cell), which is set to one in what follows. We choose the Brillouin zone as $k_x, k_y \in [-\pi/2, \pi/2)$.

The energy levels of the Hamiltonian (4.9)-(4.10) are doubly degenerate. Therefore there is only one doubly degenerate gapless Fermi point in the Brillouin zone, that is located at the momentum $\boldsymbol{Q} = (0,0)$. In the vicinity of this point the dispersion is described by Dirac fermions and we can define continuum fermion fields. We choose the following representation for two copies of spinor field $\psi_{a\alpha}(\boldsymbol{k})$:

$$\psi_1(\boldsymbol{k}) \sim \frac{1}{\sqrt{2}} \begin{pmatrix} \mathrm{i}f_{\boldsymbol{k}2} + f_{\boldsymbol{k}4} \\ -\mathrm{i}f_{\boldsymbol{k}1} - f_{\boldsymbol{k}3} \end{pmatrix}, \tag{4.11a}$$

$$\psi_2(\boldsymbol{k}) \sim \frac{1}{\sqrt{2}} \begin{pmatrix} f_{\boldsymbol{k}1} + \mathrm{i}f_{\boldsymbol{k}3} \\ -f_{\boldsymbol{k}2} - \mathrm{i}f_{\boldsymbol{k}4} \end{pmatrix}, \tag{4.11b}$$

where the index $a = 1, 2$ labels different Dirac points, $K_{\pm}$, both located at the Γ point of the Brillouin zone. Consequently, the low-energy continuum Hamiltonian is written as

$$H_{\mathrm{Dirac}} = v_F \int \frac{d^2\boldsymbol{k}}{(2\pi)^2} \psi^{\dagger}_{\sigma a}(k_x\tau^x + k_y\tau^y)\psi_{\sigma a}, \tag{4.12}$$

where made spinor index implicit. Fermi velocity, provided lattice constant is set to one, coincides with J, $v_F = J$.

The continuous fields $\psi_{a\alpha}(\boldsymbol{k})$ realize a projective representation of the lattice symmetry group. This representation is fully specified if one knows the action of group generators on continuous fields. The relevant lattice symmetry group in this case, denoted as C'_{4v}, is different from the point symmetry group of square C_{4v} due to enlarged unit cell. Consequently, the group C'_{4v}, in addition to elements from C_{4v}, contains translations by a unit vectors of square lattice along x and y-axes. The full set of generators, action of which is to be specified below, contains rotation for angle $\pi/2$, $\mathcal{R}_{\pi/2}$, reflection of x-axis, $\mathcal{R}_x$ (these are generators of C_{4v}) and lattice translation by vector $\boldsymbol{a}_1$, T_x. In addition we also have to specify the action of time-reversal symmetry, $\mathcal{T}$, and charge conjugation operators, $\mathcal{C}$.

Let us illustrate the derivation of the action of reflection generator on the contin-

uous fields. Action of $\mathcal{R}_x$ on the unit cell may be symbolically shown as

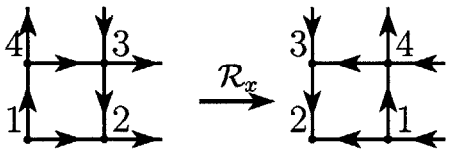

(4.13)

From here we can understand the action of $\mathcal{R}_x$ on the lattice fermion fields, as exchanging fermionic operators with indices $1 \leftrightarrow 2$ and $3 \leftrightarrow 4$. However, in order to leave Hamiltonian (4.7) invariant, this has to be supplemented by gauge transform that changes the sign of all hoppings [thus reversing the direction of all arrows in the r.h.s. of Eq. (4.13)]. One can easily check that transformation

$$f_{r1} \to f_{r'2}, \quad f_{r2} \to -f_{r'1}, \tag{4.14a}$$

$$f_{r3} \to f_{r'4}, \quad f_{r4} \to -f_{r'3}, \tag{4.14b}$$

$$\boldsymbol{r}' = \mathcal{R}_x \boldsymbol{r} = (-r_x, r_y) \tag{4.14c}$$

leaves Hamiltonian (4.7) invariant. The action of $\mathcal{R}_x$ on operators f_{rn} is easy to translate into representation of $\mathcal{R}_x$ on the continuous fermionic fields using their definition (4.11). In terms of different sets of Pauli matrices introduced above, it can be written as

$$\psi \to \mathcal{R}_x \psi \quad \text{with} \quad \mathcal{R}_x = \mathrm{i}\mu^z \tau^y. \tag{4.15}$$

Using analogous procedure we get the representation of the remaining generators to be

$$\mathcal{R}_{\pi/2} = \frac{1}{2}(\mu^x + \mu^y)(1 + \mathrm{i}\tau^z), \tag{4.16}$$

$$T_x = \mu^y. \tag{4.17}$$

Finally, for the π-flux phase there exist two additional SU(2) transformations not related to lattice symmetry group. These are time reversal, $\mathcal{T}$, defined as a antiunitary operator which flips the direction of spin operator (4.2), and charge conjugation, $\mathcal{C}$. The latter operation may be viewed an $SU(2)$ rotation in the spin space by π around

y-axis [23], supplemented by the particle-hole transformation. On the lattice level (in momentum space) these can be conveniently represented by

$$\mathcal{T}: \quad f_{k\sigma 1,3} \leftrightarrow f^{\dagger}_{k\sigma 1,3}, \qquad f_{k\sigma 2,4} \leftrightarrow -f^{\dagger}_{k\sigma 2,4}, \tag{4.18a}$$

$$\mathcal{C}: \quad f_{k\uparrow n} \rightarrow f^{\dagger}_{-k\downarrow n}, \qquad f_{k\downarrow n} \rightarrow -f^{\dagger}_{-k\uparrow n}, \tag{4.18b}$$

where $\mathcal{T}$-reversal also includes complex conjugation operation, spin indices were restored. Although these definitions may look counterintuitive, one can check that the charge conjugation (4.18b) indeed leaves the spin operator invariant, whereas the time-reversal symmetry, defined as in (4.18a), flips the direction of spin operator in Eq. (4.2). Mapping this action to continuous fermionic fields, we have:

$$\mathcal{T}: \quad \psi \rightarrow \ \mu^z \tau^z (\psi^{\dagger})^T, \tag{4.19a}$$

$$\mathcal{C}: \quad \psi \rightarrow \ (\mathrm{i}\sigma^y)(\mathrm{i}\mu^x \tau^x)(\psi^{\dagger})^T. \tag{4.19b}$$

As we pointed out earlier, the representation of the lattice symmetry group on fermions is projective. This can be easily seen from the action of generators, Eqs. (4.15)-(4.17), if one tries to test some group identities. For example, $(\mathcal{R}_{\pi/2})^4$ is a trivial transformation. However, using the explicit form of the representation of $\mathcal{R}_{\pi/2}$ for continuous fermionic fields, Eq. (4.16), we find

$$(\mathcal{R}_{\pi/2})^4 = -\mathbb{1}. \tag{4.20}$$

Thus all group identities hold only up to some gauge transformation, which leaves the Hamiltonian invariant.

4.3 Spinon-phonon interaction

Having a low energy description of Dirac spin liquid phases at our disposal, in this section we consider the spinon-phonon interaction.

As we explained in the introduction, the hydrodynamic approach [47, 162, 163],

applicable for the case of spin liquid with the Fermi surface, is not straightforward to use in our case. It is the presence of spinor structure, inherently related to the microscopic details such as two inequivalent sublattices, that prevents application of hydrodynamical arguments. Of course one can always resort to the microscopic derivation of spinon-phonon interaction. Despite the advantage of giving specific values of coupling constants, this route is highly non-universal and is not guaranteed to yield all possible couplings.

We present universal procedure for finding all possible terms in spinon-phonon interaction Hamiltonian, allowed by symmetry. First, we introduce phonons and the general form of the spinon-phonon interaction Hamiltonian. After this the general idea behind the procedure is described. Implementation of this procedure for the πF$\square$ phase serves as an example. Finally, we present results for other Dirac spin liquid phases and discuss the underlying physics. The derivation of these results extensively relies on a representation theory for finite groups. Necessary concepts, as well as basic facts about point groups of square, kagome and honeycomb lattices are listed in Appendix C.1.

4.3.1 Spinon-phonon interaction Hamiltonian from symmetry considerations

We start with specifying conventions for the spinon-phonon interaction Hamiltonian. It is written using the operator $\hat{H}_{\text{s-ph}}(\boldsymbol{k}, \boldsymbol{q})$ as

$$\mathcal{H}_{\text{s-ph}} = \sum_{\boldsymbol{k},\boldsymbol{q}} \psi^\dagger(\boldsymbol{k}+\boldsymbol{q}) \hat{H}_{\text{s-ph}}(\boldsymbol{k}, \boldsymbol{q}) \psi(\boldsymbol{k}). \tag{4.21}$$

In what follows we will refer to the operator $\hat{H}_{\text{s-ph}}(\boldsymbol{k}, \boldsymbol{q})$ itself as a spinon-phonon interaction Hamiltonian. Normally, the operator $\hat{H}_{\text{s-ph}}(\boldsymbol{k}, \boldsymbol{q})$ obtained from the procedure described above, would contain only zeroth order terms in the distance from the Dirac point, $\boldsymbol{k}$, $\hat{H}_{\text{s-ph}}(\boldsymbol{k}, \boldsymbol{q}) = \hat{H}_{\text{s-ph(0)}}(\boldsymbol{q})$. As we shall see, in some cases, all such terms vanish. Then, to find a non-zero interaction Hamiltonian, we allow the pres-

ence of terms, linear in $\boldsymbol{k}$, $\hat{H}_{\text{s-ph(1)}}(\boldsymbol{k},\boldsymbol{q})$ and the total Hamiltonian will be written as a sum:

$$\hat{H}_{\text{s-ph}}(\boldsymbol{k},\boldsymbol{q}) = \hat{H}_{\text{s-ph(0)}}(\boldsymbol{q}) + \hat{H}_{\text{s-ph(1)}}(\boldsymbol{k},\boldsymbol{q}), \tag{4.22}$$

In what follows, we restrict ourselves to the first non-vanishing term in this expansion. Phonons enter $\hat{H}_{\text{s-ph}}(\boldsymbol{k},\boldsymbol{q})$ via the $\boldsymbol{q}$ Fourier component of displacement field, $\boldsymbol{u}(t,\boldsymbol{r})$. In the second quantized language the displacement field is written as

$$\boldsymbol{u}(t,\boldsymbol{r}) = \sum_{\boldsymbol{q},\mu} \sqrt{\frac{\hbar}{2S\rho\omega_{\boldsymbol{q}}}} \boldsymbol{e}_{\boldsymbol{q}\mu}(a_{\boldsymbol{q}\mu}e^{-\mathrm{i}\omega_{\boldsymbol{q}}t+\mathrm{i}\boldsymbol{q}\cdot\boldsymbol{r}} + a^{\dagger}_{-\boldsymbol{q}\mu}e^{\mathrm{i}\omega_{\boldsymbol{q}}t-\mathrm{i}\boldsymbol{q}\cdot\boldsymbol{r}}), \tag{4.23}$$

where index μ = L,T labels longitudinal and transverse modes of acoustic phonons, and $\boldsymbol{e}_{\boldsymbol{q}\mu}$ is the corresponding polarization vector. The dispersion of phonons is assumed in the form $\omega_{\boldsymbol{q}} = v_s|\boldsymbol{q}|$, where v_s is the sound velocity. The ρ is defined as a mass density per layer, and S is the area. For simplicity we consider only in-plane phonon modes.

Although we work in continuum limit, it is the lattice symmetry group and its representations, which determines the properties of low energy (acoustic) phonons and spinon excitations. Phonons are described using vector $\boldsymbol{u}(t,\boldsymbol{r})$, describing displacement at a given point $\boldsymbol{r}$ due to deformation. As a uniform displacement of the entire lattice, $\boldsymbol{u}(t,\boldsymbol{r}) = \boldsymbol{u}_0$, leaves system invariant, acoustic phonons can couple to spinons only via spatial derivatives of $\boldsymbol{u}(\boldsymbol{r})$ [we ignore coupling to the time derivative, as it is suppressed by the ratio of sound and Fermi velocities]. Set of all spatial derivatives, $\partial_i u_j(\boldsymbol{r})$ or $-\mathrm{i}q_i u_j(\boldsymbol{q})$ in the Fourier space, transforms as a rank-two tensor under lattice symmetry group. Representation of a lattice symmetry group on a rank-two tensor can be split as a sum of irreducible representations. Symbolically this is written as

$$E_1 \times E_1 = \sum_j \oplus D_j^{\text{ph}}, \tag{4.24}$$

where E_1 is vector representation, and D_j^{ph} are (possibly repeating) irreducible representations. Acoustic phonon modes can be classified using irreducible components, present in this decomposition.

Rep.	A_1	A_2	B_1'	B_2'	E_1	E_2	E_1'	E_3	E_4	E_5
Basis	$\mathbb{1}$	τ^z	μ^z	$\mu^z\tau^z$	$\tau^{x,y}$	$\mu^{x,y}$	$\mu^z\tau^{x,y}$	$\mu^{x,y}\tau^z$	$\mu^x\tau^y, \mu^y\tau^x$	$\mu^x\tau^x, \mu^y\tau^y$
$\mathcal{T}$-inv	$-$	$-$	$-$	$-$	$+$	$+$	$+$	$+$	$-$	$-$
$\mathcal{C}$-inv	$-$	$+$	$+$	$-$	$-$	$-$	$+$	$+$	$-$	$-$

Table 4.1: Explicit form of basis in terms of tensor products of Pauli matrices for irreducible representations of C_{4v}' contained within $G_{\psi^\dagger\psi}^{\pi F}$. Last two rows show properties of basis elements under time-reversal and charge conjugation. Plus implies invariance, whereas minus indicates a change of sign under the action of corresponding symmetry.

Spinons have fermionic statistic, thus minimal coupling to phonons must involve bilinears of ψ field. In contrary to phonons, continuous spinon fields ψ realize *projective* representation of the lattice symmetry group. Action of lattice symmetries on ψ in general includes the gauge transformation, and all identities between generators are valid modulus gauge transformation [for example, see Eq. (4.20)]. Similar to a single field ψ, general spinon bilinear also realizes projective representation of lattice symmetry group. However, there exists a *subset* of spinon bilinears which transform under regular representation of symmetry group. For the case when the gauge group is SU(2) these are bilinears which are singlets under SU(2). Whereas for abelian gauge groups, like U(1) or $\mathbb{Z}_2$, *all* bilinears realize regular representation, as gauge component cancels.

Regular representation of the lattice symmetry group on (a subset of) spinon bilinears can be split into irreducible representations $D_j^{\psi^\dagger\psi}$,

$$G_{\psi^\dagger\psi} = \sum_j \oplus D_j^{\psi^\dagger\psi}. \tag{4.25}$$

We note, that invariant fermionic bilinears for πF$\square$, sF$\square$ and πF$\hexagram$ phases were identified in Refs. [5, 6, 23]. This corresponds to finding all trivial components contained within decomposition (4.25).

The product of two irreducible representations, $D_i^{\text{ph}} \times D_j^{\psi^\dagger\psi}$ contains a trivial representation within itself if, and only if these representations coincide, $D_i^{\text{ph}} \equiv D_j^{\psi^\dagger\psi}$. As the spinon-phonon interaction Hamiltonian has to be invariant under the action

of the symmetry group, we can construct all symmetry allowed couplings by pairing identical irreducible components between splittings (4.24) and (4.25). The presence of additional symmetry operations, such as time-reversal or charge conjugation may impose further restrictions on the obtained set.

4.3.2 Example: derivation for the π-flux phase

We use the πF phase as an example for an illustration of the abstract procedure outlined above. For phonons, the underlying symmetry group is C_{4v} (see Appendix C.1.2). Using characters Table C.1, we find explicit form of the decomposition (4.24) for the present case:

$$E_1 \times E_1 = A_1 \oplus A_2 \oplus B_1 \oplus B_2. \tag{4.26}$$

A_1 here and in what follows always denotes the trivial representation. All other representations are also one-dimensional, thus the action of corresponding group elements can be inferred from Table C.1 in the Appendix. In terms of components of two vectors (q_x, q_y) and (u_x, u_y), the basis functions of these representations are

$$A_1 : u_{xx} + u_{yy}, \qquad A_2 : u_{xy} - u_{yx}, \tag{4.27a}$$

$$B_1 : u_{xx} - u_{yy}, \qquad B_2 : u_{xy} + u_{yx}, \tag{4.27b}$$

where we introduced shorthand notation

$$u_{ij} \equiv q_i u_j. \tag{4.28}$$

While introducing the ansatz for πF$\Box$ phase in Section 4.2.2 we used unit cell consisting of four lattice sites. This allowed us to write relations between continuous fields and microscopic spinon operators in a simple form. However, the price to pay is that spinons now transform under the symmetry group C'_{4v} which is larger than point symmetry group of the square lattice. In addition to transformations from the point group of the square C_{4v}, group C'_{4v} includes lattice translations by unit vector in $\hat{x}$ and $\hat{y}$ directions. The details about irreducible representations of group C'_{4v} are worked out

in Appendix C.1.2. It has eight one-dimensional irreducible representations labelled as $A_{1,2}, B_{1,2}$ and $A'_{1,2}, B'_{1,2}$ in Table C.3, and six two-dimensional representations denoted as $E_1, E'_1, E_{2,\ldots,5}$. To find the splitting of representation of C'_{4v} on spinon bilinears into irreducible components we use natural basis: all spin singlet bilinears can be enumerated using tensor products of Pauli matrices acting in sublattice and valley space,

$$\psi^\dagger M \psi, \qquad M \in \{\mathbb{1}, \tau^i, \mu^i, \tau^i\mu^j\}. \tag{4.29}$$

With the help of the characters Table C.3, the 16-dimensional representation $G^{\pi F}_{\psi^\dagger\psi}$ is reduced into direct sum of four one-dimensional and six two-dimensional representations as

$$G^{\pi \mathrm{F}}_{\psi^\dagger\psi} = A_1 \oplus A_2 \oplus B'_1 \oplus B'_2 \oplus E_1 \oplus E'_1 \oplus E_2 \oplus E_3 \oplus E_4 \oplus E_5. \tag{4.30}$$

Using the explicit basis (4.29), we can find to what irreducible representation a given matrix belongs. Identity matrix $\mathbb{1}$ corresponds to the trivial representation, A_1. Next, one can check that both matrices μ^z, τ^z, and their product, $\mu^z\tau^z$, are invariant (up to a sign) under the action of all generators of C'_{4v}, Eqs. (4.15)-(4.17). Therefore the matrices μ^z, τ^z, and $\mu^z\tau^z$ form the basis of one-dimensional representations A_2, B'_1 and B'_2 respectively. Matrices (τ^x, τ^y), $(\mu^z\tau^x, \mu^z\tau^y)$, and (μ^x, μ^y) constitute basis of two-dimensional irreducible representations E_1, E'_1 and E_2 respectively. Finally, after some algebra, the remaining six matrices from (4.29) can be split into pairs that realize the basis for representations $E_3, \ldots, E_5$ as shown in the Table 4.1. The last two rows in Table 4.1 display the symmetry of corresponding matrices under the action of time reversal and charge conjugation operations.

Explicit decompositions, Eqs. (4.26) and (4.30) give us allowed couplings between spinons and phonons. Only identical irreducible representations can be coupled between themselves. Comparing Eqs. (4.26) and (4.30) we see that only two first terms in both direct sums coincide. Thus one may expect the allowed couplings to be described by contraction between A_1 (A_2) components in different sums. However, according to Table 4.1, the bilinear $\psi^\dagger\mathbb{1}\psi$ is odd under both time-reversal and charge

Rep.	A_2	B_1	B_1'	A_2'	E_1'	E_3	E_4	E_5
Basis	τ^z	$\tau^z\mu^z$	μ^z	$\mathbb{1}$	$\tau^{x,y}, \mu^z\tau^{x,y}$	$\mu^{x,y}, \tau^z\mu^{x,y}$	$\mu^{x,y}(\tau^x \mp \tau^y)$	$\mu^{x,y}(\tau^x \pm \tau^y)$
$\mathcal{T}$-inv	$-$	$-$	$-$	$-$	$+$	$+$	$-$	$-$

Table 4.2: Explicit form of basis for different irreducible representations of C_{4v}' contained within $G_{\psi^\dagger\psi}^{\text{sF}\square}$. Action of the group generators coincides with Ref. [5]. Last row summarizes the transformation of basis elements under time-reversal symmetry.

conjugation, and $\psi^\dagger\tau^z\psi$ is odd under time reversal. As different components of u_{ij} are invariant under time-reversal and charge conjugation, we conclude that at the leading order no couplings of spinons to phonons are allowed by symmetry, $\hat{H}^{\pi\text{F}\square}_{\text{s-ph(0)}}(\boldsymbol{q}) = 0$.

To find a non-zero coupling of spinons to phonons, we allow for the presence of spinon momentum, $\boldsymbol{k}$ in the coupling Hamiltonian. This corresponds to the next order in the expansion around the Dirac points. The spinon momentum, $\boldsymbol{k}$, transforms under the usual vector representation E_1 [this can be inferred from the fact that Dirac Hamiltonian, Eq. (4.12) is invariant] and is invariant under time reversal, but odd under charge conjugation. The product $E_1 \times G_{\psi^\dagger\psi}^{\pi\text{F}}$ is reduced as

$$E_1 \times G_{\psi^\dagger\psi}^{\pi\text{F}} = A_1 \oplus A_2 \oplus B_1 \oplus B_2 \oplus A_1' \oplus A_2' \oplus B_1' \oplus B_2' \\ \oplus 2(E_1 \oplus E_1' \oplus E_2 \oplus E_3 \oplus E_4 \oplus E_5). \quad (4.31)$$

The first four irreducible representations, which are of interest for us [compare with Eq. (4.26)], originate from the E_1 component within $G_{\psi^\dagger\psi}^{\pi\text{F}}$. Consequently, their basis is analogous to Eq. (4.27). The first four irreducible representations $A_1 \ldots B_2$ from Eq. (4.31) can be coupled to corresponding irreducible representations in Eq. (4.26). For example, coupling representation A_1 with basis $k_x\tau^x + k_y\tau^y$ to A_1 component with basis $u_{xx} + u_{yy}$ results in contribution

$$\hat{H}^{\pi\text{F}\square}_{\text{s-ph(1)}} = g^{(1)}_{A_1}(u_{xx} + u_{yy})\left[k_x\tau^x + k_y\tau^y\right], \quad (4.32)$$

with a phenomenological coupling constant $g^{(1)}_{A_1}$. Dependence on $\boldsymbol{k}, \boldsymbol{q}$ will be suppressed for brevity in what follows, $\hat{H}_{\text{s-ph(1)}} \equiv \hat{H}_{\text{s-ph(1)}}(\boldsymbol{k}, \boldsymbol{q})$. Collecting all contri-

butions at this order, and rearranging phenomenological coupling constants (*e.g.* $g^{(1)}_{1,4} = g^{(1)}_{A_1} \pm g^{(1)}_{B_1}$) we get the most general form of the spinon-phonon interaction Hamiltonian in the πF phase to be

$$\hat{H}^{\pi\mathrm{F}\square}_{\text{s-ph}} = g^{(1)}_1(u_{xx}k_x\tau^x + u_{yy}k_y\tau^y) + g^{(1)}_2(u_{xy}k_x\tau^x + u_{yx}k_y\tau^y) + g^{(1)}_3(u_{yx}k_x\tau^x + u_{xy}k_y\tau^y) + g^{(1)}_4(u_{xx}k_y\tau^y + u_{yy}k_x\tau^x). \quad (4.33)$$

4.3.3 Results for the sF□, πF✡, and 0F○ phases

After detailed derivation of spinon-phonon interaction for the π-flux phase on a square lattice, we present results for other algebraic spin liquid phases considered in this work.

The staggered-flux phase on a square lattice is similar to the πF□ phase, considered above. However, in contrary to the π-flux phase, there is no charge conjugation present among additional symmetries. As we shall shortly demonstrate, due to reduced symmetry, the number of allowed couplings is going to be larger. Splitting of $G^{\mathrm{sF}\square}_{\psi^\dagger\psi}$ into irreducible components works as

$$G^{\mathrm{sF}\square}_{\psi^\dagger\psi} = A_2 \oplus B_1 \oplus B_1' \oplus A_2' \oplus 2E_1' \oplus 2E_3 \oplus E_4 \oplus E_5. \quad (4.34)$$

The basis of corresponding components in terms of tensor product of Pauli matrices are listed in Table 4.2. One can notice, that all one-dimensional representation present in the decomposition (4.34) are odd under time-reversal. Just like the case of the πF□ phase, no couplings with phonons are allowed by symmetry at this order. To find non-zero coupling we consider next order in $\boldsymbol{k}$.

Explicit expression for $\hat{H}_{\text{s-ph}(1)}(\boldsymbol{k})$ can be found using decomposition of the product $E_1' \times G^{\mathrm{sF}\square}_{\psi^\dagger\psi}$ [where E_1' corresponds to spinon momentum[2]] into irreducible representa-

[2]Naively, the fact that $\boldsymbol{k}$ transforms under E_1' rather than E_1 seems to contradict the expectation, that as the staggered flux becomes exactly equal to π, the sF□ phase continuously evolves into the πF□ phase. In reality, there is no contradiction: the sF□ phase at the value of flux of π indeed turns into the πF□ phase, however, realized with a different ansatz.

Rep.	A_1	A_2	E_1	F_1	F_2	$F_3\&F_4$
Basis	$\mathbb{1}$	τ^z	$\tau^{x,y}$	$\tau^z\mu^{x,y,z}$	$\mu^{x,y,z}$	$\tau^{x,y}\mu^{x,y,z}$
$\mathcal{T}$-inv	+	−	−	+	−	+

Table 4.3: Explicit form of basis for irreducible representations of C'_{6v} contained within $G^{\pi\mathrm{F}\Box}_{\psi^\dagger\psi}$. Notations and action of group generators coincide with those used by Hermele *et al.* [6].

tions,

$$E'_1 \times G^{\mathrm{sF}\Box}_{\psi^\dagger\psi} = 2(A_1 \oplus A_2 \oplus B_1 \oplus B_2 \oplus E_1 \oplus E'_1 \oplus E_2 \oplus E_3 \oplus E_4 \oplus E_5). \tag{4.35}$$

The overall factor of two indicates that there are two distinct copies of each irreducible representation in the decomposition. Four one dimensional irreducible representation in the first line of Eq. (4.35) coincide with the decomposition of $E_1 \times E_1$ into irreducible representations. As all irreducible components are encountered twice in the decomposition (4.35), we have eight different couplings between spinons and phonons.

The basis for the two copies one-dimensional representations $A_1 \ldots B_2$ in Eq. (4.35) can be deduced using the fact that all these irreducible representations originate from the tensor product $E'_1 \times E'_1$:

$$A_1 : k_x\tau^x + k_y\tau^y, \qquad A_2 : k_x\tau^y - k_y\tau^x, \tag{4.36a}$$

$$B_1 : k_x\tau^x - k_y\tau^y, \qquad B_2 : k_x\tau^y + k_y\tau^x. \tag{4.36b}$$

The bases for the second copy of irreducible representations in Eq. (4.35) have the same form as in Eq. (4.36), but with an extra Pauli matrix μ^z. Physically, this corre-

Rep.	A_1	B_1	A_2	B_2	E_1	E_2	A_1	B_1	A_2	B_2	E_1	E_2
Basis	$\mathbb{1}$	μ^z	τ^z	$\mu^z\tau^z$	$\tau^{x,y}$	$\pm\mu^z\tau^{x,y}$	$\mu^x\tau^z$	$\mu^y\tau^z$	μ^x	μ^y	$\mp\mu^x\tau^{x,y}$	$\mu^y\tau^{x,y}$
$\mathcal{T}$-inv	+	−	−	+	−	+	+	+	−	−	+	+

Table 4.4: Irreducible representations of C_{6v} contained within $G^{0\mathrm{F}\circ}_{\psi^\dagger\psi}$ and their basis. Each irreducible component occurs twice: first six representations in the Table are diagonal in the valley space, whereas remaining six are their off-diagonal counterparts. Adopted from Table III in Ref. [7].

sponds to the fact that the anisotropy in Fermi velocity is not prohibited by symmetry in the sF$\square$ phase [5]. Time-reversal invariance does not reduce the number of allowed couplings, as all combinations in Eq. (4.36) are invariant under $\mathcal{T}$. The resulting spinon-phonon interaction Hamiltonian, has eight terms, four of which coincide with the case of the πF$\square$ phase, Eq. (4.33), while remaining four terms contain an extra μ^z and correspond to a phonon-induced valley anisotropy in a Fermi velocity.

The π-flux phase on a kagome lattice has a symmetry group C'_{6v}. Just like in the case of square lattice, it is an extension of a conventional symmetry group of hexagon, C_{6v}, to the case of enlarged unit cell [6]. The point group of hexagon governs the properties of phonons. The generators of C_{6v} are rotations for an angle of $\pi/3$, $\mathcal{R}_{\pi/3}$, and reflection with respect to x-axis, $\mathcal{R}_x$. Using character Table C.4, the tensor product of two vector representations is decomposed as

$$E_1 \times E_1 = A_1 \oplus A_2 \oplus E_2. \tag{4.37}$$

On the other hand, using character table for the group C'_{6v} from Ref. [6], one can reduce representation on fermion bilinears as

$$G^{\pi\mathrm{F}\hexagon}_{\psi^\dagger\psi} = A_1 \oplus A_2 \oplus E_1 \oplus F_1 \oplus F_2 \oplus F_3 \oplus F_4. \tag{4.38}$$

Comparing Eqs. (4.37) and (4.38), we see that, in principle, couplings between corresponding A_1 and A_2 components are possible. However, if we consider properties of representations under time reversal, listed in Table 4.3, we see that basis of A_2 is odd under time reversal and only coupling to density fluctuations remains:

$$\hat{H}^{\pi\mathrm{F}\hexagon}_{\text{s-ph(0)}} = g_0^{(0)}(u_{xx} + u_{yy})\mathbb{1}. \tag{4.39}$$

This coupling vanishes for transverse phonon modes, and we consider terms which are next order in $\boldsymbol{k}$. Higher order terms can be found from decomposing of $E_1 \times G^{\pi\mathrm{F}\hexagon}_{\psi^\dagger\psi}$

into irreducible components,

$$E_1 \times G^{\pi \mathrm{F} \hexagon}_{\psi^\dagger \psi} = A_1 \oplus A_2 \oplus 2E_1 \oplus E_2 \oplus 2(F_1 \oplus F_2 \oplus F_3 \oplus F_4), \tag{4.40}$$

and pairing those with irreducible representations contained within $E_1 \times E_1$, Eq. (4.37). Only irreducible representations A_1, A_2 and E_2 in Eq. (4.40) are of interest as the same components are also present in decomposition (4.37). The basis for these representations can be written in terms of basis of E_1, (k_x, k_y) and E_1 component within $G^{\pi \mathrm{F} \hexagon}_{\psi^\dagger \psi}$, [$\boldsymbol{\tau} = (\tau^x, \tau^y)$, see Table 4.3]:

$$A_1 \ : \ \boldsymbol{k} \cdot \boldsymbol{\tau} \tag{4.41a}$$

$$A_2 \ : \ \boldsymbol{k} \times \boldsymbol{\tau} \tag{4.41b}$$

$$E_2 \ : \ (k_x \tau^y + k_y \tau^x, k_x \tau^x - k_y \tau^y). \tag{4.41c}$$

From here, we can read off the most general form of the spinon-phonon interaction Hamiltonian to be

$$\begin{aligned} \hat{H}^{\pi \mathrm{F} \hexagon}_{\text{s-ph}} = {} & g_1^{(1)}(u_{xx} + u_{yy})(\boldsymbol{k} \cdot \boldsymbol{\tau}) + g_2^{(1)}(u_{xy} - u_{yx})(\boldsymbol{k} \times \boldsymbol{\tau}) \\ & + g_3^{(1)}\big[(u_{xy} + u_{yx})(k_x \tau^y + k_y \tau^x) + (u_{xx} - u_{yy})(k_x \tau^x - k_y \tau^y)\big]. \end{aligned} \tag{4.42}$$

The uniform phase on a honeycomb lattice is also governed by the symmetry group C_{6v}. The notable difference compared to the cases considered above, is that the honeycomb lattice is not Bravais and has a unit cell consisting of two atoms. Derivation of spinon-phonon interaction is analogous to the case of graphene [7]. We neglect the optical phonon modes related to the presence of two atoms in the unit cell. Tensor product of two vector representations is given by Eq. (4.37). Whereas, decomposition of $G^{0\mathrm{F}\circ}_{\psi^\dagger \psi}$ into irreducible representations works as [7]:

$$G^{0\mathrm{F}\circ}_{\psi^\dagger \psi} = 2(A_1 \oplus A_2 \oplus B_1 \oplus B_2 \oplus E_1 \oplus E_2), \tag{4.43}$$

where two copies describe matrices diagonal and non-diagonal in valley space. Bases

of different irreducible components are given in Table 4.4. Terms which are off-diagonal in the valley space are not considered, as we do not allow for the intervalley scattering due to phonons. At the zeroth order in $\boldsymbol{k}$, in addition to the density coupling, Eq. (4.39), there are terms which do not vanish for transverse phonon modes,

$$\hat{H}^{0\mathrm{F}\bigcirc}_{\text{s-ph}} = g_1\big[(u_{xx} - u_{yy})\tau^x - (u_{xy} + u_{yx})\tau^y\big]\mu^z. \tag{4.44}$$

Thus there is no need to consider next order in $\boldsymbol{k}$. Note, that as basis of A_2 is odd under time reversal, we omit otherwise possible term $(\partial_x u_y - \partial_y u_x)\tau_z$ from Eq. (4.44).

4.3.4 Comparison between different phases

It is instructive to compare the above results for the spinon-phonon interaction in different realizations of Dirac spin liquid. In all derivations we considered Dirac fermions describing low energy excitations. The Dirac dispersion arises as an approximation of the band structure in vicinity of $K_\pm$ points in the Brillouin zone. Consequently, the interaction with acoustic phonons may be understood from the influence of lattice deformations on the low energy band structure. The coupling of phonons to the density of spinons is very easy to explain from this perspective. The local changes in the volume of the lattice, described exactly by $\operatorname{div}\boldsymbol{u} = u_{xx} + u_{yy}$, correspond to the density modulations of spinons, yielding the interaction Hamiltonian (4.39). In the case of the 0F$\bigcirc$ phase, remaining terms given by Eq. (4.44) are can be interpreted as a relative shift of $K_\pm$ points with respect to each other by lattice deformations. In other words, strain is translated into a gauge field, which coupled with opposite sign in different valleys – well known effect for the case of graphene [7, 171].

The presence of fluxes and non-trivial action of projective symmetry group prohibits density coupling for πF$\square$ and sF$\square$ phases. In the πF$\hexagram$ phase, the density coupling is the only allowed coupling at this order. To find a non-trivial couplings, we considered next order expansion in vicinity of the Dirac points. These couplings may be readily understood as a *deformation* of the band structure in vicinity of $K_\pm$ point, which, nevertheless leaves the position of the Dirac point within the Brillouin

zone intact. This is exactly what we see in couplings (4.33) and (4.42), which can be interpreted as the change in Fermi velocity, v_F. Note, that the position of Dirac points in the Brillouin zone is non-universal, and depends on the choice of the implementation of the given phase. Therefore, it is natural, that the (physical) lattice deformation does not have any impact on the (unphysical) position of the Dirac points.

4.4 Sound attenuation

We continue with a discussion of observable consequences of spinon-phonon interaction. Interaction of acoustic phonons with gapless spinons opens another channel for decay of phonons. Thus, it is expected to contribute to the attenuation of ultrasound. To get an estimate of the this effect, we perform a simple calculation in this Section. As an example, we consider the algebraic spin liquid phase with staggered flux on a square lattice. We comment on the differences for the πF✡ and 0F⬡ phases. We do not consider the πF□ phase, to avoid the complications related to the presence of an SU(2) gauge field.

4.4.1 Framework

We start with establishing the framework and introducing the basic elements required to calculate the ultrasound attenuation. These are the gauge field propagator and the phonon self-energy.

The gauge field, strongly coupled to spinon emerges from a microscopic constraint and fluctuations around mean field anzatz. On a microscopic level it originates from constraint and is not dynamical. Non-trivial dynamics of the gauge field is generated due to the coupling to fermions [172, 173]. First, the Maxwell term will be generated while integrating out high energy degrees of freedom. Another contribution, which is singular compared to the Maxwell term, comes from the Dirac band touching and can be written via vacuum polarization operator for massless Dirac fermions. Total

Figure 4-2: Double wavy line shows the gauge field propagator in the RPA approximation. Thin wavy line is the bare Maxwell propagator.

action of gauge field then becomes

$$S_a = \frac{1}{2}\int \frac{d^3\vec{q}}{(2\pi)^3} a_\mu(\vec{q})[(D^{\mathrm{M}})^{-1}_{\mu\nu}(\vec{q}) - \Pi_{\mu\nu}(\vec{q})]a_\nu(-\vec{q}), \tag{4.45}$$

where we use covariant notations in Euclidean space, $\vec{q} = (i\omega, v_F\boldsymbol{q})$. $\Pi_{\mu\nu}(\vec{q})$ is the polarization bubble of Dirac fermions (see Fig. 4-2), and $(D^{\mathrm{M}})^{-1}_{\mu\nu}$ is the inverse Maxwell propagator of the gauge field (we work in the Lorentz gauge, $\vec{k}\cdot\vec{a} = 0$),

$$(D^{\mathrm{M}})^{-1}_{\mu\nu}(\vec{q}) = \left(\delta_{\mu\nu} - \frac{\vec{q}_\mu \vec{q}_\nu}{\vec{q}^2}\right)\Pi^{\mathrm{M}}(\vec{q}), \tag{4.46}$$

where $\Pi^{\mathrm{M}}(\vec{q})$ corresponds to the inverse propagator without tensor structure:

$$\Pi^{\mathrm{M}}(\vec{q}) = \frac{\vec{q}^2}{e^2}. \tag{4.47}$$

The polarization bubble at zero temperature (projector tensor structure is again omitted) is given by [174–176]:

$$\Pi(\vec{q}) = -\frac{N}{8}\sqrt{\vec{q}^2}, \tag{4.48}$$

where we introduced the integer number of flavors of four-component Dirac fermions, N, in our theory. The physical case corresponds to $N = 2$ coming from spin. Action (4.45) translates into the total propagator for the gauge field, Fig. 4-2, given by

$$D(q) = \frac{8}{N}\frac{1}{\sqrt{\vec{q}^2} + 8\vec{q}^2/(Ne^2)}. \tag{4.49}$$

In what follows we will need the polarization bubble at finite temperature, which may be written as

$$\Pi_{\mu\nu} = A_{\mu\nu}\Pi^A + B_{\mu\nu}\Pi^B. \tag{4.50}$$

The tensors $A_{\mu\nu}$ and $B_{\mu\nu}$,

$$A_{\mu\nu} = \left(\delta_{\mu 0} - \frac{q_\mu q_0}{\vec{q}^2}\right) \frac{\vec{q}^2}{\boldsymbol{q}^2} \left(\delta_{0\nu} - \frac{q_0 q_\nu}{\vec{q}^2}\right), \tag{4.51}$$

$$B_{\mu\nu} = \delta_{\mu i} \left(\delta_{\mu 0} - \frac{q_\mu q_0}{\vec{q}^2}\right) \delta_{j\nu}, \tag{4.52}$$

are orthogonal to each other and their sum reproduces the original zero-temperature tensor structure, Eq. (4.46). Explicit expressions for $\Pi^{A,B}$ along with detailed calculations are available in the literature [176]. We need the asymptotic expression for Π^A in the limit $T \gg v_F|\boldsymbol{q}| \gg \omega$:

$$\Pi^A = -\frac{2NT \log 2}{\pi} \left(1 + \mathrm{i}\frac{\omega}{v_F q}\right). \tag{4.53}$$

Sound attenuation, α_{s}, will be calculated from the self-energy of phonons, $\Pi_{\mathrm{ph}}(\omega, \boldsymbol{q})$, arising due to interactions with spinons. More precisely, α_{s} is given by the imaginary part of the retarded self-energy [47],

$$\alpha_{\mathrm{s}} = -\frac{2}{v_s} \operatorname{Im} \left[\Pi^R_{\mathrm{ph}}(\omega, |\boldsymbol{q}|)\right]_{\omega = v_s|\boldsymbol{q}|}, \tag{4.54}$$

with frequency and momentum related by the dispersion relation of the acoustic phonons, $\omega = v_s|\boldsymbol{q}|$, where v_s is the sound velocity.

Let us discuss the approximations to be used in the calculation of the sound attenuation. For simplicity, we consider the clean case, i.e. we assume that the mean free path of spinons, l, is much larger than the ultrasound wavelength, $ql \gg 1$. Also, we assume that the sound velocity is much smaller than the Fermi velocity, $v_F \gg v_s$. Under this condition, we immediately find that if ω and q are the phonon energy and the wave vector, $v_F q = (v_F/v_s)\omega \gg \omega$. Finally, in contrary to the case of spin liquid with a Fermi surface [47], non-zero temperature is required to get non-vanishing sound attenuation in a Dirac spin liquid. This is a consequence of the energy and momentum conservation in the scattering process. Acoustic phonon cannot excite a particle-hole pair of spinons since the maximum momentum change for such a pair

with energy ω, $\Delta k = \omega/v_F$, is much smaller than phonon momentum, $q = \omega/v_s$. Therefore, we assume that the system is at a finite temperature $T \gg (v_F/v_s)\omega \gg \omega$.

As noted above, there is a gauge field strongly coupled to the spinons. In order to have a control over its effects we artificially introduced the number of flavors, N, being equal to two in the physical case. Since gauge field propagator, Eq. (4.49), is proportional to $1/N$, effects of gauge field are suppressed for large N. We will perform calculations of sound attenuation to the leading order within $1/N$ expansion, commenting on the higher order terms.

4.4.2 Sound attenuation in the sF□ phase

Having the basic ingredient for the calculation of sound attenuation at our disposal, we consider α_s for longitudinal phonons in the sF□ phase. As shown in Section 4.3.2, there is no allowed coupling at the leading order in $\boldsymbol{k}$. All possible couplings at the next order are given by Eq. (4.33). For simplicity, we consider only first term in Eq. (4.33) [see Eq. (4.32)]. Combining Eqs. (4.23) and (4.32), corresponding spinon-phonon interaction vertex reads:

$$M^{(1)}_{\boldsymbol{k}}(\boldsymbol{q}) = \tilde{g}^{(1)}_1 q\, \tilde{M}^{(1)}_{\boldsymbol{k}}(\hat{\boldsymbol{q}}), \tag{4.55a}$$

$$\tilde{M}^{(1)}_{\boldsymbol{k}}(\hat{\boldsymbol{q}}) = \hat{q}_x^2 k_x \tau^x + \hat{q}_y^2 k_y \tau^y, \tag{4.55b}$$

where $\hat{\boldsymbol{q}} = (\hat{q}_x, \hat{q}_y)$ is the unit vector pointing along $\boldsymbol{q}$. In what follows, coupling constants with tilde are defined as:

$$\tilde{g} = \sqrt{\frac{1}{2\rho\omega_{\boldsymbol{q}}}}\, g. \tag{4.56}$$

To leading order in $1/N$, the polarization operator of phonons due to interaction with spinons is given by the sum of two diagrams in Fig. 4-3 with the spinon-phonon interaction vertex from Eq. (4.55). Indeed, the first diagram in Fig. 4-3 has one fermionic bubble and is proportional to N. An extra fermionic bubble in the diagram Fig. 4-3 (b) is compensated by factor of $1/N$ from the gauge field propagator. We

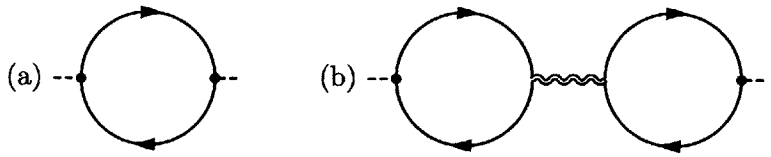

Figure 4-3: Contribution of spinons to the longitudinal sound attenuation. The bare contribution from spinons is given by the diagram (a). Diagram (b) accounts for the screening due to fluctuations of the gauge field. Black dots represent spinon-phonon interaction vertex, specified in the main text.

have for the first contribution, Fig. 4-3 (a):

$$\alpha_s = \frac{2}{v_s}\left[\tilde{g}_1^{(1)}\right]^2 q^2 \operatorname{Im}\Pi^{R(1)}(\omega, \boldsymbol{q}). \tag{4.57}$$

The imaginary part of the bubble diagram with spinons is calculated in the Appendix C.2 and behaves as $\operatorname{Im}\Pi^{R(1)}(\omega, \boldsymbol{q}) \propto N\omega T^3/(v_F^3 q)$ at the leading order. One can show that the contribution from the diagrams with an extra gauge field propagator, Fig. 4-3 (b), has the same order of magnitude as Fig. 4-3 (a). Thus, using dispersion relation of acoustic phonons, we get the following estimate for the sound attenuation:

$$\alpha_s \propto N\left[\tilde{g}_1^{(1)}\right]^2 \frac{\omega^4 T}{{v_s}^2 v_F^3}. \tag{4.58}$$

The value of the coupling constant, $g_1^{(1)}$, may be estimated from the sensitivity of the velocity of Dirac spinons to the changes of the lattice constant, a:

$$g_1^{(1)} \sim a\frac{\partial v_F}{\partial a} \sim v_F. \tag{4.59}$$

Using this estimate, we obtain for the sound attenuation:

$$\alpha_s \sim N\left(\frac{T}{\omega_D}\right)^2 \alpha_s^{(0)}, \tag{4.60}$$

where $\alpha_s^{(0)}$ defined as

$$\alpha_s^{(0)} \sim q\frac{k_T}{m_{\text{ion}} v_s} = \frac{qT}{m_{\text{ion}} v_s v_F}. \tag{4.61}$$

The Debye frequency has been estimated as $\omega_D \propto v_s/a$, and $k_T = T/v_F$ is a wave vector of spinons with the energy equal to the temperature. The $\alpha_s^{(0)}$, introduced above, gives the estimate for the sound attenuation coefficient in the case of spinon Fermi surface if one substitute the Fermi momentum for the k_T, $k_T \to k_F$. We see that in a Dirac spin liquid, contribution of spinons to the sound attenuation is suppressed compared to the Fermi surface case by two factors. The first factor, $T/\mu_F \ll 1$ is generic for any Dirac spin liquid and originates from the vanishing density of states at zero temperature in the Dirac spectrum. The second factor $(T/\omega_D)^2$, which is also expected to be smaller than one, arises due to peculiar form of spinon-phonon coupling.

Finally, we comment on the next order in $1/N$ terms, contributing to the sound attenuation. There is a much larger number of diagrams at the order $O(1)$. The most obvious are the vertex corrections, where gauge field dresses the interaction vertex of spinons with phonons or gauge field itself. Note, that if the spinon-phonon interaction vertex corresponded to some conserved current, it would be protected from logarithmic corrections [173]. However, there is no such protection here and in general we expect logarithmic corrections to arise at the order $O(1)$. There is also another type of contribution $O(1)$, which is more unusual. Indeed, in order to maintain the gauge invariance, $\boldsymbol{k}$ in Eq. (4.55) has to be extended to include the gauge field as well. This leads to the vertex where a phonon can generate a quanta of the gauge field *in addition* to the particle-hole pair of spinons. Similar type of vertex has been considered in Ref. [42].

4.4.3 Sound attenuation in πF✡ and 0F○ phases

As we have shown above, the peculiar form of the coupling between phonons and spinons in the sF□ phase leads to the suppression of the sound attenuation coefficient by additional small factors. One may expect, that since in the πF✡ and 0F○ phases longitudinal phonons couple to the density of spinons, the sound attenuation will be parametrically larger than for the sF□ phase. Below, we are going to demonstrate that these naive expectations do not hold. Due to the presence of the gauge field, the

density coupling gets screened and does not contribute to the sound attenuation at leading order in $1/N$.

Using explicit form of the coupling, Eq. (4.39), we write corresponding spinon-phonon interaction as:

$$M_{\boldsymbol{k}}^{(0)}(\boldsymbol{q}) = \tilde{g}_0^{(0)} q \, \mathbb{1}. \tag{4.62}$$

The identity matrix corresponds to the spinon density, thus justifying the use of the term "density couping". The self-energy of phonons, required to find the sound attenuation, can be expressed via time component of electron polarization bubble Π_{00}. In addition, one have to account for the effect of gauge field, including the scalar potential (unlike the case of spinons with Fermi surface, scalar potential of the gauge field is not screened by Dirac fermions). These two contributions to Π_{ph} are shown in Fig. 4-3, where now black dots correspond to the interaction vertex (4.62). Accounting for the both diagrams in Fig. 4-3, we get:

$$\Pi_{\text{ph}}(\vec{q}) = \left[\tilde{g}_0^{(0)}\right]^2 q^2 \left[\Pi_{00}(\vec{q}) + \Pi_{0\mu}(\vec{q}) D_{\mu\nu}(\vec{q}) \Pi_{\nu 0}(\vec{q})\right], \tag{4.63}$$

where propagator and self-energy are taken on a phonon mass shell, $\omega = v_s|\boldsymbol{q}|$. Using the finite-temperature expression for the polarization operator, Eq. (4.50), we find that only Π^A contributes in the present case. Two terms in the sum in Eq. (4.63) partially cancel each other and we arrive at:

$$\Pi_{\text{ph}}(\vec{q}) = \tilde{g}_0^2 q^2 \frac{q^2}{\vec{q}^2} \frac{\Pi^{\text{M}}(\vec{q}) \Pi^A(\vec{q})}{\Pi^{\text{M}}(\vec{q}) - \Pi^A(\vec{q})}. \tag{4.64}$$

Since $\Pi^A(\vec{q})$ is more important than the Maxwell term, at the leading order we can neglect the latter term in the denominator, and get $\Pi_{\text{ph}}(\vec{q}) \propto -\Pi^{\text{M}}(q)$. Note, that this term is of order of $O(1)$, compared to the naive expectation $\Pi_{\text{ph}}(\vec{q}) \sim O(N)$. Moreover, this term does not contribute to the imaginary part of the self-energy: Maxwell propagator originates from high-energy modes, whereas we are interested in the decay of phonons into low-energy Dirac-like spinons. Omitting the leading order

term, and including next order contribution, we get the result

$$\Pi_{\rm ph}(\vec{q}) = -\tilde{g}_0^2 q^2 \frac{q^2}{\vec{q}^2} \frac{[\Pi^{\rm M}(\vec{q})]^2}{\Pi^A(\vec{q})}, \tag{4.65}$$

which is proportional to $1/N$. Qualitatively, cancellation of two leading terms can be understood as an effect of screening due to gauge field.

Now that we have shown that the contribution of the density coupling to the sound attenuation is proportional to $1/N$ and thus negligible, we consider other terms in the coupling Hamiltonian, contributing at the order $O(N)$. For the πF✡ phase, these terms, listed in Eq. (4.42), are first order in $\boldsymbol{k}$. Thus, the sound attenuation is expected to be of the same order as the results for the sF□ phase, listed in Eq. (4.60).

However, for the 0F○ phase there are couplings allowed without an extra $\boldsymbol{k}$, see Eq. (4.44). Contribution from these couplings is expected to be of order of $\alpha_s^{(0)}$ [see Eq. (4.61)]. We note that contribution of gauge field vanishes in the present case. Indeed, it couples with an opposite sign in different valleys [note the presence of the extra μ^z matrix in Eq. (4.44)], thus diagram in Fig. 4-3 (b) is identically zero.

4.5 Discussion and outlook

We presented the general procedure for the derivation of the coupling between spinons and acoustic phonons in the Dirac spin liquid. Our procedure is based on the symmetry arguments. Although general fermionic bilinear transforms under projective representation of the lattice symmetry group, spin singlet bilinears realize conventional (i.e., not projective) representation of the microscopic symmetry group. We found the decomposition of this representations into irreducible for π-flux and staggered flux phases on a square lattice, as well as for π-flux phase on kagome lattice and a Dirac spin liquid phase on a honeycomb lattice. By pairing corresponding irreducible representations with those for acoustic phonons, we were able to identify all symmetry allowed couplings. Note, that such decomposition can have other applications. For instance, it can be used to derive symmetry allowed couplings to optical

phonons or some other excitations.

In a continuum limit all considered spin liquid phases have similar low energy Dirac excitations, and hardly can be distinguished. Nevertheless, the allowed interactions with phonons have different form. For the Dirac spin liquid phase on a honeycomb lattice the coupling to acoustic phonons is similar to the case of graphene. The only difference is that the coupling to the density of spinons, naively expected to be the largest, is screened by the gauge field (this is true for all Dirac spin liquid phases). As a result, for spin liquid phases on a square and kagome lattices considered in this work, the leading couplings contains an extra small parameter $(T/\omega_D)^2$, compared to U(1) Dirac spin liquid on honeycomb lattice. Qualitatively, in these phases, the lattice deformations with small wave vectors couple to the changes or anisotropies in Fermi velocity. Whereas in the case of zero-flux phase on honeycomb lattice such lattice deformations shift the position of Dirac points, acting similarly to the gauge field.

The difference between couplings arises naturally from the fact that they are controlled by the representation of the corresponding symmetry group, acting on a lattice level. Thus the interaction of spinons with phonons retains some information about microscopic structure of the phase. It would be instructive to check if one can distinguish between different projective realizations of the same symmetry group by looking at couplings to spinons. The simplest example[3] of such two phases are two $\mathbb{Z}_2$ spin liquid phases on a square lattice (Z2A0013 and Z2Azz13 in notations of Refs. [22, 177]). This, however, requires generalization of the present approach to the case of $\mathbb{Z}_2$ spin liquid phases, which is an interesting open question. Another open question is to understand the effect of projective realization of spin SU(2) symmetry, which has been proposed recently [178].

In order to understand the perspectives of spinon-phonon interaction as a probe of fermionic spinons, we carried out a simple calculations within $1/N$ expansion. Assuming that our results can be extrapolated to the physical case $N = 2$, we see that the in a generic Dirac spin liquid exemplified by the zero flux phase in the honeycomb lattice, sound attenuation is suppressed due to vanishing density of states

[3]X.-G.Wen, private communication.

at zero temperature and $\alpha_S \propto qT/(m_{\rm ion} v_F v_s)$. On the other hand, the peculiar form of spinon-phonon coupling in the π-flux and staggered flux phases contributes an additional suppression of the form $(T/\omega_D)^2$. Nevertheless, the effect from phonons is still potentially observable, as the sound attenuation due to phonon-phonon scattering (caused by non-liearities) behaves as $\alpha \sim T^4$ for $T \ll \omega_D$ [179].

We note that our calculations should be viewed as a simple estimate due to the nature of approximations used. Currently, to the best of our knowledge there is no experimental data available on the sound attenuation in Dirac spin liquids. Provided such data becomes available, more extensive theoretical work is required, in order to construct a realistic description. In particular, for the prospective spin liquid phase on a kagome lattice [28, 29], the clean limit, assuming mean free path $l \gg q^{-1}$ does not apply. Also, the estimate for v_F suggests that $v_F \sim v_s$, rather than $v_F \gg v_s$ as was assumed. Another question, which can be relevant for a spin liquid on a kagome lattice is the effect of transition from U(1) to $\mathbb{Z}_2$ spin liquid and its possible manifestation in the ultrasound attenuation.

Appendix A

Variational Monte Carlo

The Variational Monte Carlo (VMC) method allows to efficiently evaluate expectation values of observables in a given many body wave function within small error bars [24, 180]. This works as follows: Let $|\psi\rangle$ be the wave function and let O be the observable we want to evaluate. Let $\{|\alpha\rangle\}$ be an "Ising" basis of the Hilbert space; i.e., $|\alpha\rangle$ is a product of local basis states. We can write

$$\langle\psi|O|\psi\rangle = \sum_{\alpha} |\psi(\alpha)|^2 \frac{\langle\alpha|O|\psi\rangle}{\langle\alpha|\psi\rangle}, \tag{A.1}$$

with $|\psi(\alpha)|^2 = |\langle\alpha|\psi\rangle|^2/\langle\psi|\psi\rangle$. Since $\sum_\alpha |\psi(\alpha)|^2 = 1$, $|\psi(\alpha)|^2$ is a probability distribution on the Ising configurations $\{\alpha\}$. Such a distribution can be generated by a Metropolis algorithm with acceptance probability

$$p(\alpha \to \alpha') = \min\{\left|\frac{\psi(\alpha')}{\psi(\alpha)}\right|^2, 1\}. \tag{A.2}$$

Note that, in (A.2), $\psi(\alpha)$ does not need to be normalized. The sequence $\{\alpha\}$ generated by a random walk with probability (A.2) can be used to efficiently calculate the expectation value,

$$\langle\psi|O|\psi\rangle \simeq \sum_{\{\alpha\}} \frac{\langle\alpha|O|\psi\rangle}{\langle\alpha|\psi\rangle}. \tag{A.3}$$

In this paper, we use ~ 200 Monte Carlo runs to estimate the error of Eq. (A.3) by its variance over the runs. The length of a run is ~ 200 steps, and the observables are measured after each step. The measurements are precessed by an equilibration skip of ~ 400 steps. Each Monte Carlo step consists of $4 \times N \sim 600$ local moves, accepted with probability (A.2). We use a lattice of $N = L \times L$ sites, with a linear size $L = 12$ in our calculations. The error bars on the variational energies shown in Figs. 2-4 and 2-6 are smaller than the symbol sizes.

Local and global constraints (projections) on the wave function $|\psi\rangle$ can be easily implemented in the VMC scheme. The Gutzwiller projection, $|\psi\rangle = P_G|\psi_0\rangle$, for example, can be taken into account by restricting the Ising configurations α to the singly occupied subspace ($n_j \equiv 1$). Similarly, projection of a spin wave function to $S_z^{\rm tot} = 0$ leads to a global restriction on the configurations α. Here, it is important to have an algorithm that generates all states α in the constrained subspace with uniform probability.

To apply VMC to a particular wave function, we first need an expression for $\psi(\alpha) \propto \langle\alpha|\psi\rangle$. Next, an efficient algorithm is needed to calculate the Metropolis acceptance probabilities (A.2) for local moves in the constrained subspace. Similarly, for each observable of interest, one has to find an efficient way to calculate the ratio of overlaps in (A.3).

A.1 Fermionic wave functions

The first class of wave functions that we are considering in this paper are Gutzwiller-projected ground states of quadratic Hamiltonians, $H_{\rm MF}$, for three flavors of fermions f_a. A similar study of wave functions with *two* flavors of fermions has been pioneered by Gros [24] for spin $S = 1/2$ models.

In our calculation of fermionic quantum spin liquid and fermionic ordered wave functions, we use the local basis of time-reversal invariant states, $|a\rangle \in \{|x\rangle, |y\rangle, |z\rangle\}$, Eq. (2.8). The Ising configurations α are restricted to singly occupied states on a lattice of $N = L \times L$ sites. Furthermore, we restrict the configurations to states with

$N_x = N_y$ and N_z kept fixed (that is, the wave functions are projected to fixed total flavor numbers; see below).

Let $\boldsymbol{r}_j^a \in \mathbb{Z}^L \times \mathbb{Z}^L$ be the lattice positions of flavor $a \in \{x, y, z\}$ in the Ising configuration α. The U(1) state and the triplet (x-y paired) quantum spin liquid states in (2.28) can be written as a product of two determinants,

$$\langle \alpha | \psi \rangle = \det[e^{\mathrm{i}\boldsymbol{k}_j^z \cdot \boldsymbol{r}_l^z}] \det[A(\boldsymbol{r}_j^x - \boldsymbol{r}_l^y)], \tag{A.4}$$

where j and l are the indices for the determinants. $\boldsymbol{k}_j^z$ are the occupied momentum states of f_z spinons inside the Fermi sea, $\epsilon_{\boldsymbol{k}_j^z} < \mu_z$. For the U(1) state, $A(\boldsymbol{r})$ is a Slater matrix [24],

$$A(\boldsymbol{r}) = \sum_{\substack{\boldsymbol{k} \in \mathrm{BZ}, \\ \epsilon_{\boldsymbol{k}} < \mu_x}} e^{\mathrm{i}\boldsymbol{k}\cdot\boldsymbol{r}}, \tag{A.5}$$

with momenta $\boldsymbol{k}$ going over filled states in the first Brillouin zone (BZ). For the triplet quantum spin liquid states (s-wave, $d + \mathrm{i}d$), we have

$$A(\boldsymbol{r}) = \sum_{\boldsymbol{k} \in \mathrm{BZ}} a_{\boldsymbol{k}}\, e^{\mathrm{i}\boldsymbol{k}\cdot\boldsymbol{r}}, \tag{A.6}$$

where $a_{\boldsymbol{k}} = v_{\boldsymbol{k}}/u_{\boldsymbol{k}} = \Delta_{\boldsymbol{k}}/(E_{\boldsymbol{k}} + \xi_{\boldsymbol{k}})$ is the ratio of BCS coherence factors for the pairing of f_x and f_y fermions.

For the quantum spin liquid states with equal-flavor pairing (f-wave, $p + \mathrm{i}p$), the wave function is a product of three Pfaffians [181, 182],

$$\langle \alpha | \psi \rangle = \prod_a \mathrm{Pf}[A^a(\boldsymbol{r}_j^a - \boldsymbol{r}_l^a)], \tag{A.7}$$

with

$$A^a(\boldsymbol{r}) = \sum_{\boldsymbol{k} \in \mathrm{BZ}} a_{\boldsymbol{k}}^a \sin(\boldsymbol{k} \cdot \boldsymbol{r}), \tag{A.8}$$

where $a_{\boldsymbol{k}}^a = v_{\boldsymbol{k}}^a/u_{\boldsymbol{k}}^a$ are the ratio of coherence factors for each paired fermion flavor.

In the case of the ordered states (2.30), the fermions are unpaired, but the flavors hybridize through terms $f_{ia}^\dagger f_{jb}$, etc. For a lattice of N sites, the corresponding wave

function is a single Slater determinant of size $N \times N$,

$$\langle \alpha | \psi \rangle = \det[A_l(\boldsymbol{r}_j^a)] \,. \tag{A.9}$$

Here, $l = 1 \ldots N$, and $A_l(\boldsymbol{r}_j^a)$ are the lowest eigenvectors of the mean-field matrix H_{ij}^{ab} with $H_{\rm ord} = \sum_{ij,ab} f_{ai}^\dagger H_{ij}^{ab} f_{bj}$. [For the three-sublattice ordered states we consider in this paper, the eigenvectors can be labeled by $l = (n, \boldsymbol{k})$, where n is a band index and $\boldsymbol{k}$ lies in the reduced Brillouin zone.]

Our calculations are done on a finite lattice with $N = L \times L$ sites. In order to avoid singularities or degeneracies in (A.4)–(A.9), we use quadratic trial Hamiltonians (2.28) and (2.30) with periodic in one and antiperiodic boundary conditions in the other lattice direction for the spinons f_{aj}. The f-wave state, however, has lines of nodes in the gap function $\Delta_{\boldsymbol{k}}$ (at momenta $\{\boldsymbol{k}_0\}$) that cannot be avoided by choosing periodic-antiperiodic boundary conditions. A singularity $|a_{\boldsymbol{k}_0}^a| \to \infty$ occurs on these lines, and (A.8) is ill defined. To cure the divergencies, we replace $a_{\boldsymbol{k}_0}^a$ by a large but finite quantity, namely, $\pm 20 \times \max_{\boldsymbol{k} \notin \{\boldsymbol{k}_0\}} |a_{\boldsymbol{k}}^a|$. The sign is chosen to be consistent with the sign of $a_{\boldsymbol{k}}^a$ as $\boldsymbol{k} \to \boldsymbol{k}_0$. We have verified that the relevant correlators do not depend on the precise factor in the regularization and that the wave function (correlators) correctly reproduces the U(1) state when $|\Delta^{aa}| \ll 1$.

We use the usual tricks for an efficient evaluation of the Metropolis acceptance probability (A.2) and the expectation values (A.3) in fermionic wave functions: The inverse of the matrices in (A.4), (A.7), and (A.9) is stored and updated during the Monte Carlo random walk [180]. This allows for efficient evaluation of determinants and Pfaffians with rows and/or columns replaced or removed [24, 182]. To update the inverse of an antisymmetric matrix with a row and column replaced, we use the Sherman-Morrison algorithm twice, followed by antisymmetrization of the matrix. This procedure greatly improves the numerical stability of the update. The "pfapack" package by Wimmer [183] is used for efficient evaluation of Pfaffians.

Flavor-number nonconservation

An important technical difficulty with fermionic RVB wave functions for spin $S = 1$ is that typical microscopic models such as (2.37), when written in terms of fermion operators, do not conserve the number of each fermion flavor separately. This issue is also present if we wish to represent the spin operator by more than three fermion flavors. We have $N_a = N - \sum_j S_{aj}^2$ and $[H_{KD}, N_a] \neq 0$, in general. Unlike in the case of spin-1/2, conservation of $S_z^{\rm tot} = \sum_j S_{zj}$ does not imply conservations of flavor number. Note, however, that N_a is conserved in the SU(3) model (2.6) or in the KD-model (2.37) at $K = 1$, where this issue does not arise. Writing (2.37) with fermions, the terms not commuting with N_a are

$$(K-1)\sum_{ab} f_{ai}^\dagger f_{bi} f_{aj}^\dagger f_{bj}\,, \tag{A.10}$$

which vanish for $K = 1$. In general, there is therefore no justification for using variational wave functions that are particle-number eigenstates. For such wave functions, the Ising configurations α in (A.2) must visit all possible total flavor numbers, with $\sum_a N_a = N$ kept fixed. In a brute force implementation, the determinants and Pfaffians in (A.4) and (A.7) may need to change sizes during a Monte Carlo run, which implies a high computational overhead. Such a simulation has recently been done in the case of spin-one chains [184].

The problem is actually absent for the quantum spin liquid states with a spinon Fermi surface. In this case, the wave function is an N_z eigenstate. N_x and N_y do fluctuate in a paired state; nevertheless, $N_x = N_y$ and all expectation values of (A.10) vanish in this class of wave functions. The difficulty is only present for equal-flavor paired quantum spin liquid states (f-wave and $p + ip$) and for the ordered states (2.30). In these cases, the expectation value of (A.10) does not vanish (before or after Gutzwiller projection). The flavor numbers N_a fluctuate independently of each other in these wave functions.

To resolve this issue, we can use the standard argument [24] that relates grand-canonical and microcanonical RVB wave functions: The paired mean-field states are

strongly peaked at some average flavor number $\tilde{\boldsymbol{N}}_0 = (\tilde{N}_x^0, \tilde{N}_y^0, \tilde{N}_z^0)$. This peak in flavor number may shift position to $\boldsymbol{N}_0$ after Gutzwiller projection, but it should still be present. Furthermore, the variance is expected to vanish in the thermodynamic limit, $\langle (N_a - N_a^0)^2 \rangle / N^2 \sim 1/N$. Therefore, it is justified to work with microcanonical wave functions that are obtained by projecting the grand-canonical wave function, $|\psi\rangle$, to fixed total flavor numbers,

$$|\boldsymbol{N}_0\rangle = P(\boldsymbol{N}_0)|\psi\rangle \,. \tag{A.11}$$

VMC calculation of expectation values of particle-number conserving operators within a microcanonical wave function is straightforward. However, off-diagonal operators such as (A.10) require some care [185]. As an example, let us consider the operator

$$R_{xy} = f_{xi}^\dagger f_{yi} f_{xj}^\dagger f_{yj} \,. \tag{A.12}$$

Its expectation value in the grand-canonical wave function can be approximated as

$$\langle \psi | R_{xy} | \psi \rangle \simeq \frac{\langle \boldsymbol{N}_0^+ | R_{xy} | \boldsymbol{N}_0 \rangle}{\sqrt{\langle \boldsymbol{N}_0^+ | \boldsymbol{N}_0^+ \rangle \langle \boldsymbol{N}_0 | \boldsymbol{N}_0 \rangle}} \,, \tag{A.13}$$

with $\boldsymbol{N}_0^\pm = (N_x^0 \pm 2, N_y^0 \mp 2, N_z^0)$, and $\boldsymbol{N}_0$ is the average particle number in $|\psi\rangle$. In VMC, the right-hand side of Eq. (A.13) cannot be calculated directly with the correct normalization. However, it is possible to calculate

$$\frac{\langle \boldsymbol{N}_0^+ | R_{xy} | \boldsymbol{N}_0 \rangle}{\langle \boldsymbol{N}_0 | \boldsymbol{N}_0 \rangle} \qquad \text{and} \qquad \frac{\langle \boldsymbol{N}_0 | R_{xy} | \boldsymbol{N}_0^- \rangle}{\langle \boldsymbol{N}_0 | \boldsymbol{N}_0 \rangle} \tag{A.14}$$

within a single Monte Carlo run. Since the last average satisfies $\left| \langle \boldsymbol{N}_0 | R_{xy} | \boldsymbol{N}_0^- \rangle / \langle \boldsymbol{N}_0 | \boldsymbol{N}_0 \rangle \right| \simeq \left| \langle \boldsymbol{N}_0^+ | R_{xy} | \boldsymbol{N}_0 \rangle / \langle \boldsymbol{N}_0^+ | \boldsymbol{N}_0^+ \rangle \right|$, the normalization factor can be calculated from the ratio of the two correlators in (A.14),

$$g_{xy} = \frac{\langle \boldsymbol{N}_0 | \boldsymbol{N}_0 \rangle}{\langle \boldsymbol{N}_0^+ | \boldsymbol{N}_0^+ \rangle} \simeq \left| \frac{\langle \boldsymbol{N}_0 | R_{xy} | \boldsymbol{N}_0^- \rangle}{\langle \boldsymbol{N}_0^+ | R_{xy} | \boldsymbol{N}_0 \rangle} \right| \,. \tag{A.15}$$

Finally, the correctly normalized expectation value (A.13) is evaluated as

$$\langle\psi|R_{xy}|\psi\rangle \simeq \sqrt{g_{xy}}\,\frac{\langle \boldsymbol{N}_0^+|R_{xy}|\boldsymbol{N}_0\rangle}{\langle \boldsymbol{N}_0|\boldsymbol{N}_0\rangle}\,. \tag{A.16}$$

It is clear that for a given wave function, g_{xy}, (A.15), does not depend on the off-diagonal operator R_{xy} (for example, R_{xy} on different sites must give the same g_{xy}). This provides a nontrivial check of our code and we found that the renormalization factors g_{ab} are indeed identical on different sites within error bars.

Of course, a particle-number projection $|\boldsymbol{N}\rangle$ is only a faithful representation of $|\psi\rangle$ if the flavor number $\boldsymbol{N}$ is sufficiently close to the average value $\boldsymbol{N}_0$ in the Gutzwiller projected wave function. Using $\boldsymbol{N}$ as a variational parameter (here with the restriction $N_x = N_y$) guarantees that the state $|\boldsymbol{N}_0\rangle \propto |\psi\rangle$ is among the variational wave functions. For the equal-flavor paired singlet wave functions, we found that the agreement between our optimal correlators and the ones calculated in the corresponding grand-canonical wave functions is very good.

For spin $S = 1/2$ systems, the investigation of (doped) RVB wave functions in the grand-canonical ensemble was pioneered by Yokohama and Shiba in Ref. [186]. These authors introduced a particle-hole transformation $c_\downarrow^\dagger \mapsto c_\downarrow$ that allows one to do fixed-particle VMC simulations. However, this trick does not easily generalize to spin-one. For spin-half RVB wave functions, the agreement between microcanonical and grand-canonical approaches was found to be very good. Note, however, that particle number renormalization by the Gutzwiller projector in grand-canonical wave functions leads to subtle effects that need to be taken into account if one wishes to apply the Gutzwiller approximation [187–189].

A.2 Huse-Elser wave functions

This appendix contains details regarding the implementation of trial wave functions of Huse-Elser type, generalized to the spin $S = 1$ case. Similar to the case of spin $S = 1/2$ [70], our construction starts from an uncorrelated product-state wave func-

tion. Quantum correlations are introduced by applying Jastrow factors to the simple product state. The resulting wave function has two sets of variational parameters: parameters controlling the product-state, and Jastrow parameters responsible for the quantum correlations.

For the Huse-Elser wave functions, we use the local basis of S_z eigenstates, i.e., the states $|0\rangle$, $|1\rangle$, and $|\bar{1}\rangle$ with $S_z = 0$, 1, and -1, respectively. The corresponding basis of Ising configurations is denoted by $|\alpha\rangle = |110\bar{1}0\bar{1}1\ldots\rangle$. As before, the singly occupied subspace corresponds to physical spin states. Furthermore, we project the wave functions to $S_z^{\rm tot} = 0$ by restricting to Ising states with $N_1 = N_{\bar{1}}$. However, here we allow the total flavor numbers to fluctuate within this subspace.

In Ref. [55] the optimal three-sublattice product states for the bilinear-biquadratic model (2.37) were calculated. It was found that the ordering patterns in this model are well captured by the antiferromagnetic and nematic states given in Eqs. (2.35) and (2.36). In the basis of S_z eigenstates, the wave function on A, B, and C sublattices is given by

$$\begin{aligned} |A\rangle &= \cos\eta\,|0\rangle + \kappa\frac{\sin\eta}{\sqrt{2}}\left(|1\rangle + |\bar{1}\rangle\right), \\ |B\rangle, |C\rangle &= \cos\eta\,|0\rangle + \kappa\frac{\sin\eta}{\sqrt{2}}\left(e^{\mp\frac{2\pi\mathrm{i}}{3}}|1\rangle + e^{\pm\frac{2\pi\mathrm{i}}{3}}|\bar{1}\rangle\right), \end{aligned} \tag{A.17}$$

where η is a variational parameter. $\kappa = 1$ corresponds to the antiferromagnetic, and $\kappa = i$ to the nematic product state. Using the Ising basis, the corresponding wave function may be written as

$$|\psi_p\rangle = \sum_\alpha e^{\tilde{H}_1}|\alpha\rangle, \tag{A.18}$$

where the sum goes over Ising states in the S_z basis. The one-body operator $\tilde{H}_1$ accounts for different weights of $|0\rangle$, $|1\rangle$, and $|\bar{1}\rangle$, as well as for site-dependent phase factors in the product-state wave function. For the particular case specified in Eq. (A.17), it can be written in terms of S_z operators as

$$\tilde{H}_1 = \sum_j \{\frac{2\pi\mathrm{i}}{3}(\delta_{j\in C} - \delta_{j\in B})S_{zj} + \log(\kappa\frac{\tan\eta}{\sqrt{2}})S_{zj}^2\}\,. \tag{A.19}$$

The Kronecker symbols $\delta_{j\in B}$ and $\delta_{j\in C}$ are nonzero only for sites j belonging to the B or C sublattice, respectively.

The advantage of the rather complicated form (A.18) for writing a simple product state is that quantum correlations can be built in easily by adding extra terms to $\tilde{H}_1$. We define

$$|\psi\rangle = \sum_{\alpha} e^{\tilde{H}}|\alpha\rangle, \tag{A.20}$$

where

$$\tilde{H} = \tilde{H}_1 + \tilde{H}_2 + \tilde{H}_3 + \ldots, \tag{A.21}$$

and $\tilde{H}_2$, $\tilde{H}_3$, ... denote many-body Jastrow factors. The correlated wave function (A.20) is easy to use in VMC, as long as $\tilde{H}$ is diagonal in the Ising basis $|\alpha\rangle$. In this paper, we only consider two-body correlation terms,

$$\tilde{H}_2 = -\sum_{\langle i,j\rangle}\{\beta(S_{zi}S_{zj}) + \gamma(S_{zi}S_{zj})^2\}\,. \tag{A.22}$$

In principle, in Eq. (A.22), the sum can go over farther-neighbor lattice sites, and the variational parameters β and γ may depend on the distance between sites. However, inclusion of farther-neighbor correlations are expected to have a small effect on the ground state energy [70]. Because of this, and also, in order to have a number of variational parameters that is similar to the number of parameters used for the spin liquid wave functions, we consider only nearest-neighbor Jastrow factors here.

The VMC algorithm can now be applied to Huse-Elser wave functions as outlined in Appendix A. The wave function is given by

$$\langle\alpha|\psi\rangle = e^{\tilde{H}(\alpha)}\,, \tag{A.23}$$

where $\tilde{H}(\alpha) = \langle\alpha|\tilde{H}|\alpha\rangle$. The Metropolis acceptance probability (A.2) and the expectation values (A.3) are straightforward to calculate. In contrast to the case of fermionic wave functions, no determinants or Pfaffians need to be evaluated or updated for this.

In contrast to similar wave functions for spin $S = 1/2$, an important subtlety arises here in the generation of the random walk. For $S = 1/2$ and $S_z^{\rm tot} = 0$, the configurations α are restricted to states with an equal number of up and down spins. Therefore, the only admissible local Monte Carlo move is an exchange of two opposite spins. For $S = 1$, due to presence of the nematic state $|0\rangle$ with $S_z = 0$, more local moves are possible. The Hilbert space for $S = 1$ and $S_z^{\rm tot} = 0$ can be written as a direct sum of orthogonal subspaces ("N_1-sectors") with a fixed number $N_1 = 0 \ldots N/2$ of sites in configuration $|1\rangle$. The dimension of each N_1-sector is $D(N_1) = \binom{N}{N_1}\binom{N-N_1}{N_1}$. There exist two types of local moves in a random walk through the Ising configurations: those leaving N_1 intact and those changing N_1 and moving to a different N_1-sector. The algorithm generating the random walk has to be unbiased with respect to moves between different sectors such that each N_1-sector is visited with probability $p(N_1) = D(N_1)/\sum_{n=0}^{N/2} D(n)$. We have checked that such a distribution is accurately generated by the following procedure. We pick two sites at random and, depending on the states found on the sites, perform the following move:

(i) $|0\rangle|1\rangle$ or $|0\rangle|\bar{1}\rangle$: exchange the states.

(ii) $|1\rangle|\bar{1}\rangle$: exchange states or change to $|0\rangle|0\rangle$, each with probabilities 1/2.

(iii) $|0\rangle|0\rangle$: change state to $|1\rangle|\bar{1}\rangle$.

(iv) $|1\rangle|1\rangle$ or $|\bar{1}\rangle|\bar{1}\rangle$: pick two different sites that are occupied by unequal flavors and exchange them.

In (iv), when the configurations $|1\rangle|1\rangle$ or $|\bar{1}\rangle|\bar{1}\rangle$ are encountered, it is important to find two flavors to exchange, thus not changing the N_1-sector. For example, if our algorithm rejected this case, and retried with another pair of sites, the random walk would be *biased* with respect to the distribution $p(N_1)$, resulting in a higher probability for visiting sectors with smaller N_1.

A.3 Symmetries of bilinear-biquadratic and SU(3)-models

In this appendix, we elaborate on the symmetry properties of the bilinear-biquadratic model (2.37) and of the SU(3) ring-exchange model (2.6) investigated in this paper.

Let us first discuss the SU(3) symmetry of these models. Writing the Heisenberg exchange operator for spin $S = 1$, Eq. (2.5), in terms of the operators $\vec{f} = (f_x, f_y, f_z)$, we have

$$\begin{aligned} \mathcal{P}_{ij} &= \vec{S}_i \cdot \vec{S}_j + (\vec{S}_i \cdot \vec{S}_j)^2 - 1 \\ &= \sum_{ab} f^\dagger_{ai} f_{bi} f^\dagger_{bj} f_{aj} = \vec{f}^\dagger_i \cdot (\vec{f}_i \cdot \vec{f}^\dagger_j) \vec{f}_j \,. \end{aligned} \tag{A.24}$$

In this notation it is clear that $\mathcal{P}_{ij}$ is invariant under a global transformation $\vec{f} \mapsto A\vec{f}$ where A is a general 3×3 unitary matrix. However, as discussed previously, the transformation $f_a \mapsto e^{i\phi} f_a$ with the same phase for all flavors does not change the corresponding spin state. Therefore, the relevant spin symmetry is SU(3) = U(3)/U(1), and we can take $A \in$ SU(3). Similar to the operators f_a that create these states, the spin states $|a\rangle$ transform in the fundamental representation of the SU(3) symmetry, by matrix multiplication with A. To find the action of the symmetry on spin operators, let us define

$$\hat{Q}_\mu = \sum_{ab} f^\dagger_a \lambda^{ab}_\mu f_b \,, \tag{A.25}$$

where $\lambda_\mu = (\lambda^{ab}_\mu)$, $\mu = 1 \ldots 8$, are the Gell-Mann matrices, generators of SU(3). Using

$$[\hat{Q}_\mu, f_a] = \sum_b \lambda^{ab}_\mu f_b \,, \tag{A.26}$$

it is clear that

$$A\vec{f} = e^{i\,\mathrm{ad}(\hat{Q})} \vec{f} = e^{i\hat{Q}} \vec{f} e^{-i\hat{Q}} \,, \tag{A.27}$$

for $A = \exp\{\mathrm{i}\sum_\mu \alpha_\mu \lambda_\mu\}$ and $\hat{Q} = \sum_\mu \alpha_\mu \hat{Q}_\mu$. Therefore, the spin operators

$$\vec{S} = -\mathrm{i}\vec{f}^\dagger \times \vec{f} \tag{A.28}$$

transform as

$$\vec{S} \mapsto e^{\mathrm{i}\hat{Q}} \vec{S} e^{-\mathrm{i}\hat{Q}} \tag{A.29}$$

under an SU(3) symmetry transformation.

Rather than explicitly writing down all eight generators of the SU(3) symmetry, Eq. (A.25), in spin language using the Gell-Mann basis, let us mention an equivalent set of generators. This set consists of the three spin rotation generators S_a and the five independent quadrupolar operators $Q_{ab} = (S_a S_b + S_b S_a)/2 - 2/3\,\delta_{ab}$ [64].

The ring-exchange model, Eq. (2.6), is written in terms of Heisenberg exchange operators $\mathcal{P}_{ij}$. Therefore, it has the large SU(3) symmetry discussed above for all values of parameter α. The bilinear-biquadratic model, Eq. (2.37), enjoys the SU(3) symmetry only at the special point $K = 1$ and $D = 0$ in parameter space (where it is equivalent to the ring-exchange model at $\alpha = 0$). Moving away from this special point, for general K but keeping $D = 0$, the symmetry is reduced to SO(3) spin rotation symmetry, generated by $\vec{S}$. Finally, for $D \neq 0$, this symmetry is further reduced to U(1) spin rotation about the z axis.

When we move away from the SU(3) symmetric point along the line $K = 1$ and $D \neq 0$, the symmetry is reduced to SU(2) on that line. Clearly, the spin rotation symmetry is reduced to S_z as $D \neq 0$. To find the remaining unbroken generators, we need to determine the SU(3) generators that commute with the biquadratic term S_z^2. These generators are $S_x S_y + S_y S_x$ and $S_x^2 - S_y^2$. Hence, $\{S_z,\ S_x S_y + S_y S_x,\ S_x^2 - S_y^2\}$ are the three generators of an SU(2) symmetry of the model (2.37) on the line $K = 1$.

Let us briefly discuss the symmetry reasons behind the degeneracy of the correlated AFM and the nematic states, (2.35) and (2.36), on the line $K = 1$. In terms of spinon operators, the relevant symmetry generator is written as

$$S_y^2 - S_x^2 = f_x^\dagger f_x - f_y^\dagger f_y\,. \tag{A.30}$$

From (A.27), we see that x and y states simply acquire an opposite phase under this transformation: $f_x \mapsto e^{i\varphi} f_x$, $f_y \mapsto e^{-i\varphi} f_y$. It is easy to check that the magnetic state (2.35) is mapped to the spin-nematic state (2.36) for $\varphi = \pi/2$, *i.e.*, when $f_x \mapsto i f_x$ and $f_y \mapsto -i f_y$. Furthermore, it is clear that the hopping term in (2.30) and the Jastrow factors in (2.31) are invariant under this transformation. Hence, the correlated ordered states are exactly mapped into each other by this transformation.

Appendix B

Calculation of RG flow of Kondo coupling

B.1 Calculation of diagrams for β-function

In this Appendix we present calculation of diagrams in Fig. 3-3 with fermion propagator, Eq. (3.9a), containing self-energy due to gauge field. Detailed calculation of these diagrams without gauge field can be found, for example, in Refs. [86, 87].

First we consider diagram in Fig. 3-3 (a), describing second order correction to the dimensionless coupling $g = \nu J_K$. We will be interested only in the logarithmically divergent part of the diagram. Using zero temperature Matsubara diagram technique and implying summation over repeated indices we can write for the correction to impurity interaction vertex:

$$\Gamma^{(a1)}_{\alpha\beta\gamma\delta} = -\left(\frac{J_K}{4}\right)^2 (\boldsymbol{\sigma}_{\alpha\rho}\cdot\boldsymbol{\sigma}_{\gamma\lambda})(\boldsymbol{\sigma}_{\rho\beta}\cdot\boldsymbol{\sigma}_{\lambda\delta})\int \frac{d\boldsymbol{k}\, d\omega_1}{(2\pi)^3} F(-\mathrm{i}\omega_1)G(\boldsymbol{k}, \mathrm{i}\omega + \mathrm{i}\omega_1). \quad \text{(B.1)}$$

Symmetric counterpart of diagram (a) with flipped direction of the propagation of the pseudofermions (not shown in Fig. 3-3) gives us,

$$\Gamma^{(a2)}_{\alpha\beta\gamma\delta} = -\left(\frac{J_K}{4}\right)^2 (\boldsymbol{\sigma}_{\alpha\rho}\cdot\boldsymbol{\sigma}_{\lambda\delta})(\boldsymbol{\sigma}_{\rho\beta}\cdot\boldsymbol{\sigma}_{\gamma\lambda})\int \frac{d\boldsymbol{k}\, d\omega_1}{(2\pi)^3} F(\mathrm{i}\omega_1)G(\boldsymbol{k}, \mathrm{i}\omega + \mathrm{i}\omega_1). \quad \text{(B.2)}$$

After integrating over ω_1 and changing integration variable from $\boldsymbol{k}$ to $\xi = \varepsilon_{\boldsymbol{k}} - \mu$, we have similar expressions for both diagrams:

$$\Gamma^{(a1,2)}_{\alpha\beta\gamma\delta} = \left(\frac{J_K}{4}\right)^2 (\mp 2\boldsymbol{\sigma}_{\alpha\beta}\cdot\boldsymbol{\sigma}_{\gamma\delta} + 3\delta_{\alpha\beta}\delta_{\gamma\delta})\nu \int d\xi \frac{\theta(\pm\xi)}{i\omega(1+\frac{1}{N\varepsilon}\left|\frac{\omega_0}{\omega}\right|^{\varepsilon/2}) - \xi}, \tag{B.3}$$

We perform integration over ξ, retaining only logarithmical part. Collecting results for both diagrams and going to real frequency domain, we get:

$$\Gamma^{(a)}_{\alpha\beta\gamma\delta} = 4\nu\left(\frac{J_K}{4}\right)^2 (\boldsymbol{\sigma}_{\alpha\beta}\cdot\boldsymbol{\sigma}_{\gamma\delta}) \log\frac{D}{|\omega|(1+\frac{1}{N\varepsilon}\left|\frac{\omega_0}{\omega}\right|^{\varepsilon/2})}. \tag{B.4}$$

We expand logarithm in ε to the leading order and collect both terms into single logarithm again:

$$\log\frac{D}{|\omega|(1+\frac{1}{N\varepsilon}\left|\frac{\omega_0}{\omega}\right|^{\varepsilon/2})} = \log\frac{D}{|\omega|} - \kappa\log\frac{\omega_0}{|\omega|} = \log\frac{D}{|\omega|^{1-\kappa}\omega_0^{\kappa}} \tag{B.5}$$

where κ is small, $\kappa \propto O(1/N)$,

$$\kappa = \frac{1}{2N}\frac{1}{1+\frac{1}{N\varepsilon}}. \tag{B.6}$$

Finally, we have

$$\Gamma^{(a)}_{\alpha\beta\gamma\delta} = -g\log\frac{D}{|\omega|^{1-\kappa}\omega_0^{\kappa}}\Gamma_{\alpha\beta\gamma\delta}, \tag{B.7}$$

where bare vertex $\Gamma_{\alpha\beta\gamma\delta}$ is defined in Eq. (3.9c), and we retained only logarithmically divergent terms. Alternatively, we could expand in Greens function in $1/N$ already in Eqs. (B.1)-(B.2), reproducing the same result.

Calculations of vertex and Z-factor renormalization, described correspondingly by diagrams (b) and (c) in Fig. 3-3 are very similar. Indeed, in order to get impurity pseudofermions Z-factor, $Z_{\rm imp}$, we have to differentiate self-energy over ω, what may be thought of as an introduction of additional vertex with zero incoming frequency. Therefore, below we present only details on the calculation for the derivative of self-energy and list the result for the vertex renormalization.

Correction to the impurity self-energy described by diagram Fig. 3-3 (c) is written as

$$\Sigma^{\rm imp}(\mathrm{i}\omega) = -6N\left(\frac{J_K}{4}\right)^2 \int \frac{d\boldsymbol{k}_1\, d\omega_1}{(2\pi)^3}\frac{d\boldsymbol{k}_2\, d\Omega_2}{(2\pi)^3} \times G(\boldsymbol{k}_1, \mathrm{i}\omega_1)G(\boldsymbol{k}_2, \mathrm{i}\omega_1 + \mathrm{i}\Omega_2)F(\mathrm{i}\omega + \mathrm{i}\Omega_2), \quad \text{(B.8)}$$

where we omitted spin indices of external pseudofermions and associated δ-function. Renormalization of $Z_{\rm imp}$ is given by the derivative of self-energy,

$$Z_{\rm imp}^{-1} = 1 - \frac{\partial\Sigma_{\rm imp}(\mathrm{i}\omega)}{\partial(\mathrm{i}\omega)}, \quad \text{(B.9)}$$

so that to the first order in the self-energy,

$$\delta Z_{\rm imp} = \frac{\partial\Sigma^{\rm imp}(\mathrm{i}\omega)}{\partial(\mathrm{i}\omega)}. \quad \text{(B.10)}$$

Integrating over Ω_2 in Eq. (B.8), we have

$$\delta Z_{\rm imp} = 6N\left(\frac{J_K}{4}\right)^2 \frac{\partial}{\partial(\mathrm{i}\omega)} \int \frac{d\boldsymbol{k}_1\, d\boldsymbol{k}_2}{(2\pi)^4} \mathcal{I}_{\boldsymbol{k}_1,\boldsymbol{k}_2,\mathrm{i}\omega}, \quad \text{(B.11)}$$

$$\mathcal{I}_{\boldsymbol{k}_1,\boldsymbol{k}_2,\mathrm{i}\omega} = \int \frac{d\omega_1}{2\pi} G(\boldsymbol{k}_1, \mathrm{i}\omega_1)G(\boldsymbol{k}_2, \mathrm{i}\omega_1 - \mathrm{i}\omega)\theta(-\xi_{\boldsymbol{k}_2}). \quad \text{(B.12)}$$

To simplify further calculations, we expand in ε and $1/N$. Self-energy, Eq. (3.13), expanded to the leading order in ε becomes:

$$\Sigma(\mathrm{i}\omega) = -\mathrm{i}\omega\left(\frac{1}{N\varepsilon} + \frac{1}{2N}\log\left|\frac{\omega_0}{\omega}\right|\right). \quad \text{(B.13)}$$

Inserting this into fermion Greens function, Eq. (3.9a), and expanding in $1/N$ we get:

$$G(\boldsymbol{k}_1, \mathrm{i}\omega_1) = \tilde{G}(\boldsymbol{k}_1, \mathrm{i}\omega_1) - \frac{1}{2N}\mathrm{i}\omega_1 \log\left|\frac{\omega_0}{\omega_1}\right| [\tilde{G}(\boldsymbol{k}_1, \mathrm{i}\omega_1)]^2, \quad \text{(B.14)}$$

where $\tilde{G}(\boldsymbol{k}_1, \mathrm{i}\omega_1)$ is defined as:

$$\tilde{G}(\boldsymbol{k}_1, \mathrm{i}\omega_1) = \frac{1}{\mathrm{i}\omega_1(1+\frac{1}{N\varepsilon}) - \xi_{\boldsymbol{k}_1}}. \tag{B.15}$$

Finally, expansion of the product of Greens function in $\mathcal{I}_{\boldsymbol{k}_1,\boldsymbol{k}_2,\mathrm{i}\omega}$, Eq. (B.12), gives us:

$$\mathcal{I}_{\boldsymbol{k}_1,\boldsymbol{k}_2,\mathrm{i}\omega} = \int \frac{d\omega_1}{2\pi}\theta(-\xi_{\boldsymbol{k}_2})\tilde{G}(\boldsymbol{k}_1, \mathrm{i}\omega_1)\tilde{G}(\boldsymbol{k}_2, \mathrm{i}\omega_1 - \mathrm{i}\omega)\left[1 - \frac{1}{2N}\mathrm{i}\omega_1 \log\left|\frac{\omega_0}{\omega_1}\right| \tilde{G}(\boldsymbol{k}_1, \mathrm{i}\omega_1)\right.$$
$$\left. -\frac{1}{2N} i(\omega_1 - \omega)\log\left|\frac{\omega_0}{\omega_1 - \omega}\right| \tilde{G}(\boldsymbol{k}_2, \mathrm{i}\omega_1 - \mathrm{i}\omega)\right]. \tag{B.16}$$

After integration over ω_1, zeroth order term in (B.16) yields

$$\mathcal{I}^{(0)}_{\boldsymbol{k}_1,\boldsymbol{k}_2,\mathrm{i}\omega} = -\frac{\theta(\xi_{\boldsymbol{k}_1})\theta(-\xi_{\boldsymbol{k}_2})}{(1+\frac{1}{N\varepsilon})[\xi_{\boldsymbol{k}_1} + |\xi_{\boldsymbol{k}_2}| - i(1+\frac{1}{N\varepsilon})\omega]}. \tag{B.17}$$

This is inserted into Eq. (B.11). After integration over momenta extra factors $(1+\frac{1}{N\varepsilon})$ drop out and we reproduce the answer for the case without gauge field, $\delta Z^{(0)}_{\mathrm{imp}} = -3Ng^2/8\log(D/|\omega|)$.

Frequency integration for terms proportional to $1/N$ in Eq. (B.16) results into cumbersome expression. However, after integrations over $\xi_{\boldsymbol{k}_1}$ and $\xi_{\boldsymbol{k}_2}$ and extracting log-divergent part we obtain $\delta Z^{(1)}_{\mathrm{imp}} = 3\kappa Ng^2/8\log(\omega_0/|\omega|)$, where κ is defined in Eq. (B.6). Combining $\delta Z^{(0)}_{\mathrm{imp}}$ and $\delta Z^{(1)}_{\mathrm{imp}}$, we have for impurity pseudofermions Z-factor:

$$Z_{\mathrm{imp}} = 1 + \delta Z_{\mathrm{imp}} = 1 - \frac{3}{8}Ng^2 \log\frac{D}{|\omega|^{1-\kappa}\omega_0^{\kappa}}. \tag{B.18}$$

Correction to the impurity interaction vertex, diagram Fig. 3-3 (b) is calculated in a similar way. Resulting contribution to the interaction vertex is

$$\Gamma^{(b)}_{\alpha\beta\gamma\delta} = \frac{N}{8}g^2 \log\frac{D}{|\omega|^{1-\kappa}\omega_0^{\kappa}}\Gamma_{\alpha\beta\gamma\delta}. \tag{B.19}$$

Finally, renormalized coupling is

$$g_R = \frac{g + \delta g}{Z_{\mathrm{imp}}}, \tag{B.20}$$

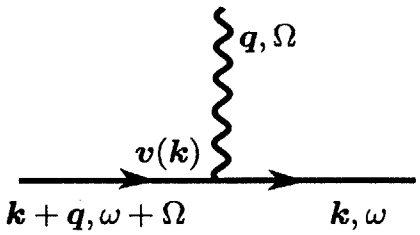

Figure B-1: Part of diagram with vertex corrections that makes the diagram vanish.

where $Z_{\rm imp}$ is given by Eq. (B.18), and δg can be read from Eqs. (B.7) and (B.19):

$$\frac{\delta g}{g} = \left(-g + \frac{N}{8}g^2\right) \log \frac{D}{|\omega|^{1-\kappa}\omega_0^{\kappa}}. \tag{B.21}$$

Using that $\omega_0 \propto D$, we obtain the β-function:

$$\beta(g) = \frac{d\log g}{d\log D} = (1-\kappa)\left(-g^2 + \frac{N}{2}g^3\right) + \ldots, \tag{B.22}$$

where ellipses denote the subleading terms $O(1/N^3)$ obtained in Ref. [97, 98] and listed in the main text. Note, that Eq. (B.22) is exact to the order $1/N^3$: corrections to subleading terms from to the gauge field are of order $O(1/N^4)$ and thus can be ignored.

B.2 Vertex corrections

In this Appendix we demonstrate that a subset of vertex corrections where gauge field propagator is connected to internal fermion Greens function vanish. Two examples of such diagrams are shown in Fig. 3-4 (a). It suffices to consider a part present in all diagrams, consisting of two Greens functions and a single gauge field vertex, Fig. B-1. Using notations adopted in Fig. B-1, we can write for the integral over momentum $\boldsymbol{k}$

$$\int dk_x\, dk_y\, v_y(\boldsymbol{k}) G(\boldsymbol{k}, \mathrm{i}\omega) G(\boldsymbol{k} + q\boldsymbol{e}_x, \mathrm{i}\omega + \mathrm{i}\Omega), \tag{B.23}$$

where we assumed that $\boldsymbol{q}$ has only x-component, $\boldsymbol{q} \parallel \boldsymbol{e}_x$ and used fact that gauge field is transverse. Note that integration over $\boldsymbol{k}$ does not involve any other functions

due to the fact that interaction with impurity is local. It is integration over k_y in Eq. (B.23) that makes the expression to be zero. Indeed, prefactor $v_y(\boldsymbol{k})$ is odd under inversion of k_y, whereas both Greens functions do not change under $k_y \to -k_y$. Since this part is present in all diagrams in Fig. 3-4 (b), all these diagrams vanish.

Appendix C

Spinon-phonon interactions

C.1 Elements of representation theory for relevant groups

This Appendix provides background on the representation theory, and gives more details for the symmetry groups used in the main text. It starts with a summary of the basic facts from the representation theory of finite groups, which are extensively used throughout the paper. The reader interested in more details or derivations of particular statements is referred to Refs. [190, 191]. Next, the symmetry group of square and its extension, relevant for the πF$\square$ and sF$\square$ phases, is considered. Finally, the basic facts about the symmetry group of hexagon and the symmetry group of the πF$\hexagon$ phase are discussed.

C.1.1 Basic facts from representation theory

We consider a point group $\mathcal{G}$, which contains $h_{\mathcal{G}}$ elements. Notion of conjugacy classes will be of great importance for us in what follows. Conjugacy class is defined as a complete set of mutually conjugate group elements, where two group elements g_1 and g_2 are defined to be conjugate if there exists another group element g_3, such that $g_1 = g_3^{-1} \circ g_2 \circ g_3$. In other words, if g belongs to a given conjugacy class, $\mathcal{C}_i$, then for

any group element

$$\forall\ g_j \in \mathcal{G}, \qquad g_j^{-1} \circ g \circ g_j \in \mathcal{C}_i, \tag{C.1}$$

still is an element from the conjugacy class $\mathcal{C}_i$. Let us assume, that the group $\mathcal{G}$ has $n_{\mathcal{G}}$ conjugacy classes, denoted as $\mathcal{C}_1, \mathcal{C}_2, \ldots \mathcal{C}_{n_{\mathcal{G}}}$. Each class contains N_k elements, and, since each group element belongs to only one conjugacy class, we have $\sum_{k=1}^{n_{\mathcal{G}}} N_k = h_{\mathcal{G}}$. The identity element, which is necessary present in any group is a conjugacy class itself, $\mathcal{C}_1 \equiv E = \{\mathbb{1}\}$ and $N_1 = 1$. For an abelian group, any element belongs to a separate conjugacy class, so that $n_{\mathcal{G}} = h_{\mathcal{G}}$, and $N_{1,\ldots,n_{\mathcal{G}}} = 1$.

In what follows, our main interest will be in classifying representations of a given group. Representation of the group can be thought of as a mappings from the group elements to operators acting on some linear space, $g \to R_g$ which respects the group multiplication, $R_{g_1} \cdot R_{g_2} = R_{g_1 \circ g_2}$. If operators from a given representations cannot be represented as a direct sum of two operators acting on a smaller subspaces, this representation is called irreducible. According to this definition, any representation D can be expressed as a direct sum of irreducible representations,

$$D = a_1 D^{(1)} \oplus a_2 D^{(2)} \oplus \ldots \oplus a_{n_{\mathcal{G}}} D^{(n_{\mathcal{G}})}, \tag{C.2}$$

where non-negative integers a_i describe how many times a given irreducible representation is encountered in the decomposition. If $D^{(i)}$ is not contained within D, corresponding a_i is zero, $a_i = 0$. In this way the problem of classifying all representations of a given group is reduced to a classification of all irreducible representations.

The number of different irreducible representations for the group $\mathcal{G}$ coincides with the number of its conjugacy classes, $n_{\mathcal{G}}$. Each irreducible representation, $D^{(i)}$ is specified by the value of its character for different conjugacy classes, defined as

$$\chi^{(i)}(\mathcal{C}_k) = \operatorname{tr} R_{g_{\mathcal{C}_k}}, \quad \text{where} \quad g_{\mathcal{C}_k} \in \mathcal{C}_k. \tag{C.3}$$

According to the definition of the conjugacy class (C.1), the value of $\chi^{(i)}(\mathcal{C}_k)$ does not depend on the choice of a particular element $g_{\mathcal{C}_k}$ from the $\mathcal{C}_k$. Operators which act

on a linear space can be expressed as matrices, and trace in Eq. (C.3) is understood in this sense.

Value of character for the conjugacy class which consists identity $E = \{\mathbb{1}\}$ is special, since it gives us the dimension of the corresponding irreducible representation. To classify all irreducible representations of a given group, it is good to know not only the number of different irreducible representations, but their dimensions as well. In such situation the following relation between the number of elements in the group, $h_{\mathcal{G}}$ and the dimensions of all irreducible representations contained within the group, $\ell_i = \chi^{(i)}(E)$ turns out to be particularly useful:

$$h_{\mathcal{G}} = \sum_{i=1}^{N_C} \ell_i^2. \tag{C.4}$$

Typically only a few sets of integers $\{\ell_1, \ldots, \ell_{N_{\mathcal{G}}}\}$ satisfy this relation, and one can usually identify the correct set of dimensions by involving other considerations.

Character table is a compact way of describing all irreducible representations of a given group. It is a square $n_{\mathcal{G}} \times n_{\mathcal{G}}$ table, where columns correspond to different conjugacy classes, and rows are labeled by different irreducible representations. The entry at an intersection of i-th row and j-th column is given by the value of the character for the i-th representation of the group elements from the j-th conjugacy class.

Using the characters table of a given group, one can easily find multiplicities a_i in the decomposition of a representation D into irreducible representations, Eq. (C.2). Provided, characters of the representation D, $\chi(\mathcal{C}_k)$, are known, we can find a_i as

$$a_i = \frac{1}{h_{\mathcal{G}}} \sum_{k=1}^{n_{\mathcal{G}}} N_k \, \chi^{(i)*}(\mathcal{C}_k) \, \chi(\mathcal{C}_k), \tag{C.5}$$

where $h_{\mathcal{G}}$ is the number of elements in $\mathcal{G}$, and N_k is the number of elements in the corresponding conjugacy class.

If representation D is obtained as the tensor product of two representations, let us say, E and F, $D = E \times F$, the characters of D, $\chi(\mathcal{C}_k) \equiv \chi^{E\times F}(\mathcal{C}_k)$, can be obtained

as a product of characters for representations E and F,

$$\chi^{E\times F}(\mathcal{C}_k) = \chi^E(\mathcal{C}_k)\chi^F(\mathcal{C}_k). \tag{C.6}$$

After this, one can easily apply formula (C.5) to find the decomposition of the $E \times F$ into irreducible representations.

C.1.2 Group of square lattice and its representations

Here we illustrate how the facts summarized above may be used to classify representations of the point symmetry group of square, C_{4v} and its extension, C'_{4v}.

Point group of square C_{4v} and its representations

We start with reviewing properties and representations of the point symmetry group of square, C_{4v}. This is the group of all symmetry operations, which leave square invariant. It can be generated by rotations for $\pi/2$ around the center of the square, $\mathcal{R}_{\pi/2}$ and a reflection of x-axis, $\mathcal{R}_x$ [190]. In total the group C_{4v} has $h_{C_{4v}} = 8$ elements. In addition to rotations for angles multiple of $\pi/2$, these include reflections around x and y-axes, as well as $\mathcal{R}_{u,v}$, standing for reflections relative to the planes containing vectors $\hat{\boldsymbol{x}} \pm \hat{\boldsymbol{y}}$, $\mathcal{R}_{u,v} = \mathcal{R}_{x,y}\mathcal{R}_{\pi/2}$.

These elements can be split into total of $n_{C_{4v}} = 5$ conjugacy classes. There are two conjugacy classes consisting of only one group element: trivial $E = \{\mathbb{1}\}$, and $\mathcal{C}_2$ consisting of rotation for π, $\mathcal{C}_2 = \{\mathcal{R}_\pi\}$. Each of the remaining three classes consists of two elements: $\mathcal{C}_4 = \{\mathcal{R}_{\pi/2}, \mathcal{R}_{3\pi/2}\}$, $\mathcal{C}_{xy} = \{\mathcal{R}_x, \mathcal{R}_y\}$, and $\mathcal{C}_{uv} = \{\mathcal{R}_u, \mathcal{R}_v\}$. Correspondingly, group C_{4v} has five irreducible representations. Using Eq. (C.4) we find that four of irreducible representations are one-dimensional and one is a two-dimensional. Characters of these irreducible representations are listed in Table C.1. One-dimensional representations are fully specified by their list of characters. Whereas two dimensional representation E_1 corresponds to a transformation of a vector. If we denote the basis

Rep.	E	C_2	C_4	C_{xy}	σ_{uv}
A_1	1	1	1	1	1
A_2	1	1	1	-1	-1
B_1	1	1	-1	1	-1
B_2	1	1	-1	-1	1
E_1	2	-2	0	0	0

Table C.1: Irreducible representations of C_{4v} and their characters.

of E_1 as $(\hat{\boldsymbol{x}}, \hat{\boldsymbol{y}})$, action of the group generators becomes

$$\mathcal{R}_{\pi/2}: \qquad \hat{\boldsymbol{x}} \to \hat{\boldsymbol{y}}, \qquad \hat{\boldsymbol{y}} \to -\hat{\boldsymbol{x}}, \tag{C.7a}$$

$$\mathcal{R}_{x}: \qquad \hat{\boldsymbol{x}} \to -\hat{\boldsymbol{x}}, \qquad \hat{\boldsymbol{y}} \to \hat{\boldsymbol{y}}. \tag{C.7b}$$

Using Table C.1 we can easily find decomposition of the Kronecker product of $E_1 \times E_1$ into irreducible representations. [190] Only two non-zero characters of $E_1 \times E_1$ are $\chi^{E_1 \times E_1}(E) = \chi^{E_1 \times E_1}(C_2) = 4$. Now, using Eq. (C.5) we can find that first four representations in Table C.1 are contained once within $E_1 \times E_1$: corresponding multiplicities are all equal to one, $a_i = 1/8 \cdot (4 + 4) = 1$. Whereas for E_1, we find corresponding a to be zero. This may be summarized as

$$E_1 \times E_1 = A_1 \oplus A_2 \oplus B_1 \oplus B_2. \tag{C.8}$$

Although formula (C.5) gives us information about representations contained within $E_1 \times E_1$, it does not give explicit expression for basis of these irreducible representations. In the present case the explicit form of the basis may be easily guessed from physical arguments. Basis of each E_1 in the product can be written as a two components of a vector, with the action of generators specified in Eq. (C.7). Having components of two vectors (q_x, q_y) and (u_x, u_y), one can easily guess that the quantity, invariant under all symmetries is the scalar product. Thus, $\boldsymbol{q} \cdot \boldsymbol{u} = q_x u_x + q_y u_y$ is a basis of A_1 component, contained in Eq. (C.8). Basis for A_2 is also easy to guess, as it has to change sign under any reflections. Thus, it is given by the vector product, $\boldsymbol{q} \times \boldsymbol{u} = q_x u_y - q_y u_x$. Finally, one can check that remaining combinations $q_x u_x - q_y u_y$

and $q_x u_y + q_y u_x$ realize the basis for B_1 and B_2 irreducible representations. This leads us to the Eq. (4.27) in the main text, which summarizes the above results.

Group C'_{4v} and its representations

From the group C_{4v} we move to the group $C'_{4v} = G_\square / G_{2t}$, which is the factor group of the space group of square lattice $G_\square$ over the group of translations for two unit cell vectors G_{2t}. In other words, group C'_{4v} is defined as group C_{4v} with added translation operations $t_{\boldsymbol{a}_1}$ and $t_{\boldsymbol{a}_2}$. In order to specify this group we will use Seitz operators $\{R|\boldsymbol{t}\}$ defined as

$$\{R|\boldsymbol{t}\} \cdot \boldsymbol{r} = R \cdot \boldsymbol{r} + \boldsymbol{t}. \tag{C.9}$$

The group

$$G_t = \{\{\mathbb{1}|0\}, \{\mathbb{1}|\boldsymbol{a}_1\}, \{\mathbb{1}|\boldsymbol{a}_2\}, \{\mathbb{1}|\boldsymbol{a}_1 + \boldsymbol{a}_2\}\} \tag{C.10}$$

is the subgroup of C'_{4v} and it contains $h_{G_t} = 4$ elements. The group C'_{4v} has $h_{C'_{4v}} = h_{G_t} \cdot h_{4v} = 32$ elements. It has $n_{C'_{4v}} = 14$ conjugacy classes, which are listed in Table C.2.

Representations of C'_{4v} can be worked out using the fact that it has a subgroup G_t. Consequently we can easily obtain five irreducible representations, one-dimensional $A_{1,2}$ and $B_{1,2}$ along with two-dimensional E_1, from corresponding irreducible representations of C_{4v}. For this we simply assume the action of translations to be trivial. Assuming that translation result in multiplying basis elements by minus one, we find additional four one-dimensional irreducible representations, denoted as $A'_{1,2}$ and $B'_{1,2}$ to emphasize that these are an extension of corresponding representations from C_{4v}. Analogous extension of E_1 is denoted as E'_1. Remaining four two-dimensional irreducible representations can be found explicitly using $SU(4)$ generators given by $\{\mu^i, \tau^i, \mu^i\tau^j\}$ as a basis. Action of translations for representations $E_2 \ldots E_5$ can be written as

$$T_{x,y}: \quad \hat{\boldsymbol{x}} \to \mp\hat{\boldsymbol{x}}, \quad \hat{\boldsymbol{y}} \to \pm\hat{\boldsymbol{y}}, \tag{C.11}$$

so that $T_x T_y = -\mathbb{1}$. However, the transformation of basis under rotation and reflection

Conj. class	E	$\mathcal{C}_t$	$\mathcal{C}_{tt}$	$\mathcal{C}_2$	$\mathcal{C}_{2t}$	$\mathcal{C}_{2tt}$	$\mathcal{C}_4$
$N_\mathcal{C}$	1	2	1	1	2	1	4
Members	$\mathbb{1}$	$\{\mathbb{1}\|\boldsymbol{a}_{1,2}\}$	$\{\mathbb{1}\|\boldsymbol{a}_3\}$	$\{\mathcal{R}_\pi\|0\}$	$\{\mathcal{R}_\pi\|\boldsymbol{a}_{1,2}\}$	$\{\mathcal{R}_\pi\|\boldsymbol{a}_3\}$	$\{\mathcal{R}^{1,3}_{\pi/2}\|0,\boldsymbol{a}_3\}$
Conj. class	$\mathcal{C}_{4t}$	$\mathcal{C}_{xy}$	$\mathcal{C}_{xyt_1}$	$\mathcal{C}_{xyt_2}$	$\mathcal{C}_{xytt}$	$\mathcal{C}_{uv}$	$\mathcal{C}_{uvt}$
$N_\mathcal{C}$	4	2	2	2	2	4	4
Members	$\{\mathcal{R}^{1,3}_{\pi/2}\|\boldsymbol{a}_{1,2}\}$	$\{\mathcal{R}_{x,y}\|0\}$	$\{\mathcal{R}_x\|\boldsymbol{a}_1\}$ $\{\mathcal{R}_y\|\boldsymbol{a}_2\}$	$\{\mathcal{R}_x\|\boldsymbol{a}_2\}$ $\{\mathcal{R}_y\|\boldsymbol{a}_1\}$	$\{\mathcal{R}_{x,y}\|\boldsymbol{a}_3\}$	$\{\mathcal{R}_{u,v}\|0,\boldsymbol{a}_3\}$	$\{\mathcal{R}_{u,v}\|\boldsymbol{a}_{1,2}\}$

Table C.2: Labeling of conjugacy classes of group C'_{4v}. Below each label, number of group elements, $N_\mathcal{C}$, belonging to a given conjugacy class, as well as explicit form of these elements in Seitz notations are given. Vector $\boldsymbol{a}_3$ is a short-hand notation for the sum of lattice vectors, $\boldsymbol{a}_3 = \boldsymbol{a}_1 + \boldsymbol{a}_2$.

Rep.	E	C_t	C_{tt}	C_2	C_{2t}	C_{2tt}	C_4	C_{4t}	C_{xy}	C_{xyt_1}	C_{xyt_2}	C_{xytt}	C_{uv}	C_{uvt}
A_1	1	1	1	1	1	1	1	1	1	1	1	1	1	1
A_2	1	1	1	1	1	1	1	1	-1	-1	-1	-1	-1	-1
B_1	1	1	1	1	1	1	-1	-1	1	1	1	1	-1	-1
B_2	1	1	1	1	1	1	-1	-1	-1	-1	-1	-1	1	1
A_1'	1	-1	1	1	-1	1	1	-1	1	-1	-1	1	1	-1
A_2'	1	-1	1	1	-1	1	1	-1	-1	1	1	-1	-1	1
B_1'	1	-1	1	1	-1	1	-1	1	1	-1	-1	1	-1	1
B_2'	1	-1	1	1	-1	1	-1	1	-1	1	1	-1	1	-1
E_1	2	2	2	-2	-2	-2	0	0	0	0	0	0	0	0
E_1'	2	-2	2	-2	2	-2	0	0	0	0	0	0	0	0
E_2	2	0	-2	2	0	-2	0	0	-2	0	0	2	0	0
E_3	2	0	-2	2	0	-2	0	0	2	0	0	-2	0	0
E_4	2	0	-2	-2	0	2	0	0	0	2	-2	0	0	0
E_5	2	0	-2	-2	0	2	0	0	0	-2	2	0	0	0

Table C.3: Irreducible representations of C_{4v}' and their characters. The first eight representations are one-dimensional, the remaining six representations are two-dimensional.

are realized differently for each of these representations. For representations E_2 and E_3 we have

$$\mathcal{R}_{\pi/2}: \quad \hat{\boldsymbol{x}} \to \hat{\boldsymbol{y}}, \quad \hat{\boldsymbol{y}} \to \hat{\boldsymbol{x}}, \tag{C.12a}$$

$$\mathcal{R}_x: \quad \hat{\boldsymbol{x}} \to \mp\hat{\boldsymbol{x}}, \quad \hat{\boldsymbol{y}} \to \mp\hat{\boldsymbol{y}}, \tag{C.12b}$$

with the minus (plus) sign corresponding to E_2 (E_3). For E_4 (E_5) we get:

$$\mathcal{R}_{\pi/2}: \quad \hat{\boldsymbol{x}} \to \mp\hat{\boldsymbol{y}}, \quad \hat{\boldsymbol{y}} \to \pm\hat{\boldsymbol{x}}, \tag{C.13a}$$

$$\mathcal{R}_x: \quad \hat{\boldsymbol{x}} \to \mp\hat{\boldsymbol{x}}, \quad \hat{\boldsymbol{y}} \to \pm\hat{\boldsymbol{y}}. \tag{C.13b}$$

The character table may be easily calculated from here, and it is summarized in Table C.3.

From characters we determine the decomposition of different representations of C_{4v}' on fermion bilinears into irreducible representations. Indeed, basis in the space of all possible fermion bilinears that are singlets in spin sector can be constructed using

$SU(4)$ generators $\{\mu^i, \tau^i, \mu^i\tau^j\}$. Therefore this problem is equivalent to reducing adjoint representation of C'_{4v} on sixteen 4×4 matrices $\{\mathbb{1}, \mu^i, \tau^i, \mu^i\tau^j\}$. Representation is fully specified by the action of generators. For the cases of the πF$\square$ phase these are given by Eqs. (4.13)-(4.19). Whereas for the sF$\square$ phase, the reader is referred to Ref. [5]. (Note, that there $\mathcal{R}_x$ is defined as a reflection with respect to the edge of square, whereas in our conventions reflection plane goes through the center of plaquette. Therefore $\mathcal{R}_x$ from Ref. [5] coincides with $T_x\mathcal{R}_x$ in our notations.) Calculating characters and applying Eq. (C.5), we find

$$G^{\pi\mathrm{F}\square}_{\psi^\dagger\psi} = A_1 \oplus A_2 \oplus B'_1 \oplus B'_2 \oplus E_1 \oplus E'_1 \oplus E_2 \oplus E_3 \oplus E_4 \oplus E_5, \tag{C.14}$$

for the πF$\square$ phase, where basis in terms of products of Pauli matrices for each irreducible componentis listed in Table 4.1 in the main text. We also obtained the same expressions for bases of different representations using the notations from Ref. 23. Analogously, for the πF$\square$ phase we have:

$$G^{\mathrm{sF}\square}_{\psi^\dagger\psi} = A_2 \oplus B_1 \oplus B'_1 \oplus A'_2 \oplus 2E'_1 \oplus 2E_3 \oplus E_4 \oplus E_5, \tag{C.15}$$

with details on the basis listed in Table 4.2. From here we immediately recover result of Refs. [5,23] that no invariant fermion bilinear terms exist in πF$\square$ and sF$\square$ phases. Indeed, G^{sF} does not contain trivial representation A_1. Whereas, even though $G^{\pi\mathrm{F}}$ contains A_1, as one can see from Table 4.1 it is not invariant under time reversal, $\mathcal{T}$, nor under charge conjugation, $\mathcal{C}$.

C.1.3 Group of honeycomb and kagome lattices

Since an extensive details for kagome and honeycomb lattices are available in the literature [6,7], we only briefly summarize the basic facts for the symmetry group of the hexagon C_{6v} and its extension for the πF$\hexagram$ phase. More details for the honeycomb lattice can be found in Ref. [7].

Point group of hexagon

For kagome and honeycomb lattices the relevant point group is that of a hexagon, denoted as C_{6v}. It has $h_{C_{6v}} = 12$ elements and can be generated by the rotation $\mathcal{R}_{\pi/3}$ and the reflection of y-axis, $\mathcal{R}_y$. It has six different conjugacy classes and six irreducible representations, of which four are one-dimensional, and remaining are two-dimensional. Using characters of C_{6v} shown in Table C.4, we can write product of $E_1 \times E_1$ as

$$E_1 \times E_1 = A_1 \oplus A_2 \oplus E_2. \tag{C.16}$$

C'_{6v} for kagome lattice

Anzats for the algebraic spin liquid on Kagome lattice has a larger unit cell than the case without any fluxes. Thus, to classify fermionic bilinears, we again have to consider enlarged group, C'_{6v}, which is the C_{6v} with added translations for primitive lattice vectors $\boldsymbol{a}_1$ and $\boldsymbol{a}_2$.

The group C'_{6v} (or, G_{s2} in notations of Ref. [6]) has been studied extensively and its conjugacy classes along with characters are listed in Tables III and IV in Ref. [6]. Using this information, we may find the decomposition of the representation on bilinears as in Eq. (4.38) with bases of corresponding irreducible components listed in Table 4.3.

In the next order, we have to decompose the $E_1 \times G^{\pi \mathrm{F} \Phi}_{\psi^\dagger \psi}$ into irreducible representations. This leads us to Eq. (4.40) in the main text, where components A_1, A_2 and E_2, which are of interest for us originate from the tensor product of E_1 with another

Rep	E	C_2	C_3	C_6	C_a	$C_{a'}$
A_1	1	1	1	1	1	1
A_2	1	1	1	1	−1	−1
B_2	1	−1	1	−1	1	−1
B_1	1	−1	1	−1	−1	1
E_1	2	−2	−1	1	0	0
E_2	2	2	−1	−1	0	0

Table C.4: Irreducible representations of the group C_{6v} and their characters.

E_1, contained within Eq. (4.38). This readily allows us to find the basis for these representations.

C.2 Calculation of the polarization operator

In this appendix we calculate the imaginary part of the polarization bubble. We work using assumptions, specified in the main text. In particular we restrict ourselves to the clean limit $ql \gg 1$ and assume the temperature to the the largest energy scale in the problem, $T \gg v_F q \gg \omega$. Note, that we use explicit value of $N = 2$ corresponding to spin. Since the polarization operator is proportional to N, one can easily restore the answer for the general case.

We write the polarization operator, $\Pi^{(i)}$, corresponding to the interaction vertex $\tilde{M}^{(i)}(\hat{\boldsymbol{q}})$ as

$$\operatorname{Im}\Pi^{(i)}(\mathrm{i}\omega_n, \boldsymbol{q}) = 2T \operatorname{Im}\int (dk) \sum_m \operatorname{tr}[\tilde{M}^{(i)}_{\boldsymbol{k}}(\hat{\boldsymbol{q}}) G_{\boldsymbol{k}+\boldsymbol{q}}(\mathrm{i}\omega_m + \mathrm{i}\omega_n) \tilde{M}^{(i)}_{\boldsymbol{k}+\boldsymbol{q}}(\hat{\boldsymbol{q}}) G_{\boldsymbol{k}}(\mathrm{i}\omega_m)], \tag{C.17}$$

where $(dk) = dk_x dk_y/(2\pi)^2$ is the short-hand notation for the momentum integration measure. The interaction vertex $\tilde{M}^{(i)}(\hat{\boldsymbol{q}})$ as well as the Greens function are matrices in spinor space, and tracing in (C.17) goes over matrix indices. After analytical continuation, the imaginary part of the the matsubara sum of two Greens functions is written as,

$$\operatorname{Im}\sum_m [G_{\boldsymbol{k}+\boldsymbol{q}}(\mathrm{i}\omega_m + \mathrm{i}\omega_n)]_{\alpha\beta} [G_{\boldsymbol{k}}(\mathrm{i}\omega_m)]_{\gamma\delta} = \frac{1}{2\pi T}\int dz \left(\tanh\frac{z}{2T} - \tanh\frac{z+\omega}{2T}\right) \operatorname{Im}[G^R_{\boldsymbol{k}+\boldsymbol{q}}(z+\omega)]_{\alpha\beta} \operatorname{Im}[G^A_{\boldsymbol{k}}(z)]_{\gamma\delta}. \tag{C.18}$$

where we restored internal indices. $G^{R,A}_{\boldsymbol{k}}(z)$ stands for retarded (advanced) Greens function for real frequencies,

$$G^{R,A}_{\boldsymbol{k}}(z, \boldsymbol{k}) = \frac{z + v_F \boldsymbol{\tau}\cdot\boldsymbol{k}}{(z \pm \mathrm{i}0)^2 - v_F^2 \boldsymbol{k}^2}. \tag{C.19}$$

In what follows, we will need the expression for the trace of numerators of two Greens functions with corresponding interaction vertices in Eq. (C.17). For the case of density coupling, defined in Eq (4.62), we have $\tilde{M}_{\boldsymbol{k}}^{(0)}(\hat{\boldsymbol{q}}) = \mathbb{1}$, and the trace is evaluated as:

$$T^{(0)}(z,\omega,\boldsymbol{k},\boldsymbol{q}) = \mathrm{tr}[\mathbb{1}\cdot(z+\omega+v_F\boldsymbol{\tau}\cdot(\boldsymbol{k}+\boldsymbol{q}))\cdot\mathbb{1}\cdot(z+v_F\boldsymbol{\tau}\cdot\boldsymbol{k})] = 4[(z+\omega)z+(v_Fk)^2+v_F^2kq\cos\theta], \quad \text{(C.20)}$$

with θ being the angle between vectors $\boldsymbol{k}$ and $\boldsymbol{q}$. Note that there is an additional factor of two in (C.20) from accounting for the (trivial) valley structure, whereas the factor of two originating from spin degrees of freedom is included in (C.17). For the case of spinon-phonon coupling, arising in the next order of expansion in $\boldsymbol{k}$, the $\tilde{M}_{\boldsymbol{k}}^{(1)}(\hat{\boldsymbol{q}})$ is given by Eq. (4.55b) and the trace results in a cumbersome expression for $T^{(1)}(z,\omega,\boldsymbol{k},\boldsymbol{q})$, which will be not listed here. Using expression for the imaginary part of Green's functions, we have:

$$\begin{aligned}\mathrm{Im}\,\Pi^{R(i)}(\omega,\boldsymbol{q}) = \pi\,\mathrm{Im}\int(dk)\int dz\left(\tanh\frac{z}{2T}-\tanh\frac{z+\omega}{2T}\right)T^{(i)}(z,\omega,\boldsymbol{k},\boldsymbol{q})\frac{1}{4v_Fk}\\ \left[\frac{\delta(z+v_Fk)\delta(\omega+v_Fk'-v_Fk)}{v_Fk-\omega}+\frac{\delta(z-v_Fk)\delta(\omega-v_Fk'+v_Fk)}{v_Fk+\omega}\right.\\ \left.+\frac{\delta(z+v_Fk)\delta(\omega-v_Fk'-v_Fk)}{v_Fk-\omega}+\frac{\delta(z-v_Fk)\delta(\omega+v_Fk'+v_Fk)}{v_Fk+\omega}\right]. \quad \text{(C.21)}\end{aligned}$$

We drop last two terms in the square brackets since they correspond to interband transitions, and for $\omega \ll v_Fq$ they are not important. Also, we expand the difference between hyperbolic tangents, thus getting the derivative of the Fermi distribution function, denoted as $n_F'(z)$:

$$\begin{aligned}\mathrm{Im}\,\Pi^{R(i)}(\omega,\boldsymbol{q}) = 2\pi\omega\int(dk)\int dz\, n_F'(z)T^{(i)}(z,\omega,\boldsymbol{k},\boldsymbol{q})\frac{1}{4v_Fk}\\ \times\left[\frac{\delta(z+v_Fk)\delta(\omega+v_Fk'-v_Fk)}{v_Fk-\omega}+\frac{\delta(z-v_Fk)\delta(\omega-v_Fk'+v_Fk)}{v_Fk+\omega}\right]. \quad \text{(C.22)}\end{aligned}$$

Using δ-functions, we may get rid of the integration over z. Integral over angle

between vectors $\boldsymbol{k}$ and $\boldsymbol{q}$, denoted as θ, can be done using the following expression:

$$\int d\theta\, \delta(\pm\omega - v_F|\boldsymbol{k}+\boldsymbol{q}| + v_F k) F(\theta) = 2\theta(2k-q) \frac{v_F k \pm \omega}{v_0^2 kq |\sin\theta_0^{\pm}|} F(\theta_0^{\pm}), \qquad \text{(C.23)}$$

where

$$\cos\theta_0^{\pm} = \frac{\omega^2}{2v_F^2 kq} \pm \frac{\omega}{v_F q} - \frac{q}{2k}. \qquad \text{(C.24)}$$

This is valid in the limit when $v_F q \gg \omega$. Note, that we included an extra factor 2 to account for two possible values of θ_0^+ (and θ_0^-), assuming that the $F(\theta_0^+)$ is the same for both solutions. The integration over θ in Eq. (C.22) yields:

$$\mathrm{Im}\,\Pi^{R(i)}(\omega,\boldsymbol{q}) = \frac{\omega}{4\pi v_0^3 q} \int_{q/2}^{\infty} dk \left[n_F'(-v_F k) \frac{T^{(i)}(-v_F k, \omega, \boldsymbol{k}, \boldsymbol{q})|_{\theta=\theta_0^-}}{k|\sin\theta_0^-|} + n_F'(v_F k) \frac{T^{(i)}(v_F k, \omega, \boldsymbol{k}, \boldsymbol{q})|_{\theta=\theta_0^+}}{k|\sin\theta_0^+|} \right]. \qquad \text{(C.25)}$$

We notice, that expression in the square brackets in Eq. (C.25) does not vanish if we put ω to zero within it for the case of density coupling [when $T(z,k,\theta)$ is given by Eq. (C.20)]. In this case, accounting for the fact that $n_F'(v_F k)$ for the vanishing chemical potential is an even function, we have:

$$\mathrm{Im}\,\Pi^{R(0)}(\omega,\boldsymbol{q}) = \frac{4\omega}{\pi v_F q} \int_{q/2}^{\infty} dk\, n_F'(v_F k) \sqrt{k^2 - (q/2)^2} = -\frac{4\omega}{\pi v_F q} T \log 2. \qquad \text{(C.26)}$$

When calculating the integral we used the fact that the main contribution to the integral comes from $v_F k \sim T$, thus we may neglect by q in the square root. This answer reproduces the results, available in the literature [174–176, 192, 193]. Recalling that this polarization operator is proportional to N, which was assumed to be $N = 2$ for this calculation, we reproduce the imaginary part of the result listed in the main text, Eq. (4.53).

The calculation for the case of the next order coupling, $\tilde{M}_{\boldsymbol{k}}^{(1)}(\hat{\boldsymbol{q}})$, requires more care. The answer depends on the direction of the phonon momentum, $\boldsymbol{q}$. We define the ϕ to be an angle of $\boldsymbol{q}$ relative to the x-axis, so that $\hat{\boldsymbol{q}} = (\cos\phi, \sin\phi)$. Lengthy,

but straightforward calculation gives for the polarization operator in this case

$$\mathrm{Im}\,\Pi^{R(1)}(\omega,\boldsymbol{q}) = \frac{\omega\sin^4 2\phi}{\pi q}\int_{q/2}^{\infty} dk\, n_F'(v_F k)\frac{k^4}{\sqrt{k^2-(q/2)^2}} = -\frac{9\zeta(3)}{2\pi}\frac{\omega}{v_F^3 q}T^3\sin^4 2\phi. \tag{C.27}$$

Noteworthy, the answer is invariant under rotations of $\pi/2$, as one may expect for our case. The angular dependence of (C.27) is very anisotropic, in particular, when $\boldsymbol{q}$ points along x or y-axes, the result vanish, indicating that the answer will be of higher order in ω.

Bibliography

[1] Maksym Serbyn, T. Senthil, and Patrick A. Lee. Exotic S=1 spin-liquid state with fermionic excitations on the triangular lattice. *Phys. Rev. B*, 84:180403, 2011.

[2] Samuel Bieri, Maksym Serbyn, T. Senthil, and Patrick A. Lee. Paired chiral spin liquid with a fermi surface in S=1 model on the triangular lattice. *Phys. Rev. B*, 86:224409, 2012.

[3] Maksym Serbyn, T. Senthil, and Patrick A. Lee. Overscreened Kondo fixed point in S=1 spin liquid. *Phys. Rev. B*, 88:024419, 2013.

[4] Maksym Serbyn and Patrick A. Lee. Spinon-phonon interaction in algebraic spin liquids. *Phys. Rev. B*, 87:174424, 2013.

[5] Michael Hermele, T. Senthil, and Matthew P. A. Fisher. Algebraic spin liquid as the mother of many competing orders. *Phys. Rev. B*, 72(10):104404, 2005.

[6] Michael Hermele, Ying Ran, Patrick A. Lee, and Xiao-Gang Wen. Properties of an algebraic spin liquid on the kagome lattice. *Phys. Rev. B*, 77(22):224413, 2008.

[7] D. M. Basko. Theory of resonant multiphonon raman scattering in graphene. *Phys. Rev. B*, 78(12):125418, 2008.

[8] P. W. Anderson. Resonating valence bonds - new kind of insulator. *Materials Research Bulletin*, 8(2):153–160, 1973.

[9] Leon Balents. Spin liquids in frustrated magnets. *Nature*, 464(7286):199–208, 2010.

[10] X.G. Wen. *Quantum Field Theory of Many-Body Systems:From the Origin of Sound to an Origin of Light and Electrons.* Oxford Graduate Texts. OUP Oxford, 2004.

[11] Xiao-Gang Wen. Topological order: From long-range entangled quantum matter to a unified origin of light and electrons. *ISRN Condensed Matter Physics*, 2013:20, 2013.

[12] Alexei Kitaev and John Preskill. Topological entanglement entropy. *Phys. Rev. Lett.*, 96:110404, 2006.

[13] Michael Levin and Xiao-Gang Wen. Detecting topological order in a ground state wave function. *Phys. Rev. Lett.*, 96:110405, 2006.

[14] Steven R. White. Density matrix formulation for quantum renormalization groups. *Phys. Rev. Lett.*, 69:2863–2866, 1992.

[15] E.M. Stoudenmire and Steven R. White. Studying two-dimensional systems with the density matrix renormalization group. *Annual Review of Condensed Matter Physics*, 3(1):111–128, 2012.

[16] Hong-Chen Jiang, Zhenghan Wang, and Leon Balents. Identifying topological order by entanglement entropy. *Nat Phys*, 8(12):902–905, 2012.

[17] Stefan Depenbrock, Ian P. McCulloch, and Ulrich Schollwöck. Nature of the spin-liquid ground state of the S=1/2 Heisenberg model on the kagome lattice. *Phys. Rev. Lett.*, 109:067201, 2012.

[18] Simeng Yan, David A. Huse, and Steven R. White. Spin-liquid ground state of the s = 1/2 kagome Heisenberg antiferromagnet. *Science*, 332(6034):1173–1176, 2011.

[19] Yi Zhang, Tarun Grover, and Ashvin Vishwanath. Entanglement entropy of critical spin liquids. *Phys. Rev. Lett.*, 107:067202, 2011.

[20] Tarun Grover, Yi Zhang, and Ashvin Vishwanath. Entanglement entropy as a portal to the physics of quantum spin liquids. *New Journal of Physics*, 15(2):025002, 2013.

[21] Michael M. Wolf. Violation of the entropic area law for fermions. *Phys. Rev. Lett.*, 96:010404, 2006.

[22] Xiao-Gang Wen. Quantum orders and symmetric spin liquids. *Phys. Rev. B*, 65:165113, 2002.

[23] Michael Hermele, T. Senthil, Matthew P. A. Fisher, Patrick A. Lee, Naoto Nagaosa, and Xiao-Gang Wen. Stability of $U(1)$ spin liquids in two dimensions. *Phys. Rev. B*, 70(21):214437, 2004.

[24] C. Gros. Physics of projected wavefunctions. *Annals of Physics*, 189(1):53–88, 1989.

[25] P. W. Anderson. Resonating valence bond state in La_2Cu0_4 and superconductivity. *Science*, 235(4793):1196–1198, 1987.

[26] Y. Shimizu, K. Miyagawa, K. Kanoda, M. Maesato, and G. Saito. Spin liquid state in an organic mott insulator with a triangular lattice. *Physical Review Letters*, 91(10), 2003.

[27] Yamashita Satoshi, Nakazawa Yasuhiro, Oguni Masaharu, Oshima Yugo, Nojiri Hiroyuki, Shimizu Yasuhiro, Miyagawa Kazuya, and Kanoda Kazushi. Thermodynamic properties of a spin-1/2 spin-liquid state in a kappa-type organic salt. *Nature Physics*, 4:459–462, 2008.

[28] J. S. Helton, K. Matan, M. P. Shores, E. A. Nytko, B. M. Bartlett, Y. Yoshida, Y. Takano, A. Suslov, Y. Qiu, J. H. Chung, D. G. Nocera, and Y. S. Lee. Spin dynamics of the spin-1/2 kagome lattice antiferromagnet ZnCu3(OH)(6)Cl-2. *Physical Review Letters*, 98(10), 2007.

[29] Tian-Heng Han, Joel S. Helton, Shaoyan Chu, Daniel G. Nocera, Jose A. Rodriguez-Rivera, Collin Broholm, and Young S. Lee. Fractionalized excitations in the spin-liquid state of a kagome-lattice antiferromagnet. *Nature*, 492(7429):406–410, 2012.

[30] Yoshihiko Okamoto, Minoru Nohara, Hiroko Aruga-Katori, and Hidenori Takagi. Spin-liquid state in the $S = 1/2$ hyperkagome antiferromagnet $Na_4Ir_3O_8$. *Phys. Rev. Lett.*, 99:137207, 2007.

[31] S. Nakatsuji, K. Kuga, K. Kimura, R. Satake, N. Katayama, E. Nishibori, H. Sawa, R. Ishii, M. Hagiwara, F. Bridges, T. U. Ito, W. Higemoto, Y. Karaki, M. Halim, A. A. Nugroho, J. A. Rodriguez-Rivera, M. A. Green, and C. Broholm. Spin-orbital short-range order on a honeycomb-based lattice. *Science*, 336(6081):559–563, 2012.

[32] J. G. Cheng, G. Li, L. Balicas, J. S. Zhou, J. B. Goodenough, Cenke Xu, and H. D. Zhou. High-pressure sequence of $Ba_3NiSb_2O_9$ structural phases: New $S = 1$ quantum spin liquids based on Ni^{2+}. *Physical Review Letters*, 107(19), 2011.

[33] Subhro Bhattacharjee, Vijay B. Shenoy, and T. Senthil. Possible ferro-spin nematic order in Ni Ga_2 S_4. *Phys. Rev. B*, 74(9):092406, 2006.

[34] Hirokazu Tsunetsugu and Mitsuhiro Arikawa. Spin nematic phase in S=1 triangular antiferromagnets. *Journal of the Physical Society of Japan*, 75(8), 2006.

[35] Zheng-Xin Liu, Yi Zhou, and Tai-Kai Ng. Fermionic theory for quantum antiferromagnets with spin S > 1/2. *Physical Review B*, 82(14), 2010.

[36] Zheng-Xin Liu, Yi Zhou, and Tai-Kai Ng. Possibility of S=1 spin liquids with fermionic spinons on triangular lattices. *Physical Review B*, 81(22), 2010.

[37] Tarun Grover and T. Senthil. Non-abelian spin liquid in a spin-one quantum magnet. *Phys. Rev. Lett.*, 107(7):077203, 2011.

[38] B. I. Halperin, Patrick A. Lee, and Nicholas Read. Theory of the half-filled landau level. *Phys. Rev. B*, 47:7312–7343, 1993.

[39] Patrick A. Lee and Naoto Nagaosa. Gauge theory of the normal state of high-t_c superconductors. *Phys. Rev. B*, 46:5621–5639, 1992.

[40] B. L. Altshuler, L. B. Ioffe, and A. J. Millis. Low-energy properties of fermions with singular interactions. *Phys. Rev. B*, 50:14048–14064, 1994.

[41] B. L. Altshuler, L. B. Ioffe, and A. J. Millis. Critical behavior of the t=0 $2k_f$ density-wave phase transition in a two-dimensional fermi liquid. *Phys. Rev. B*, 52:5563–5572, 1995.

[42] Yong Baek Kim, Akira Furusaki, Xiao-Gang Wen, and Patrick A. Lee. Gauge-invariant response functions of fermions coupled to a gauge field. *Phys. Rev. B*, 50:17917–17932, 1994.

[43] Olexei I. Motrunich. Variational study of triangular lattice spin-12 model with ring exchanges and spin liquid state in. *Phys. Rev. B*, 72:045105, 2005.

[44] Sung-Sik Lee. Low-energy effective theory of fermi surface coupled with U(1) gauge field in $2+1$ dimensions. *Phys. Rev. B*, 80:165102, 2009.

[45] David F. Mross, John McGreevy, Hong Liu, and T. Senthil. Controlled expansion for certain non-fermi-liquid metals. *Phys. Rev. B*, 82:045121, 2010.

[46] M. A. Metlitski, D. F. Mross, S. Sachdev, and T. Senthil. Are non-Fermi-liquids stable to Cooper pairing? *ArXiv e-prints*, 2014.

[47] Yi Zhou and Patrick A. Lee. Spinon phonon interaction and ultrasonic attenuation in quantum spin liquids. *Phys. Rev. Lett.*, 106:056402, 2011.

[48] Patrick A. Lee. Physics - an end to the drought of quantum spin liquids. *Science*, 321(5894):1306–1307, 2008.

[49] O. I. Motrunich. Variational study of triangular lattice spin-1/2 model with ring exchanges and spin liquid state in kappa-(et)(2)cu-2(cn)(3). *Physical Review B*, 72(4), 2005.

[50] S. S. Lee and P. A. Lee. U(1) gauge theory of the hubbard model: Spin liquid states and possible application to kappa-(bedt-ttf)(2)cu-2(cn)(3). *Physical Review Letters*, 95(3), 2005.

[51] Cenke Xu, Fa Wang, Yang Qi, Leon Balents, and Matthew P. A. Fisher. Spin liquid phases for spin-1 systems on the triangular lattice. *Physical Review Letters*, 108(8), 2012.

[52] G. Chen, M. Hermele, and L. Radzihovsky. Frustrated quantum critical theory of putative spin-liquid phenomenology in 6H-B-Ba3NiSb2O9. *Physical Review Letters*, 109(1), 2012.

[53] N. Papanicolaou. Unusual phases in quantum spin-1 systems. *Nuclear Physics B*, 305(3):367 – 395, 1988.

[54] Andreas Laeuchli, Frederic Mila, and Karlo Penc. Quadrupolar phases of the S=1 bilinear-biquadratic Heisenberg model on the triangular lattice. *Physical Review Letters*, 97(8), 2006.

[55] T. A. Tóth. *Quadrupolar Ordering in Two-Dimensional Spin-One Systems.* PhD thesis, EPFL, 2011.

[56] Peng Li, Guang-Ming Zhang, and Shun-Qing Shen. SU(3) bosons and the spin nematic state on the spin-1 bilinear-biquadratic triangular lattice. *Phys. Rev. B*, 75(10):104420, 2007.

[57] Kedar Damle and T. Senthil. Spin nematics and magnetization plateau transition in anisotropic kagome magnets. *Phys. Rev. Lett.*, 97(6):067202, 2006.

[58] M. Granath and S. Ostlund. Degenerate three-band hubbard model with anti-hund's rule interactions: A model for a(x)c(60). *Physical Review B*, 68(20), 2003.

[59] A. H. Macdonald, S. M. Girvin, and D. Yoshioka. T/u expansion for the hubbard-model. *Physical Review B*, 37(16):9753–9756, 1988.

[60] Guang-Ming Zhang and Xiaoguang Wang. Spin swapping operator as an entanglement witness for quantum Heisenberg spin-s systems. *Journal of Physics a-Mathematical and General*, 39(26):8515–8526, 2006.

[61] D. J. Thouless. Exchange in solid 3he and Heisenberg hamiltonian. *Proceedings of the Physical Society of London*, 86(553P):893, 1965.

[62] A. Lauchli, J. C. Domenge, C. Lhuillier, P. Sindzingre, and M. Troyer. Two-step restoration of SU(2) symmetry in a frustrated ring-exchange magnet. *Physical Review Letters*, 95(13), 2005.

[63] W. LiMing, G. Misguich, P. Sindzingre, and C. Lhuillier. From neel long-range order to spin liquids in the multiple-spin exchange model. *Physical Review B*, 62(10):6372–6377, 2000.

[64] Karlo Penc and Andreas M. Laeuchli. *Spin Nematic Phases in Quantum Spin Systems*, volume 164 of *Springer Series in Solid-State Sciences*, pages 331–362. Springer, 2011.

[65] R. P. Feynman. *Statistical Mechanics.* Addison-Wesley, Reading, MA, 1972.

[66] Jan Brinckmann and Patrick A. Lee. Renormalized mean-field theory of neutron scattering in cuprate superconductors. *Phys. Rev. B*, 65(1):014502, 2001.

[67] X. G. Wen, F. Wilczek, and A. Zee. Chiral spin states and superconductivity. *Physical Review B*, 39(16):11413–11423, 1989.

[68] E. Fradkin and S. H. Shenker. Phase-diagrams of lattice gauge-theories with higgs fields. *Physical Review D*, 19(12):3682–3697, 1979.

[69] P. A. Lee, N. Nagaosa, and X. G. Wen. Doping a mott insulator: Physics of high-temperature superconductivity. *Reviews of Modern Physics*, 78(1):17–85, 2006.

[70] D. A. Huse and V. Elser. Simple variational wave-functions for two-dimensional Heisenberg spin-1/2 antiferromagnets. *Physical Review Letters*, 60(24):2531–2534, 1988.

[71] Bela Bauer, Philippe Corboz, Andreas M. Laeuchli, Laura Messio, Karlo Penc, Matthias Troyer, and Frederic Mila. Three-sublattice order in the SU(3) Heisenberg model on the square and triangular lattice. *Physical Review B*, 85(12), 2012.

[72] G. E. Volovik. On edge states in superconductors with time inversion symmetry breaking. *Jetp Letters*, 66(7):522–527, 1997.

[73] T. Senthil, J. B. Marston, and M. P. A. Fisher. Spin quantum hall effect in unconventional superconductors. *Physical Review B*, 60(6):4245–4254, 1999.

[74] K. Sengupta, I. Zutic, H. J. Kwon, V. M. Yakovenko, and S. Das Sarma. Midgap edge states and pairing symmetry of quasi-one-dimensional organic superconductors. *Physical Review B*, 63(14), 2001.

[75] M. Stone and R. Roy. Edge modes, edge currents, and gauge invariance in p(x)+ip(y) superfluids and superconductors. *Physical Review B*, 69(18), 2004.

[76] H. Takayama, Y. R. Linliu, and K. Maki. Continuum model for solitons in polyacetylene. *Physical Review B*, 21(6):2388–2393, 1980.

[77] D. A. Ivanov. Non-abelian statistics of half-quantum vortices in p-wave superconductors. *Physical Review Letters*, 86(2):268–271, 2001.

[78] X. G. Wen. Gapless boundary excitations in the quantum hall states and in the chiral spin states. *Physical Review B*, 43(13):11025–11036, 1991.

[79] Hosho Katsura, Naoto Nagaosa, and Patrick A. Lee. Theory of the thermal hall effect in quantum magnets. *Physical Review Letters*, 104(6), 2010.

[80] C. L. Kane and M. P. A. Fisher. Quantized thermal transport in the fractional quantum hall effect. *Physical Review B*, 55(23):15832–15837, 1997.

[81] N. Read and D. Green. Paired states of fermions in two dimensions with breaking of parity and time-reversal symmetries and the fractional quantum hall effect. *Physical Review B*, 61(15):10267–10297, 2000.

[82] Roland Bastardis, Nathalie Guihery, and Coen de Graaf. Microscopic origin of isotropic non-Heisenberg behavior in S=1 magnetic systems. *Physical Review B*, 76(13), 2007.

[83] C. Kittel. Model of exchange-inversion magnetization. *Physical Review*, 120(2):335–342, 1960.

[84] A. V. Gorshkov, M. Hermele, V. Gurarie, C. Xu, P. S. Julienne, J. Ye, P. Zoller, E. Demler, M. D. Lukin, and A. M. Rey. Two-orbital SU(N) magnetism with ultracold alkaline-earth atoms. *Nature Physics*, 6(4):289–295, 2010.

[85] Jun Kondo. Free-energy shift of conduction electrons due to the *s-d* exchange interaction. *Progress of Theoretical Physics*, 40(4):683–694, 1968.

[86] A. A. Abrikosov. Electron scattering on magnetic impurities in metals and anomalous resistivity effects. *Physics (Long Island City, N. Y.)*, 2:5, 1965.

[87] A. A. Abrikosov and A. A. Migdal. On the theory of the Kondo effect. *J. Low Temp. Phys.*, 3:519, 1970.

[88] Ph. Nozières and A. Blandin. Kondo effect in real metals. *Journal de Physique*, 41(3):19, 1980.

[89] N Read and D M Newns. On the solution of the coqblin-schreiffer hamiltonian by the large-n expansion technique. *Journal of Physics C: Solid State Physics*, 16(17):3273, 1983.

[90] Ian Affleck. A current algebra approach to the Kondo effect. *Nuclear Physics B*, 336(3):517 – 532, 1990.

[91] Ian Affleck and Andreas W.W. Ludwig. Critical theory of overscreened Kondo fixed points. *Nuclear Physics B*, 360(2-3):641 – 696, 1991.

[92] Ian Affleck and Andreas W.W. Ludwig. The Kondo effect, conformal field theory and fusion rules. *Nuclear Physics B*, 352(3):849 – 862, 1991.

[93] Olivier Parcollet and Antoine Georges. Transition from overscreening to underscreening in the multichannel Kondo model: Exact solution at large N. *Phys. Rev. Lett.*, 79:4665–4668, 1997.

[94] Olivier Parcollet, Antoine Georges, Gabriel Kotliar, and Anirvan Sengupta. Overscreened multichannel SU(n) Kondo model: Large-n solution and conformal field theory. *Phys. Rev. B*, 58:3794–3813, 1998.

[95] Anirvan M. Sengupta and Yong Baek Kim. Overscreened single-channel Kondo problem. *Phys. Rev. B*, 54:14918–14921, 1996.

[96] Michele Fabrizio and Gergely Zaránd. Mapping between multichannel exchange models. *Phys. Rev. B*, 54:10008–10013, 1996.

[97] J. Gan, N. Andrei, and P. Coleman. Perturbative approach to the non-fermi-liquid fixed point of the overscreened Kondo problem. *Phys. Rev. Lett.*, 70:686–689, 1993.

[98] J Gan. On the multichannel Kondo model. *Journal of Physics: Condensed Matter*, 6(24):4547, 1994.

[99] M. Fabrizio and Alexander O. Gogolin. Toulouse limit for the overscreened four-channel Kondo problem. *Phys. Rev. B*, 50:17732–17735, 1994.

[100] R. M. Potok, I. G. Rau, Hadas Shtrikman, Yuval Oreg, and D. Goldhaber-Gordon. Observation of the two-channel Kondo effect. *Nature*, 446:167, 2007.

[101] A. C. Hewson. *The Kondo problem to heavy fermions.* Cambridge University Press, Cambridge, 1993.

[102] D. L. Cox and A. Zawadowski. Exotic Kondo effects in metals: Magnetic ions in a crystalline electric field and tunnelling centres. *Advances in Physics*, 47(5):599–942, 1998.

[103] P. Schlottmann and P. D. Sacramento. Multichannel Kondo problem and some applications. *Advances in Physics*, 42(6):641–682, 1993.

[104] A.M. Tsvelick and P.B. Wiegmann. Exact results in the theory of magnetic alloys. *Advances in Physics*, 32(4):453–713, 1983.

[105] A.M. Tsvelick and P.B. Wiegmann. Exact results in the theory of magnetic alloys. *Z. Phys. B*, 54:201, 1984.

[106] A.M. Tsvelick and P.B. Wiegmann. Exact solution of the multichannel Kondo problem, scaling, and integrability. *J. Stat. Phys*, 38:125, 1985.

[107] A.M. Tsvelick. The thermodynamics of multichannel Kondo problem. *J. Phys. C*, 18:159, 1985.

[108] N. Andrei, K. Furuya, and J. H. Lowenstein. Solution of the Kondo problem. *Rev. Mod. Phys.*, 55:331–402, 1983.

[109] B. Béri and N. R. Cooper. Topological Kondo effect with majorana fermions. *Phys. Rev. Lett.*, 109:156803, 2012.

[110] Matthias Vojta. Impurity quantum phase transitions. *Philosophical Magazine*, 86(13-14):1807–1846, 2006.

[111] David Withoff and Eduardo Fradkin. Phase transitions in gapless fermi systems with magnetic impurities. *Phys. Rev. Lett.*, 64:1835–1838, 1990.

[112] Carlos R. Cassanello and Eduardo Fradkin. Kondo effect in flux phases. *Phys. Rev. B*, 53:15079–15094, 1996.

[113] Matthias Vojta and Lars Fritz. Upper critical dimension in a quantum impurity model:critical theory of the asymmetric pseudogap Kondo problem. *Phys. Rev. B*, 70:094502, 2004.

[114] Matthias Vojta and Lars Fritz. Upper critical dimension in a quantum impurity model:critical theory of the asymmetric pseudogap Kondo problem. *Phys. Rev. B*, 70:094502, 2004.

[115] Lars Fritz and Matthias Vojta. Phase transitions in the pseudogap anderson and Kondo models: critical dimensions, renormalization group, and local-moment criticality. *Phys. Rev. B*, 70:214427, 2004.

[116] Lars Fritz, Serge Florens, and Matthias Vojta. Universal crossovers and critical dynamics of quantum phase transitions: A renormalization group study of the pseudogap Kondo problem. *Phys. Rev. B*, 74:144410, 2006.

[117] G. Khaliullin, R. Kilian, S. Krivenko, and P. Fulde. Impurity-induced moments in underdoped cuprates. *Phys. Rev. B*, 56:11882–11888, 1997.

[118] Naoto Nagaosa and Tai-Kai Ng. Nonmagnetic impurity in the spin-gap state. *Phys. Rev. B*, 51:15588–15591, 1995.

[119] Naoto Nagaosa and Patrick A. Lee. Kondo effect in high- T_c cuprates. *Phys. Rev. Lett.*, 79:3755–3758, 1997.

[120] Catherine Pépin and Patrick A. Lee. Order from disorder: Nonmagnetic impurities in the spin-gap phase of the cuprates. *Phys. Rev. Lett.*, 81:2779–2782, 1998.

[121] Ziqiang Wang and Patrick A. Lee. Local moment formation in the superconducting state of a doped mott insulator. *Phys. Rev. Lett.*, 89:217002, 2002.

[122] Subir Sachdev, Chiranjeeb Buragohain, and Matthias Vojta. Quantum impurity in a nearly critical two-dimensional antiferromagnet. *Science*, 286(5449):2479–2482, 1999.

[123] Subir Sachdev and Matthias Vojta. Quantum impurity in an antiferromagnet: Nonlinear sigma model theory. *Phys. Rev. B*, 68:064419, 2003.

[124] Kaj H. Höglund and Anders W. Sandvik. Anomalous curie response of impurities in quantum-critical spin-1/2 Heisenberg antiferromagnets. *Phys. Rev. Lett.*, 99:027205, 2007.

[125] Kaj H. Höglund, Anders W. Sandvik, and Subir Sachdev. Impurity induced spin texture in quantum critical 2d antiferromagnets. *Phys. Rev. Lett.*, 98:087203, 2007.

[126] Max A. Metlitski and Subir Sachdev. Valence bond solid order near impurities in two-dimensional quantum antiferromagnets. *Phys. Rev. B*, 77:054411, 2008.

[127] Serge Florens, Lars Fritz, and Matthias Vojta. Kondo effect in bosonic spin liquids. *Phys. Rev. Lett.*, 96:036601, 2006.

[128] Serge Florens, Lars Fritz, and Matthias Vojta. Boundary quantum criticality in models of magnetic impurities coupled to bosonic baths. *Phys. Rev. B*, 75:224420, 2007.

[129] Alexei Kolezhuk, Subir Sachdev, Rudro R. Biswas, and Peiqiu Chen. Theory of quantum impurities in spin liquids. *Phys. Rev. B*, 74:165114, 2006.

[130] Ki-Seok Kim and Mun Dae Kim. Kondo physics in the algebraic spin liquid. *Journal of Physics: Condensed Matter*, 20(12):125206, 2008.

[131] Kusum Dhochak, R. Shankar, and V. Tripathi. Magnetic impurities in the honeycomb kitaev model. *Phys. Rev. Lett.*, 105:117201, 2010.

[132] P. Ribeiro and P. A. Lee. Magnetic impurity in a $U(1)$ spin liquid with a spinon fermi surface. *Phys. Rev. B*, 83:235119, 2011.

[133] Satoru Nakatsuji, Yusuke Nambu, Hiroshi Tonomura, Osamu Sakai, Seth Jonas, Collin Broholm, Hirokazu Tsunetsugu, Yiming Qiu, and Yoshiteru Maeno. Spin disorder on a triangular lattice. *Science*, 309(5741):1697–1700, 2005.

[134] E. M. Stoudenmire, Simon Trebst, and Leon Balents. Quadrupolar correlations and spin freezing in $S = 1$ triangular lattice antiferromagnets. *Phys. Rev. B*, 79:214436, 2009.

[135] Hirokazu Tsunetsugu and Mitsuhiro Arikawa. Spin nematic phase in $S = 1$ triangular antiferromagnets. *Journal of the Physical Society of Japan*, 75(8):083701, 2006.

[136] Zheng-Xin Liu, Yi Zhou, and Tai-Kai Ng. Possibility of $S = 1$ spin liquids with fermionic spinons on triangular lattices. *Phys. Rev. B*, 81(22):224417, 2010.

[137] Zheng-Xin Liu, Yi Zhou, and Tai-Kai Ng. Fermionic theory for quantum antiferromagnets with spin $S = 1/2$. *Phys. Rev. B*, 82(14):144422, 2010.

[138] Tarun Grover and T. Senthil. Non-abelian spin liquid in a spin-one quantum magnet. *Phys. Rev. Lett.*, 107:077203, 2011.

[139] Maksym Serbyn, T. Senthil, and Patrick A. Lee. Exotic $S = 1$ spin-liquid state with fermionic excitations on the triangular lattice. *Phys. Rev. B*, 84:180403, 2011.

[140] Cenke Xu, Fa Wang, Yang Qi, Leon Balents, and Matthew P. A. Fisher. Spin liquid phases for spin-1 systems on the triangular lattice. *Phys. Rev. Lett.*, 108:087204, 2012.

[141] Olexei I. Motrunich. Orbital magnetic field effects in spin liquid with spinon fermi sea: Possible application to κ-$(ET)_2cu_2(CN)_3$. *Phys. Rev. B*, 73:155115, 2006.

[142] M. R. Norman and T. Micklitz. How to measure a spinon fermi surface. *Phys. Rev. Lett.*, 102:067204, 2009.

[143] Wing-Ho Ko, Zheng-Xin Liu, Tai-Kai Ng, and Patrick A. Lee. Raman signature of the U(1) Dirac spin-liquid state in the spin-$\frac{1}{2}$ kagome system. *Phys. Rev. B*, 81:024414, 2010.

[144] Wing-Ho Ko and Patrick A. Lee. Proposal for detecting spin-chirality terms in mott insulators via resonant inelastic x-ray scattering. *Phys. Rev. B*, 84:125102, 2011.

[145] David F. Mross and T. Senthil. Charge friedel oscillations in a mott insulator. *Phys. Rev. B*, 84:041102, 2011.

[146] P. Coleman and C. Pépin. Singular fermi liquid behavior in the underscreened Kondo model. *Phys. Rev. B*, 68:220405, 2003.

[147] Pankaj Mehta, Natan Andrei, P. Coleman, L. Borda, and Gergely Zarand. Regular and singular fermi-liquid fixed points in quantum impurity models. *Phys. Rev. B*, 72:014430, 2005.

[148] D. C. Ralph and R. A. Buhrman. Observations of Kondo scattering without magnetic impurities: A point contact study of two-level tunneling systems in metals. *Phys. Rev. Lett.*, 69:2118–2121, 1992.

[149] D. C. Ralph, A. W. W. Ludwig, Jan von Delft, and R. A. Buhrman. 2-channel Kondo scaling in conductance signals from 2 level tunneling systems. *Phys. Rev. Lett.*, 72:1064–1067, 1994.

[150] Max A. Metlitski and Subir Sachdev. Quantum phase transitions of metals in two spatial dimensions. i. ising-nematic order. *Phys. Rev. B*, 82:075127, 2010.

[151] P. Nozieres. A fermi-liquid description of the Kondo problem at low temperatures. *Journal of Low Temperature Physics*, 17:112, 1974.

[152] N. Andrei and C. Destri. Solution of the multichannel Kondo problem. *Phys. Rev. Lett.*, 52:364–367, 1984.

[153] G. Fáth and J. Sólyom. Period tripling in the bilinear-biquadratic antiferromagnetic S =1 chain. *Phys. Rev. B*, 44:11836–11844, 1991.

[154] G. Fáth and J. Sólyom. Isotropic spin-1 chain with twisted boundary condition. *Phys. Rev. B*, 47:872–881, 1993.

[155] Chigak Itoi and Masa-Hide Kato. Extended massless phase and the haldane phase in a spin-1 isotropic antiferromagnetic chain. *Phys. Rev. B*, 55:8295–8303, 1997.

[156] Ian Affleck, Masaki Oshikawa, and Hubert Saleur. Boundary critical phenomena in SU(3) "spin" chains. *Journal of Physics A: Mathematical and General*, 34(6):1073, 2001.

[157] Andreas Läuchli, Guido Schmid, and Simon Trebst. Spin nematics correlations in bilinear-biquadratic $S = 1$ spin chains. *Phys. Rev. B*, 74:144426, 2006.

[158] P. A. Lee and N. Nagaosa. A Proposal to Use Neutron Scattering to Measure Scalar Spin Chirality Fluctuations in Kagome Lattices. *ArXiv e-prints*, 2012.

[159] Oleg A. Starykh and Leon Balents. Ordering in spatially anisotropic triangular antiferromagnets. *Phys. Rev. Lett.*, 98:077205, 2007.

[160] A. C. Potter, T. Senthil, and P. A. Lee. Mechanisms for Sub-Gap Optical Conductivity in Herbertsmithite. *ArXiv e-prints*, 2013.

[161] D. V. Pilon, C. H. Lui, T. Han, D. B. Shrekenhamer, A. J. Frenzel, W. J. Padilla, Y. S. Lee, and N. Gedik. Spin Induced Optical Conductivity in the Spin Liquid Candidate Herbertsmithite. *ArXiv e-prints*, 2013.

[162] Eugene I. Blount. Ultrasonic attenuation by electrons in metals. *Phys. Rev.*, 114:418–436, 1959.

[163] T. Tsuneto. Ultrasonic attenuation in superconductors. *Phys. Rev.*, 121(2):402–415, 1961.

[164] S. Rodriguez and E. Kartheuser. Deformation potentials and the electron-phonon interaction in crystals. *Superlattices and Microstructures*, 1(6):503 – 510, 1985.

[165] F. S. Khan and P. B. Allen. Deformation potentials and electron-phonon scattering: Two new theorems. *Phys. Rev. B*, 29:3341–3349, 1984.

[166] J. L. Mañes. Symmetry-based approach to electron-phonon interactions in graphene. *Phys. Rev. B*, 76:045430, 2007.

[167] Walter Rantner and Xiao-Gang Wen. Electron spectral function and algebraic spin liquid for the normal state of underdoped high T_c superconductors. *Phys. Rev. Lett.*, 86:3871–3874, 2001.

[168] Walter Rantner and Xiao-Gang Wen. Spin correlations in the algebraic spin liquid: Implications for high-T_c superconductors. *Phys. Rev. B*, 66:144501, 2002.

[169] O. Vafek, Z. Tešanović, and M. Franz. Relativity restored: Dirac anisotropy in qed_3. *Phys. Rev. Lett.*, 89:157003, 2002.

[170] M. Franz, Z. Tešanović, and O. Vafek. QED_3 theory of pairing pseudogap in cuprates: From d-wave superconductor to antiferromagnet via an algebraic fermi liquid. *Phys. Rev. B*, 66:054535, 2002.

[171] M.A.H. Vozmediano, M.I. Katsnelson, and F. Guinea. Gauge fields in graphene. *Physics Reports*, 496:109 – 148, 2010.

[172] L. B. Ioffe and A. I. Larkin. Gapless fermions and gauge fields in dielectrics. *Phys. Rev. B*, 39:8988–8999, 1989.

[173] Don H. Kim and Patrick A. Lee. Theory of spin excitations in undoped and underdoped cuprates. *Annals of Physics*, 272(1):130 – 164, 1999.

[174] N. Dorey and N. E. Mavromatos. QED3 and two-dimensional superconductivity without parity violation. *Nuclear Physics B*, 386(3):614 – 680, 1992.

[175] D. V. Khveshchenko. Coulomb-interacting dirac fermions in disordered graphene. *Phys. Rev. B*, 74:161402, 2006.

[176] Oskar Vafek. *Quasiparticles and Vortices in the High Temperature Cuprate Superconductors.* PhD thesis, Johns Hopkins University, Baltimore, MD, 2003.

[177] X. G. Wen. Quantum orders and symmetric spin liquids (the original version), 2001.

[178] Gang Chen, Andrew Essin, and Michael Hermele. Majorana spin liquids and projective realization of SU(2) spin symmetry. *Phys. Rev. B*, 85:094418, 2012.

[179] T. O. Woodruff and H. Ehrenreich. Absorption of sound in insulators. *Phys. Rev.*, 123(5):1553–1559, 1961.

[180] D. Ceperley, G. V. Chester, and M. H. Kalos. Monte-carlo simulation of a many-fermion study. *Physical Review B*, 16(7):3081–3099, 1977.

[181] J. P. Bouchaud and C. Lhuillier. A new variational description of liquid-he-3 - the superfluid glass. *Europhysics Letters*, 3(12):1273–1280, 1987.

[182] M. Bajdich, L. Mitas, L. K. Wagner, and K. E. Schmidt. Pfaffian pairing and backflow wavefunctions for electronic structure quantum monte carlo methods. *Physical Review B*, 77(11), 2008.

[183] M. Wimmer. Algorithm 923: Efficient numerical computation of the pfaffian for dense and banded skew-symmetric matrices. *Acm Transactions on Mathematical Software*, 38(4), 2012.

[184] Zheng-Xin Liu, Yi Zhou, Hong-Hao Tu, Xiao-Gang Wen, and Tai-Kai Ng. Gutzwiller projected wave functions in the fermionic theory of S=1 spin chains. *Physical Review B*, 85(19), 2012.

[185] Samuel Bieri and Dmitri Ivanov. Quasiparticle spectral weights of gutzwiller-projected high-t-c superconductors. *Physical Review B*, 75(3), 2007.

[186] H. Yokoyama and H. Shiba. Variational monte-carlo studies of superconductivity in strongly correlated electron systems. *Journal of the Physical Society of Japan*, 57(7):2482–2493, 1988.

[187] B. Edegger, N. Fukushima, C. Gros, and V. N. Muthukumar. Particle number renormalization in nearly half-filled mott hubbard superconductors. *Physical Review B*, 72(13), 2005.

[188] P. W. Anderson and N. P. Ong. Theory of asymmetric tunneling in the cuprate superconductors. *Journal of Physics and Chemistry of Solids*, 67(1-3):1–5, 2006.

[189] Noboru Fukushima. Grand canonical gutzwiller approximation for magnetic inhomogeneous systems. *Physical Review B*, 78(11), 2008.

[190] M. Hamermesh. *Group Theory and its Application to Physical Group Theory and its Application to Physical Problems.* Addison-Wesley Series in Physics. Addison-Wesley, Reading, MA, 1962.

[191] Frank Porter. Notes on representation theory. http://www.hep.caltech.edu/ fcp/math/groupTheory/represen.pdf.

[192] B Wunsch, T Stauber, F Sols, and F Guinea. Dynamical polarization of graphene at finite doping. *New Journal of Physics*, 8(12):318, 2006.

[193] E. H. Hwang and S. Das Sarma. Dielectric function, screening, and plasmons in two-dimensional graphene. *Phys. Rev. B*, 75(20):205418, 2007.